

**THE EFFECT OF OPTICAL SPATIAL FILTERING
ON THE STATISTICS OF LASER RADIATION
PROPAGATING THROUGH THE
TURBULENT ATMOSPHERE**

Libo Sun
B.S. Chinese University of Science and Technology, 1967
M.S. Chinese Academy of Sciences, 1981

**A dissertation submitted to the faculty
of the Oregon Graduate Center
in partial fulfillment of the
requirements for the degree
Doctor of Philosophy
in
Applied Physics**

September, 1988

To My Parents

The dissertation "The Effect of Optical Spatial Filtering on the Statistics of Laser Radiation Propagating through Turbulent Atmosphere" by Libo Sun has been examined and approved by the following Examination Committee:

J. Fred Holmes, Advisor
Professor

Paul R. Davis
Professor

V. S. Rao Gudimetla
Assistant Professor

Aslam Khalil
Professor

ACKNOWLEDGEMENTS

I am most grateful for the advise and guidance of my advisor, Prof. J. Fred Holmes for his support and the advisory during and after my years at Oregon Graduate Center.

I especially value his understanding and encouragement in finishing my Ph. D. degree.

I also thank Dr. V.S.R. Gudimetla for his many helpful discussions and friedship.

Much gratitude is due to senior engineer J. Hunt for his valuable contribution in the design and manufacture of the optical system and data processing equipment used in this project. I wish to thank Drs. Richard A. Elliott, J.Fred. Holmes, Paul R. Davis, and other faculties at OGC for the beneficial lectures that directly related to my research area.

I would express my sincere thanks to friedship and help from my classmates, Drs. Jia Zheng Li, Mark Gesley, Rick DeFreez, Jack Biles, and Feng Qian.

I appreciate the help from Beverly Kyler for her help in the past years and word-processing of research papers.

At last, I would indicate that the Computer Laboratory of the Department of APEE, OGC, along with its rich software, provides and ideal environment for scientific research, I benefitted a lot from using it.

Table of Contents

ACKNOWLEDGEMENTS	iii
LIST OF FIGURES	vii
LIST OF TABLES	ix
ABSTRACT	x
1. Introduction	1
2. The Green Function of the System	8
2.1 The Image Plane Green Function	8
2.2 The Output Plane Green Function	11
3. Mean Intensity	17
3.1 Mean Intensity on Image Plane	17
3.1.1 Line of Sight Propagation	17
3.1.2 Speckle Propagation	22
3.2 Mean Intensity on Output Plane	23
3.2.1 Line of Sight Propagation	23
3.2.2 Speckle Propagation	26
3.2.3 Phase Contrast Filtering	29
3.3 Quadratic Approximation	34
3.3.1 Line of Sight propagation	35

3.3.2 Speckle Propagation	37
4. Intensity variance (Line of sight case)	39
4.1 Introduction	39
4.2 General Expression for Intensity Correlation	39
4.3 Variance	43
5. The Intensity Variance (Speckle case)	53
5.1 Introduction	53
5.2 The fourth order moment of input field	54
5.3 Variance of Intensity after Spatial Filtering	60
6. Experimental results	69
6.1 Introduction	69
6.2 Mean Intensity measurement	73
6.2.1 Experiment in Laboratory Simulated Turbulence	74
6.2.2 Line of Sight Propagation in Turbulent Atmosphere	78
6.2.3 Speckle Propagation in Turbulent Atmosphere	80
6.3 Intensity Variance	84
7. Conclusions	87
References	89
APPENDIX 1: Transformation in Eight-Dimensional Space	93
1. Introduction	93
2. Linear Transformation (1)	94

3. Linear Transformation (2)	98
References	104
APPENDIX 2: Closed Form Expansion of the Four-Point, Wave Structure Function for a Turbulent Atmosphere	
1. Introduction	105
2. Analysis	107
3. Approximate Expansion	110
3.1 Step 1	114
3.2 Step 2	115
3.3 Step 3	116
4. Final Results	117
5. Example: Line of Sight Spherical Wave Propagation	118
References	125
VITA	127

List of Figures

Fig. 2.1 Basic structure of optical spatial filtering system	9
Fig. 3.1 Line of sight remote sensing system	18
Fig. 3.2 Line of sight propagation. Intensity distribution on image plane as a function of received aperture and turbulence levels	21
Fig. 3.3 Speckle propagation. Intensity distribution on image plane as a function of received aperture and turbulence levels	24
Fig. 3.4 Mean intensity of line of sight propagation. effect of receiver aperture	27
Fig. 3.5 Mean intensity of line of sight propagation. effect of filter center transmission	28
Fig. 3.6 Mean intensity of speckle propagation. effect of transmitter aperture	30
Fig. 3.7 Mean intensity of speckle propagation. effect of receiver aperture	31
Fig. 3.8 Mean intensity of line of sight propagation. Phase contrast filter	32
Fig. 3.9 Mean intensity of speckle propagation. Phase contrast filter	33
Fig. 3.10 Mean intensity of line of sight propagation, compared with	

quadratic approximation (line of sight propagation)	36
Fig. 3.11 Mean intensity of line of sight propagation, compared with quadratic approximation (speckle propagation)	38
Fig. 4.1 Second order statistics of line of sight propagation	47
Fig. 4.2 Intensity variance of line of sight propagation with different filter sizes (C_n^2 scale)	48
Fig. 4.3 Intensity variance of line of sight propagation with different filter sizes (σ_x^2 scale)	49
Fig. 4.4 Normalized intensity variance of line of sight propagation with different receiver apertures	50
Fig. 4.5 Second order statistics under typical propagation parame- ters (OGC field site geometry)	51
Fig. 5.1 Second order statistics of speckle propagation	63
Fig. 5.2 Normalized intensity variance of speckle propagation with different transmitter apertures	64
Fig. 5.2 Intensity variance of speckle propagation with different transmitter apertures	65
Fig. 5.4 Second order statistics under typical propagation parame- ters (OGC campus site geometry)	66
Fig. 5.5 Normalized intensity variance of speckle propagation with different filter sizes	67
Fig. 6.1 Schematic illustration of the turbulence simulation tank	

and instrumentations for turbulence measurement	75
Fig. 6.2 Output of optical intensity variance versus turbulence levels	76
Fig. 6.3 Output of mean intensity of the optical spatial filtering receiver versus turbulence levels	77
Fig. 6.4 Mean intensity after spatial filtering for line of sight atmo- sphere propagation	79
Fig. 6.5 Structure of Transmitter in a Single Ended Remote Sens- ing System	81
Fig. 6.6 Structure of Receiver in a Single Ended Remote Sensing System	82
Fig. 6.7 Speckle propagation. Experimental results of mean inten- sity after optical spatial filtering vs. σ_x^2	83
Fig. 6.8 Speckle propagation. Experimental results of normalized variance vs. σ_x^2	85
Fig. A1.1 Original Space and New Space.	100
Fig. A1.2 Integration Region on θ_1, θ_2 Plane.	101
Fig. A2.1 Numerical Integration of I as a Function of ρ	111
Fig. A2.2 Numerical Integration of I as a Function of θ	112
Fig. A2.3 Relative Error of Expansion 1.	119
Fig. A2.4 Relative Error of Expansion 2.	120
Fig. A2.5 Relative Error of Expansion 3.	121

List of Tables

Table 1. Coefficients of first order harmonics	122
Table 2. Coefficients of second order harmonics	123
Table 3. Coefficients of third order harmonics	124

ABSTRACT

THE EFFECT OF OPTICAL SPATIAL FILTERING ON THE STATISTICS OF LASER RADIATION PROPAGATING THROUGH THE TURBULENT ATMOSPHERE

Libo Sun, Ph. D.
Oregon Graduate Center, 1988

Supervising Professor: J. Fred Holmes

Speckle-turbulence interaction has the potential for allowing single ended remote sensing of the path averaged strength of turbulence (structure constant) along the limit of sight to a remote object. Unfortunately, the fluctuations in received intensity due to speckle and those due to the turbulence cannot be directly separated. It was therefore proposed that by utilizing optical spatial filtering (OSF) before measuring the received intensity, that the effects of speckle and turbulence could be separated. Consequently, the research for this dissertation was directly toward a better understanding of laser and laser generated speckle propagation through turbulence, the effect of optical spatial filtering on the received intensity and its application to optical remote sensing of the strength of turbulence.

The work involved both analysis of the statistics for the received intensity after OSF and experimental work to verify the analysis. The mean and the variance of the received intensity after OSF both for the line of sight case and the single ended case were analyzed and the results studied. These

results indicated that the OSF mean intensity in both cases could be used very effectively to remote sense the strength of turbulence, but that the variance was not useful for that purpose.

Experimental work was conducted for both the line of sight and single ended cases in the atmosphere and also utilizing the OGC turbulence simulation tank. The results agree with the theoretical predictions and demonstrate that OSF can be used in both the line of sight case and the single ended case for optically remote sensing the strength of turbulence. The technique should be useful for turbulence levels from around 10^{-16} to $10^{-12}m^{-2/3}$ by choosing appropriate laser wavelengths and the high-pass spatial filter sizes.

1. Introduction

Optical images have the inherent property that they possess two degrees of freedom as represented by the two independent variables. An additional property of an optical system is that a Fourier transform relation exists between the field distributions at the front and back focal planes of a lens used in such a system. Hence, in a coherent optical system, an optical arrangement which presents a space-domain function and successive Fourier transforms can easily be implemented. As a result, integral transforms and filtering in the spatial frequency domain may often be carried out more conveniently in an optical system than in an equivalent electronic channel.

Historically, the basic Fourier transform relations upon which the spatial filtering is based are essentially established by Huygens, Fresnel and Kirchoff. The first attempt in performing optical spatial filtering (OSF) were made by Abbe¹ and Porter² in their studies on microscope vision³ in the years 1893 and 1903 respectively. In their experiments, the effects of OSF were demonstrated by inserting a narrow slit in the focal plane of a transform lens. The change in the orientation of the slot would produce a change in the contents of the vertical or horizontal component which can best be seen from the image of a meshed screen made of thin wire. Several filtering methods have been developed with the advancement of optical manufacturing techniques. The Schlieren technique⁴ (1866) provides a sensitive approach to detect light diffractions due to changes in the refractive

index along the path. A typical Schlieren system consists of two concave mirrors that produce and refocus a parallel beam of light from a monochromatic source; A knife edge is placed at the location of the focal point of the second mirror. The knife edge is placed in such a way as to obscure half of the image when there is no diffraction on the path, the effect of diffraction will form a shifted image. Due to the coherence of the primary and diffracted light, the illumination of the output will be altered. It is evident that the output is proportional to the integrated gradient throughout the path in a direction normal to the knife-edge. This fact, together with the effect of the finite aperture of the system, makes quantitative analysis of the Schlieren photography difficult. The anisotropy of the Schlieren method can be removed by utilizing a two-dimensional knife-edge shaped to fit the shape of the source. Opaque stops of circular⁵ and square⁶ shape have been used as spatial filters for corresponding light sources. The well known experiment by Zernike⁷ (1942) successfully solved the vision of a thin transparent phase object by introducing a phase shift filter.

In the fifties, the concept of electric filtering began to be accepted by scientists in optics. Because of the Fourier transform relations of coherent optical systems they behave in many ways, analogously to electrical-filters. The ease of synthesis of optical system has made them useful in some areas where complex electric networks were previously used. Since then, the OSF technique has developed rapidly and the communication theory approach has widely been used in the analysis of such system. O'Neill⁸ and Cutrona⁹ provided good review papers summarizing the details of this development.

In comparison to the electric filter counterpart, the optical filtering system features a huge information volume, instant processing and parallel processing. On the other hand, there are some disadvantages associated with using the optical approach. First, the two-dimensional nature of the filtering makes quantitative analysis difficult. In some cases of application, the effect of OSF can only be described in qualitative terms or be displayed in pictorial images before and after filtering. Second, the resolution of the optical system is always limited by the diffraction of the finite aperture. The output of the optical system is the convolution of the input image with the delta-response of the apertures involved. In electronic systems, the accuracy and the bandwidth of a filter can be implemented in response to the requirement up to a specified degree. In optical systems, high-quality filters are usually expensive to make and hard to implement. For example, under monochromatic collimated input, a circular aperture produces an amplitude distribution in the form of a zero order Bessel function which features a rich zero-frequency component within the disk with radius $r = 1.22\lambda f/d$, where d is the diameter of the aperture. The upper limit of resolution of the optical system, according to the Rayleigh criterion, is determined by r . In order to increase the resolution beyond this limit, the only possible choice is to use a larger aperture. In addition, various aberrations of the optical system will introduce more errors and thus decrease the resolution. Hence, it is expensive to build a high-resolution system and it is also tedious to analyze such a system quantitatively. Another difficulty associated with the OSF system is the requirement for high-mechanical precision. The theoretical resolution of

a lens 20 centimeters in diameter and with a focal length of one meter is about 3.6 micrometers. To match such resolution, the edge shape as well as the positioning of the filter need to be controlled within the order of micrometer. It is relatively easier to manufacture a half-plane filter by using a sharp edged knife as in the Schlieren apparatus. But, it is much more expensive to implement a small circular disk with the same edge sharpness.

More recently, efforts have been made to probe the quantitative aspects of the OSF technique and to design precision measurement system based on the analysis. Taylor¹⁰ completed an analysis on gas flow visualization using a phase contrast filter and a physical apparatus based on a Schlieren system was used to study the gas flow. He pointed out that in order to realize the full sensitivity of the method, the image of the input pinhole, in the absence of a phase object, must exactly coincide with the phase shifting filter spot. The need for accurately matching the image of the source with the phase shifting spot requires that all aberrations in the optical system be kept to a minimum and that all the optical components be of the highest possible quality. The numerical discrete Fourier transform (DFT) was adopted¹¹ to discuss the quantitative properties of the phase shift filtering. The performance of the optical matched filter, i.e. the Vander-Lugt filter, in regard to the signal-to-noise ratio was analyzed by Shanker and Gupta¹² in their studies on the multiplicative speckle noise of digital information storage system.

An object with low contrast and soft edges possesses rich low frequency components which overlap the spectrum of the aperture. Numerous techniques have been developed to overcome this difficulty with various degree of

success. A two-stage spatial filtering scheme was proposed by Blodgett and Easton¹³ with an attempt to separate the spectrum generated by the aperture and that generated by the object. A cross-shaped high-pass spatial filter was introduced in the focal plane of the first stage to match the square input window. The filter is analytically represented by the following formula

$$T = [1 - \text{rect}(\frac{x}{a})][1 - \text{rect}(\frac{y}{b})]$$

where a and b are the half-width of the elements of the cross in the x and y directions respectively. By using optimum parameters, the aperture spectrum energy is reduced by a factor of 10^4 . This technique, however, can only be used successfully when the object is in the format of a transparency.

The optical spatial filtering techniques can also be applied to speckle interferometry¹⁴. This is a technique that uses a double-exposure specklegram to detect small displacement and strain in mechanical structures. In this arrangement, a filtering aperture is located at the transform plane to allow a particular spatial frequency of the spectrum to pass through the reconstruction lens and to form fringes. Chen and Chiang¹⁵ performed a quantitative analysis of the effect of the size and location of the band-pass filter on the visibility of the fringes.

Obviously, the OSF technique has become a powerful tool in the area of precision measurement. The purpose of this research is to provide a systematic approach in modeling and analysis of OSF systems. With special application in the remote sensing of turbulence in the atmosphere, formulations for the mean intensity as well as the intensity variance are given in

closed form. The formulation contains important system parameters such as the lens aperture, focal length, filter size, center transmission, phase-shift, etc. In order to verify the theory, several experiments were designed and measurements conducted by using the equipment and computer facilities of the Laboratory of Atmospheric Optics at Oregon Graduate Center.

This paper is divided into seven chapters. Chapter 1 is an introduction which provides a review of the development of the OSF technique. In chapter 2, we introduce the Green function of the standard OSF system in a close form representation. All system parameters are involved in the discussion so the effect of each of them can be studied separately. This function is given for a general center-symmetrical-structured system and can thus be used elsewhere for analysis purposes. In chapter 3, the mean intensity of spatially filtered laser radiation propagated through the turbulent atmosphere is studied. Here, the mean intensities as functions of the system parameters and of the turbulence index are given for two planes of interest: the image plane and the output plane. The performances of high-pass and also phase-shift filtering are displayed under typical system parameter configurations. We have also considered the quadratic approximation of the wave structure function of the turbulent atmosphere and discussed the error introduced into the spatially filtered mean intensity. The analyses of spatially filtered intensity variance for the line of sight case and for speckle propagation case in the turbulent atmosphere are discussed in chapters 4 and 5 respectively. To avoid cumbersome mathematical complexity, the results are given using the quadratic approximation for the wave structure function.

The experiments that were designed and performed to support the theory are described in detail in chapter 6. The major results of this paper are summarized in chapter 7. Appendix 1 presents a transformation in 8-dimensional space which enables us to simplify some mathematical expressions in the text. The numerical expansions of the four-point structure function of spherical wave propagation in turbulent atmosphere are given in the closed forms in the appendix 2, which has much better accuracy of numerical evaluation in comparison with the quadratic approximation.

2. The Green functions of the Spatial Filtering System

The Green function of a two-dimensional system is often called the 'point spread function'¹⁶ in optics literature, which is the system response to a two-dimensional delta function input. In the following, we use the Green function to represent the input/output relation between field amplitude of a two-dimensional optical image processing system.

2.1. Image Plane Green Function

Fig. 2.1 shows a schematic diagram of the receiver system. A receiver consists of two lenses with diameter $D = 2\sqrt{2}a$, where D is the actual diameter of the lens and a is a normalized parameter. A spatial filter is put between these two lenses.

There are two planes of interest in Fig. 2.1, i.e the image plane and the output plane. The image plane q is defined via the expression

$$\frac{1}{d_o} + \frac{1}{d_i} = \frac{1}{f} \quad (2.1)$$

where d_o is the object distance, d_i is the image distance and f is the focal length of the lens. We stress the term 'image plane' to distinguish it from the popular term 'focal plane' in our spatial filtering system. In most cases of remote sensing, the object is usually far away from the receiver and

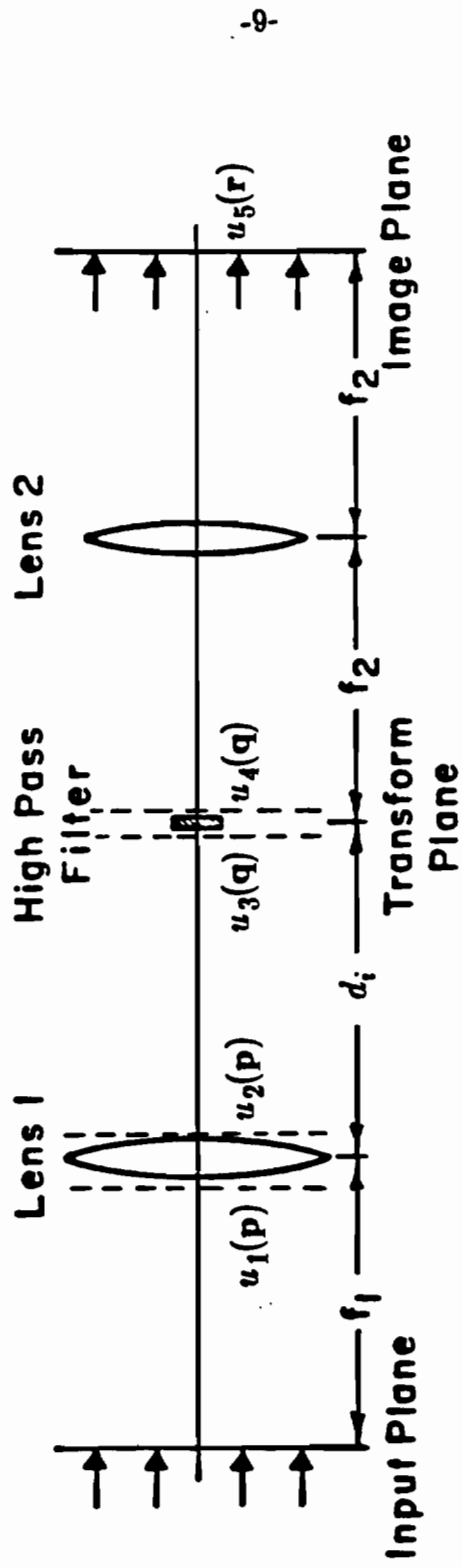


Fig. 2.1 Basic structure of optical spatial filtering system.

thus the image plane is very close to the focal plane. But, in practice, it is much easier to place the filter on the image plane which is well defined, has the sharpest image and is observable. The 'focal' plane, although also well defined conceptually for an aberration free lens, is hard to find in actual measurement. For an object situated at a distance of 500 meters, the distance between the two planes is only 2 mm for a lens with a focal length of 1 meter. But this produces a substantial difference in the results of spatial filtering. In order to have good consistency, our theory is developed in terms of image plane filtering and in our experimental work, efforts are made to place the filter on a plane having the sharpest image.

We introduce two Green functions which are required to complete the theory: the image plane and output plane Green function.

The input plane is assumed to be just in front of lens L_1 . The image Green function $G_3(\mathbf{q}, \mathbf{p})$ can be constructed in terms of the field distribution $u_3(\mathbf{q})$ on the image plane due to a point source located at point \mathbf{p}_0 on the input plane. The output Green function $G_5(\mathbf{r}, \mathbf{p})$ is similarly defined in terms of the field $u_5(\mathbf{r})$ on the output plane generated by the point source. Thus we assume

$$u_1(\mathbf{p}) = \delta(\mathbf{p} - \mathbf{p}_0) \quad (2.2)$$

The lens is represented by a Gaussian transfer function

$$t(\mathbf{p}) = \exp\left(-\frac{p^2}{a^2} - i\frac{kp^2}{2f}\right) \quad (2.3)$$

Where a is the aperture parameter and f is the focal length of the lens.

Under the thin lens assumption¹⁷, the field behind the lens is given by

$$u_2(\mathbf{p}) = \delta(\mathbf{p}-\mathbf{p}_0)\exp\left(-\frac{p^2}{a^2} - ik\frac{p^2}{2f}\right) \quad (2.4)$$

The field on the \mathbf{q} plane before filtering is the result of a free propagation of u_2 and is given using the Huygens-Fresnel formulation and the paraxial approximation by:

$$\begin{aligned} u_3(\mathbf{q}) &= \frac{e^{ikd_i}}{i\lambda d_i} e^{i\frac{k}{2d_i}q^2} \iint u_2(\mathbf{p}) \exp\left[i\frac{k}{2d_i}p^2 - i\frac{k}{d_i}\mathbf{p}\cdot\mathbf{q}\right] d\mathbf{p} \\ &= \frac{e^{ikd_i}}{i\lambda d_i} \exp\left[i\frac{k}{2d_i}q^2 - \frac{p_0^2}{a^2} + i\frac{k}{2}\left(\frac{1}{d_i} - \frac{1}{f}\right)p_0^2 - i\frac{k}{d_i}\mathbf{p}_0\cdot\mathbf{q}\right] \end{aligned} \quad (2.5)$$

where $d\mathbf{p} = p dp d\theta$. Thus the image Green function of the system is given by

$$G_3(\mathbf{q}, \mathbf{p}) = \frac{e^{ikd_i}}{i\lambda d_i} \exp\left\{i\frac{k}{2d_i}q^2 - \left[\frac{1}{a^2} - i\frac{k}{2}\left(\frac{1}{d_i} - \frac{1}{f}\right)\right]p^2 - i\frac{k}{d_i}\mathbf{p}\cdot\mathbf{q}\right\} \quad (2.6)$$

2.2. The Output Plane Green Function

The spatial filtering is implemented by putting a Gaussian type spatial filter on the image plane. The transfer function of the filter is defined as:

$$F(\mathbf{q}) = [b + (\alpha e^{i\delta} - b)\exp(-\frac{q^2}{q_0^2})] \quad (2.7)$$

Where q_0 is the normalized filter size defined by $q_0 = \frac{\sqrt{2}}{4}D$ and D is the actual diameter of the center spot of the filter. Different filter configurations can be simulated by properly choosing the parameters. Typical examples are :

1. High-pass filter: $b = 1, \alpha = 0, \delta = 0$
2. Low-pass filter: $b = 0, \alpha = 1, \delta = 0$
3. $\pi/2$ Phase-contrast filter: $b = 1, \alpha = 1, \delta = \frac{\pi}{2}$

The field immediately behind the filter is given by

$$u_4(\mathbf{q}) = u_3(\mathbf{q})F(\mathbf{q}) \quad (2.8)$$

The field $u_5(\mathbf{r})$ is related to $u_4(\mathbf{q})$ by¹⁶:

$$u_5(\mathbf{r}) = \frac{e^{2ikf}}{i\lambda f} \iint u_4(\mathbf{q})A(\mathbf{r}+\mathbf{q})\exp(-i\frac{k}{f}\mathbf{r}\cdot\mathbf{q})d\mathbf{q} \quad (2.9)$$

where $d\mathbf{q}=qdq d\theta$, $A(\mathbf{x})$ is the aperture function of the second lens and is given by $A(\mathbf{x}) = \exp(-\frac{x^2}{a^2})$.

Substituting (2.7) , (2.8) and (2.5) into (2.9) , writing $u_5 = u_5^1 + u_5^2$, we have

$$u_5^1(\mathbf{r}) = -b \frac{e^{ik(d_i+2f)}}{\lambda^2 d_i f} e^{-[\frac{1}{a^2} - i\frac{k}{2}(\frac{1}{a} - \frac{1}{f})]p_0^2 - \frac{r^2}{a^2}} \iint e^{-i(\frac{1}{a^2} - i\frac{k}{2d_i})q^2 - [(\frac{2}{a^2} + i\frac{k}{f})\mathbf{r} + i\frac{k}{d_i}\mathbf{p}_0]\cdot\mathbf{q}} d\mathbf{q}$$

The integral can be worked out as :

$$I_1 = \frac{\pi}{\frac{1}{a^2} - i\frac{k}{2d_i}} \exp\left[-\frac{i(\frac{k}{f} - i\frac{2}{a^2})\mathbf{r} + \frac{k}{d_i}\mathbf{p}_0 \cdot \mathbf{r}}{4(\frac{1}{a^2} - i\frac{k}{2d_i})}\right]$$

u_5^1 can thus be rearranged as the following;

$$u_5^1 = \pi b \frac{e^{ik(d_i+2f)}}{-\lambda^2 d_i f (\frac{1}{a^2} - i\frac{k}{2d_i})} \exp\left\{-\left[\frac{1}{a^2} - i\frac{k}{2}\left(\frac{1}{d_i} - \frac{1}{f}\right) + \frac{k^2}{4d_i\left(\frac{1}{a^2} - i\frac{k}{2d_i}\right)}\right]p_0^2\right\}$$

$$-\left[\frac{k\left(\frac{k}{f} - \frac{2i}{a^2}\right)}{2d_i\left(\frac{1}{a^2} - i\frac{k}{2d_i}\right)} \right] p_0 \cdot r - \left[\frac{1}{a^2} + \frac{\left(\frac{k}{f} - i\frac{2}{a^2}\right)^2}{4\left(\frac{1}{a^2} - i\frac{k}{2d_i}\right)} \right] r^2 \quad (2.11)$$

Similarly, the second term of $u_5^2(\mathbf{q})$ is

$$u_5^2 = \frac{(\alpha e^{i\delta} - b)\pi e^{ik(d_i+2f)}}{-\lambda^2 d_i f \left(\frac{1}{a^2} + \frac{1}{q_0^2} - i\frac{k}{2d_i}\right)} \exp \left\{ \left[-\frac{1}{a^2} - i\frac{k}{2}\left(\frac{1}{d_i} - \frac{1}{f}\right) + \frac{k^2}{4d_i^2\left(\frac{1}{a^2} + \frac{1}{q_0^2} - i\frac{k}{2d_i}\right)} \right] p_0^2 \right. \\ \left. - \left[i\frac{k\left(\frac{k}{f} - i\frac{2}{a^2}\right)}{2d_i\left(\frac{1}{a^2} + \frac{1}{q_0^2} - i\frac{k}{2d_i}\right)} \right] \mathbf{r} \cdot \mathbf{p} - \frac{\left[\frac{1}{a^2} + \left(\frac{k}{f} - i\frac{2}{a^2}\right)\right]^2}{4\left(\frac{1}{a^2} + \frac{1}{q_0^2} - i\frac{k}{2d_i}\right)} r^2 \right\} \quad (2.12)$$

After rearrangement and combining terms, we have the output Green function of the system defined in the following form

$$G_5(\mathbf{r}, \mathbf{p}) = \sum_{i=1}^2 A_i \exp[-B_i p^2 - C_i r^2 - D_i \mathbf{r} \cdot \mathbf{p}] \quad (2.13)$$

where the coefficients are given by:

$$A_1 = \pi b \frac{e^{ik(d_i+2f)}}{-\lambda^2 d_i f \left(\frac{1}{a^2} - i\frac{k}{2d_i}\right)} \quad (2.14)$$

$$A_2 = \pi(\alpha e^{i\delta} - b) \frac{e^{ik(d_i+2f)}}{-\lambda^2 d_i f \left(\frac{1}{a^2} + \frac{1}{q_0^2} - i\frac{k}{2d_i}\right)} \quad (2.15)$$

$$B_1 = \frac{1}{a^2} - i\frac{k}{2}\left(\frac{1}{d_i} - \frac{1}{f}\right) + \frac{k^2}{4d_i\left(\frac{1}{a^2} - i\frac{k}{2d_i}\right)} \quad (2.16)$$

$$B_2 = \frac{1}{a^2} - i\frac{k}{2}\left(\frac{1}{d_i} - \frac{1}{f}\right) + \frac{k^2}{4d_i^2\left(\frac{1}{a^2} + \frac{1}{q_0^2} - i\frac{k}{2d_i}\right)} \quad (2.17)$$

$$C_1 = \frac{1}{a^2} + \frac{\left(\frac{k}{f} - i\frac{2}{a^2}\right)^2}{4\left(\frac{1}{a^2} - i\frac{k}{2d_i}\right)} \quad (2.18)$$

$$C_2 = \frac{1}{a^2} + \frac{\left(\frac{k}{f} - i\frac{2}{a^2}\right)^2}{4\left(\frac{1}{a^2} + \frac{1}{q_0^2} - i\frac{k}{2d_i}\right)} \quad (2.19)$$

$$D_1 = \frac{k\left(\frac{k}{f} - i\frac{2}{a^2}\right)}{2d_i\left(\frac{1}{a^2} - i\frac{k}{2d_i}\right)} \quad (2.20)$$

$$D_2 = \frac{k\left(\frac{k}{f} - i\frac{2}{a^2}\right)}{2d_i\left(\frac{1}{a^2} + \frac{1}{q_0^2} - i\frac{k}{2d_i}\right)} \quad (2.21)$$

The statistical quantities needed are the second and fourth moments of the field. Under the new coordinate system defined by

$$\mathbf{p}_1 - \mathbf{p}_2 = \mathbf{p} \quad ; \quad \mathbf{q}_1 - \mathbf{q}_2 = \mathbf{q} \quad ; \quad \mathbf{r}_1 - \mathbf{r}_2 = \mathbf{r} \quad (2.22)$$

$$\mathbf{p}_1 + \mathbf{p}_2 = 2\mathbf{P} \quad ; \quad \mathbf{q}_1 + \mathbf{q}_2 = 2\mathbf{Q} \quad ; \quad \mathbf{r}_1 + \mathbf{r}_2 = 2\mathbf{R} \quad (2.23)$$

The second moment is given by

$$\Gamma_i(\mathbf{Q}, \mathbf{q}) = \langle u_i(\mathbf{q}_1) u_i^*(\mathbf{q}_2) \rangle \quad (2.24)$$

where the subscript i is 3 or 5 depending on whether image or output plane statistics is derived. For the output plane, \mathbf{Q} and \mathbf{q} are replaced by \mathbf{R} and \mathbf{r} . The field quantities u_i can be expressed in terms of the Green function as

$$\begin{aligned}
 u_i(\mathbf{q}) &= G_i(\mathbf{q}, \mathbf{p}) * u_1(\mathbf{p}) \\
 &= \int G_i(\mathbf{q}, \mathbf{p}) u_1(\mathbf{p}) d\mathbf{p}
 \end{aligned} \tag{2.25}$$

Using equation (2.25) in (2.24), the second moment of the fields becomes

$$\begin{aligned}
 \Gamma_i(\mathbf{Q}, \mathbf{q}) &= \iint G_i(\mathbf{q}_1, \mathbf{p}_1) G_i^*(\mathbf{q}_2, \mathbf{p}_2) \langle u_1(\mathbf{p}_1) u_1^*(\mathbf{p}_2) \rangle d\mathbf{p}_1 d\mathbf{p}_2 \\
 &= \iint G_i G_i^*(\mathbf{Q}, \mathbf{q}; \mathbf{P}, \mathbf{p}) \Gamma_1(\mathbf{P}, \mathbf{p}) d\mathbf{P} d\mathbf{p}
 \end{aligned} \tag{2.26}$$

Proceeding in a similar manner, the fourth moment of the field is given by

$$\begin{aligned}
 B_i(\mathbf{r}_1, \mathbf{r}_2, \mathbf{r}_3, \mathbf{r}_4) &= \langle u_i(\mathbf{r}_1) u_i^*(\mathbf{r}_2) u_i(\mathbf{r}_3) u_i^*(\mathbf{r}_4) \rangle \\
 &= \iiint\int G_i(\mathbf{r}_1, \mathbf{p}_1) G_i^*(\mathbf{r}_2, \mathbf{p}_2) G_i(\mathbf{r}_3, \mathbf{p}_3) G_i^*(\mathbf{r}_4, \mathbf{p}_4) \times \\
 &\quad \langle u_1(\mathbf{p}_1) u_1^*(\mathbf{p}_2) u_1(\mathbf{p}_3) u_1^*(\mathbf{p}_4) \rangle d\mathbf{p}_1 d\mathbf{p}_2 d\mathbf{p}_3 d\mathbf{p}_4 \\
 &= \iiint\int G_i G_i^* G_i G_i^*(\mathbf{r}_1, \mathbf{p}_1; \mathbf{r}_2, \mathbf{p}_2; \mathbf{r}_3, \mathbf{p}_3; \mathbf{r}_4, \mathbf{p}_4) B_1(\mathbf{p}_1, \mathbf{p}_2, \mathbf{p}_3, \mathbf{p}_4) d\mathbf{p}_1 d\mathbf{p}_2 d\mathbf{p}_3 d\mathbf{p}_4
 \end{aligned} \tag{2.27}$$

The second order image and output Green functions as given by:

$$\begin{aligned}
 G_3 G_3^*(\mathbf{Q}, \mathbf{q}; \mathbf{P}, \mathbf{p}) &= G_3(\mathbf{Q} + \frac{1}{2}\mathbf{q}, \mathbf{P} + \frac{1}{2}\mathbf{p}) G_3^*(\mathbf{Q} - \frac{1}{2}\mathbf{q}, \mathbf{P} - \frac{1}{2}\mathbf{p}) \\
 &= [\frac{1}{\lambda d_i}]^2 \exp[i\frac{k}{d_i} \mathbf{Q} \cdot \mathbf{q} - \frac{2}{a^2} (P^2 + \frac{1}{4} p^2 - ik(\frac{1}{f} - \frac{1}{d_i}) \mathbf{P} \cdot \mathbf{p} - i\frac{k}{d_i} (\mathbf{P} \cdot \mathbf{q} + \mathbf{p} \cdot \mathbf{Q}))]
 \end{aligned} \tag{2.28}$$

$$G_5 G_5^*(\mathbf{R}, \mathbf{r}; \mathbf{P}, \mathbf{p}) = \sum_{i=1}^2 \sum_{j=1}^2 A_i A_j^* \exp \left\{ -(C_i + C_j^*) (R^2 + \frac{1}{4} r^2) + (C_i - C_j^*) \mathbf{R} \cdot \mathbf{r} \right.$$

$$- (B_i + B_j^*)(P^2 + \frac{1}{4}p^2) + (B_i - B_j^*)\mathbf{P} \cdot \mathbf{p} + (D_i + D_j^*)(\mathbf{R} \cdot \mathbf{P} + \frac{1}{4}\mathbf{r} \cdot \mathbf{p}) + (D_i - D_j^*)(\frac{1}{2}(\mathbf{R} \cdot \mathbf{p} + \mathbf{r} \cdot \mathbf{P})) \Big\} \quad (2.29)$$

and the fourth order output Green function by

$$\begin{aligned} G_5 G_5^* G_5 G_5^*(\mathbf{r}_1, \mathbf{r}_2, \mathbf{r}_3, \mathbf{r}_4; \mathbf{p}_1, \mathbf{p}_2, \mathbf{p}_3, \mathbf{p}_4) &= G_5(\mathbf{r}_1, \mathbf{p}_1) G_5^*(\mathbf{r}_2, \mathbf{p}_2) G_5(\mathbf{r}_3, \mathbf{p}_3) G_5^*(\mathbf{r}_4, \mathbf{p}_4) \\ &= \sum_{i=1}^2 \sum_{j=1}^2 \sum_{k=1}^2 \sum_{l=1}^2 A_i A_j^* A_k A_l^* \exp \left\{ - (B_i p_1^2 + B_j^* p_2^2 + B_k p_3^2 + B_l^* p_4^2) \right. \\ &\quad \left. - (C_i r_1^2 + C_j^* r_2^2 + C_k r_3^2 + C_l^* r_4^2) - (D_i \mathbf{p}_1 \cdot \mathbf{r}_1 + D_j^* \mathbf{p}_2 \cdot \mathbf{r}_2 + D_k \mathbf{p}_3 \cdot \mathbf{r}_3 + D_l^* \mathbf{p}_4 \cdot \mathbf{r}_4) \right\} \quad (2.30) \end{aligned}$$

3. Mean Intensity

3.1. Mean Intensity on Image Plane

The intensity statistics on the focal plane of a receiver lens have been discussed by several authors¹⁸⁻²¹ for a laser beam propagating through turbulence and a method for optical measurement of the turbulence parameter has been developed^{22,23} based on theoretical analysis. As we mentioned earlier, the focal plane is conceptually different from the image plane. The image plane statistics of the intensity is essential to the spatial filtering system. It is also important to study the intensity distribution on the image plane in order to optimize the filter parameter. We will first discuss the image plane intensity under two different cases of interest, i.e. line of sight and speckle propagation.

3.1.1. Line of Sight Propagation

We first try to find the field mutual coherence function (MCF) at the input of the system. Since the system is linear, the intensity on the image plane is given by the convolution of the MCF of the input field with the system Green function $G_3 G_3^*$. The geometry of the remote sensing system is shown in Fig. 3.1. A raw laser beam is propagating through turbulent atmosphere and is received by the spatial filtering receiver. By utilizing of the extended Huygens-Fresnel principle²⁴, the input field on the p plane can be

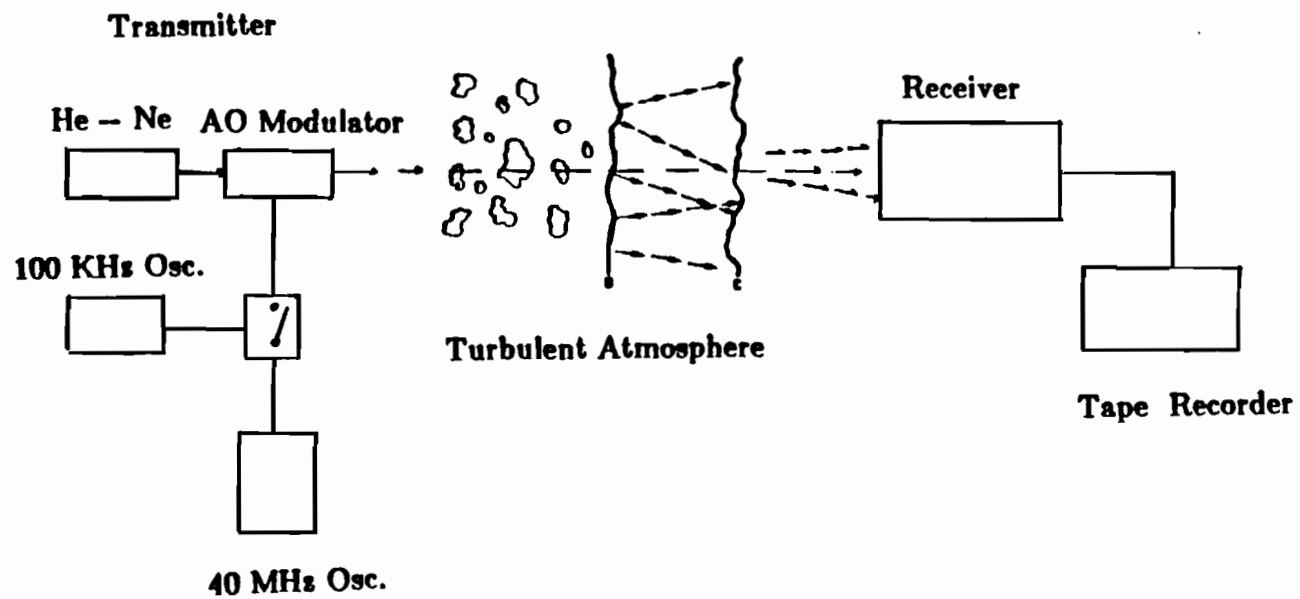


Fig. 3.1 Line of Sight Remote Sensing System

expressed by

$$u_1(\mathbf{p}) = \frac{e^{ikd_o}}{i\lambda d_o} \iint u_o(\mathbf{p}) \exp\left[i\frac{k}{2d_o} |\mathbf{p}-\mathbf{p}'|^2 + \psi(\mathbf{p},\mathbf{p}')\right] d\mathbf{p}' \quad (3.1)$$

where d_o is the object distance measured from the source to the receiver, and $\psi(\mathbf{p},\mathbf{p}')$ is the random phase perturbation by the atmosphere.

The laser source can well be modeled by a spherical wave for long distance propagation and using a relatively small receiver aperture. For simplicity, we assume that

$$u_o(\mathbf{p}) = \delta(\mathbf{p}) \quad (3.2)$$

Thus

$$u_1(\mathbf{p}) = \frac{e^{ikd_o}}{i\lambda d_o} \exp\left[i\frac{k}{2d_o} p^2 + \psi(\mathbf{p},0)\right] \quad (3.3)$$

So the MCF of the field at the input plane is given by

$$\begin{aligned} \Gamma_1(\mathbf{P}, \mathbf{p}) &= \langle u_1(\mathbf{P} + \frac{1}{2}\mathbf{p}) u_1^*(\mathbf{P} - \frac{1}{2}\mathbf{p}) \rangle \\ &= \frac{1}{\lambda^2 d_o^2} \exp\left[i\frac{k}{d_o} \mathbf{P} \cdot \mathbf{p} - \left(\frac{p}{\rho_o}\right)^{5/3}\right] \end{aligned} \quad (3.4)$$

where $\rho_o = (0.546 C_n^2 k^2 L)^{5/3}$ is the coherence length of a spherical wave propagating in the random medium.

The mean intensity on the image plane can be obtained from the following double convolution:

$$\Gamma_3(\mathbf{Q}, \mathbf{q}) = \iint G_3 G_3^*(\mathbf{Q}, \mathbf{q}; \mathbf{P}, \mathbf{p}) \Gamma_1(\mathbf{P}, \mathbf{p}) d\mathbf{P} d\mathbf{p} \quad (3.5)$$

Here, we use subscript 1 and 3 for the input and image plane respectively and the four dimensional integration is with respect to $d\mathbf{P}d\mathbf{p}=PdPd\theta_p p dp d\theta_p$. Using (2.28) and (3.4) in (3.5), we have

$$\begin{aligned} \Gamma_3(\mathbf{Q}, \mathbf{q}) = & \iint \left[\frac{1}{\lambda d_i} \right]^2 \exp \left[i \frac{k}{d_i} \mathbf{Q} \cdot \mathbf{q} - \frac{2}{a^2} (P^2 + \frac{1}{4} p^2) - ik \left(\frac{1}{f} - \frac{1}{d_i} \right) \mathbf{P} \cdot \mathbf{p} - i \frac{k}{d_i} (\mathbf{P} \cdot \mathbf{q} + \mathbf{p} \cdot \mathbf{Q}) \right] \\ & \times \frac{1}{\lambda^2 d_o^2} \exp \left[i \frac{k}{d_o} \mathbf{P} \cdot \mathbf{p} - \left(\frac{p}{\rho_0} \right)^{5/3} \right] d\mathbf{P} d\mathbf{p} \end{aligned}$$

By using the imaging condition (2.1), this can be simplified to

$$\begin{aligned} \Gamma_3(\mathbf{Q}, \mathbf{q}) = & \frac{\pi}{2} \left[\frac{a}{\lambda d_o d_i} \right]^2 \times \\ & \exp \left[i \frac{k}{d_i} \mathbf{Q} \cdot \mathbf{q} - \frac{1}{2} \left(\frac{\pi a}{\lambda d_i} \right)^2 q^2 \right] \int \exp \left[- \frac{1}{2a^2} p^2 + \left(\frac{1}{\rho_0} \right)^{5/3} - i \frac{k}{d_i} \mathbf{p} \cdot \mathbf{Q} \right] dp \end{aligned} \quad (3.6)$$

The intensity distribution on the image plane is a function of radial coordinate Q and turbulence index C_n^2 . Let $\mathbf{q} = 0$ in (3.6). The result is

$$I(Q) = \Gamma_3(Q, 0) = \left[\frac{\pi a}{\lambda d_o d_i} \right]^2 \int \exp \left[- \frac{1}{2a^2} p^2 - \left(\frac{p}{\rho_0} \right)^{5/3} \right] J_0 \left(\frac{k}{d_i} \mathbf{p} \cdot \mathbf{Q} \right) dp \quad (3.7)$$

where J_0 is the Bessel function of zero order.

The numerical integration result of (3.7) with different aperture sizes and filter parameters is shown in Fig. 3.2.

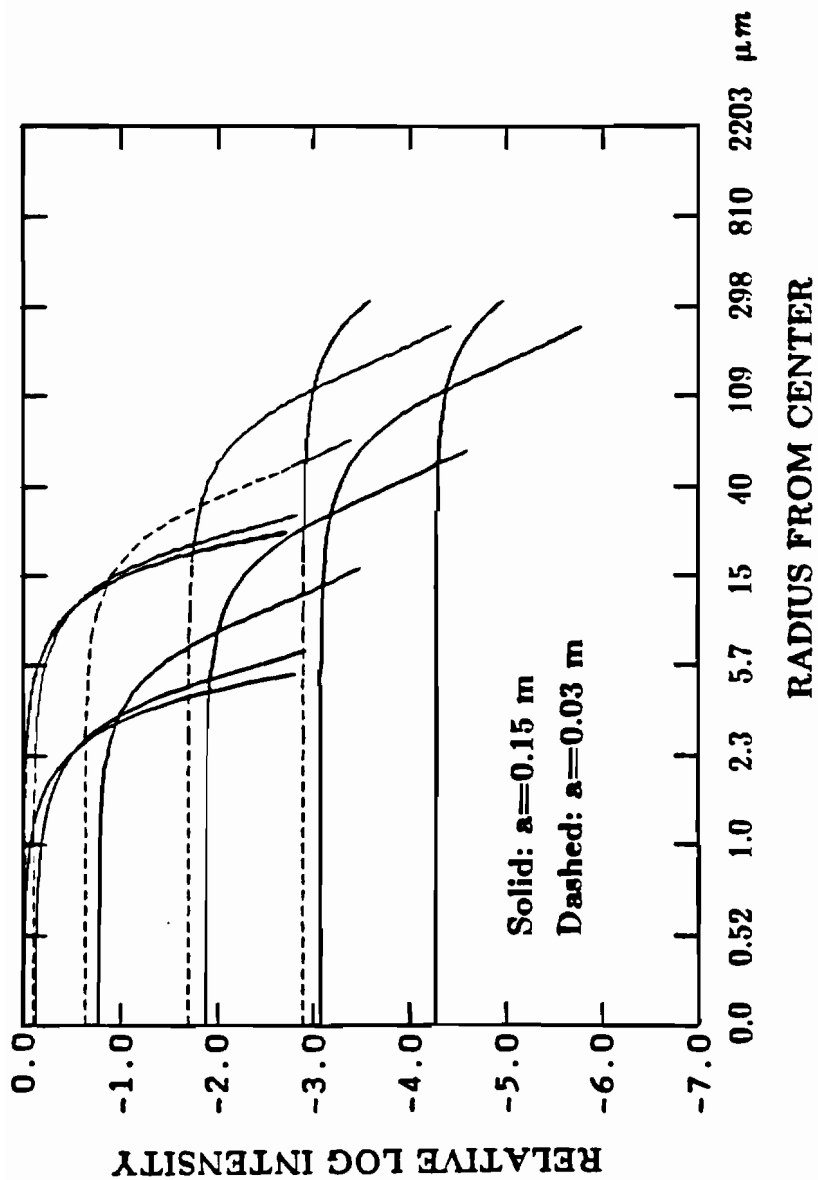


Fig. 3.2 Line of sight propagation. Intensity distribution on image plane as a function of receiver aperture and turbulence level. C_n^2 from $1 \times 10^{-17} m^{-2/3}$ (top) to $1 \times 10^{-12} m^{-2/3}$ (bottom).

3.1.2. Speckle Propagation

In the speckle propagation case, the transmitter and the receiver are at the same end of the propagation path and a diffuse target is placed at the other end. The laser beam is focused on the target and generates speckles that propagate back to the receiver.

The laser source has a finite aperture α_0 . As it is focused on the target, we have $f = d_o$, so

$$u_0(r) = U_0 \exp\left(-\frac{r^2}{2\alpha_0^2} - i\frac{kr^2}{2d_o}\right) \quad (3.8)$$

The intensity distribution on the target is given by

$$I(\rho) = \left(\frac{k}{d_o}\right)^2 U_0^2 \frac{\alpha_0^2}{2} \int_0^\infty r dr J_0\left(\frac{k}{d_o} \rho r\right) \exp\left[-\frac{r^2}{4\alpha_0^2} - \left(\frac{r}{\rho_0}\right)^{5/3}\right] \quad (3.9)$$

The target is assumed to be a Lambertian reflector and provides a δ spatial correlation. It can be shown that the MCF of the field at the input of the receiver is ²⁵

$$\Gamma(\mathbf{P}, \mathbf{P}) = \frac{U_0^2 \alpha_0^2}{d_o^2} \exp\left[-\frac{P^2}{4\alpha_0^2} - 2\left(\frac{P}{\rho_0}\right)^{5/3} + i\frac{k}{d_o} \mathbf{P} \cdot \mathbf{P}\right] \quad (3.10)$$

Comparing (3.10) with (3.4), it can be seen that the effect of the turbulence on the MCF has 'doubled'. Putting (2.13) and (3.10) into (3.5), going through the procedure used for the case of line of sight propagation, one can find the MCF distribution as

$$\Gamma_3(\mathbf{Q}, \mathbf{q}) = \frac{\pi}{2} \left[\frac{u_0 \alpha_0 a}{\lambda^2 d_o d_i} \right]^2 \exp\left[i\frac{k}{d_i} \mathbf{Q} \cdot \mathbf{q} - \frac{1}{2} \left(\frac{ka}{2d_i}\right)^2 q^2\right]$$

$$\times \int \exp\left[-\left(\frac{1}{2a^2} + \frac{1}{4\alpha_0^2}\right)p^2 - \left(\frac{p}{\rho_0}\right)^{5/3} - i\frac{k}{d_i}\mathbf{p}\cdot\mathbf{Q}\right] d\mathbf{p} \quad (3.11)$$

The intensity distribution on the image plane is a function of radial coordinate Q and turbulence index C_n^2 . Letting $q = 0$ in (3.11), the intensity is obtained,

$$I(Q) = \left[\frac{\pi a}{\lambda d_o d_i} \right]^2 \int \exp\left[-\left(\frac{1}{2a^2} + \frac{1}{4\alpha_0^2}\right)p^2 - \left(\frac{p}{\rho_0}\right)^{5/3}\right] J_0\left(\frac{k}{d_i}\mathbf{p}\cdot\mathbf{Q}\right) d\mathbf{p} \quad (3.12)$$

It is worth noting that in the speckle case, the transmitter aperture effect on the image plane spot size is combined with the receiver aperture under a geometrical rule. We can define the effective aperture a_{eff} as

$$\frac{1}{2a_{eff}^2} = \frac{1}{2a^2} + \frac{1}{4\alpha_0^2}$$

Fig. (3.3) shows the dependence of the intensity distribution versus the turbulence as a function of radial coordinate Q for the geometry of the remote sensing used to gather experimental data.

3.2. Mean Intensity on Output Plane

3.2.1. Line of Sight Propagation

The field correlation on the output plane of the spatial filtering system is given by the convolution of (3.4) with (2.28) :

$$\Gamma_{\mathfrak{s}}(\mathbf{R}, \mathbf{r}) = \iint G_{\mathfrak{s}} G_{\mathfrak{s}}^*(\mathbf{R}, \mathbf{r}; \mathbf{P}, \mathbf{p}) \Gamma_1(\mathbf{P}, \mathbf{p}) d\mathbf{P} d\mathbf{p} \quad (3.13)$$

Using (2.15) and (3.4) in (3.13), we get the output MCF as

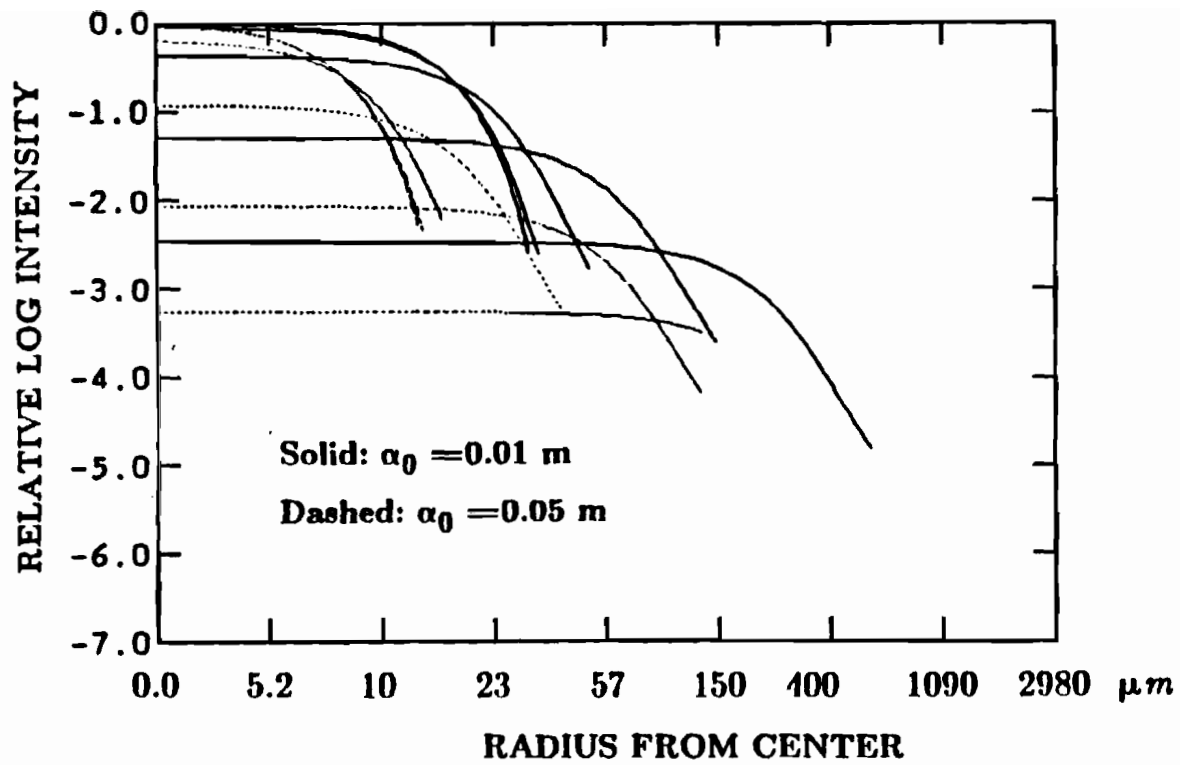


Fig. 3.3 Speckle propagation. Intensity distribution on image plane as a function of transmitter aperture and turbulence level. C_n^2 from $1 \times 10^{-16} \text{ m}^{-2/3}$ (top) to $1 \times 10^{-12} \text{ m}^{-2/3}$ (bottom), path length = 290m.

$$\begin{aligned} \Gamma_5(\mathbf{R}, \mathbf{r}) &= \frac{1}{\lambda^2 d_o^2} \sum_{i=1}^2 \sum_{j=1}^2 A_i A_j^* \exp \left[-(C_i + C_j^*)(R^2 + \frac{1}{4} r^2) - (C_i - C_j^*) \mathbf{R} \cdot \mathbf{r} \right] \\ &\times \iint \exp \left\{ -[(B_i + B_j^*)(P^2 + \frac{1}{4} p^2) + (B_i - B_j^*) \mathbf{P} \cdot \mathbf{p} + (D_i + D_j^*)(\mathbf{R} \cdot \mathbf{P} + \frac{1}{4} \mathbf{r} \cdot \mathbf{p}) \right. \\ &\left. + (D_i - D_j^*)(\frac{1}{2}(\mathbf{R} \cdot \mathbf{p} + \mathbf{r} \cdot \mathbf{P})) - (\frac{\mathbf{p}}{\rho_0})^{5/3} + \frac{k}{d_o} \mathbf{P} \cdot \mathbf{p}] \right\} d\mathbf{P} d\mathbf{p} \end{aligned} \quad (3.14)$$

Using

$$\begin{aligned} E_1 &= \frac{k^2}{4d_i^2(\frac{1}{a^2} - i\frac{k}{2d_i})} \\ E_2 &= \frac{k^2}{4d_i^2(\frac{1}{a^2} + \frac{1}{q_0^2} - i\frac{k}{2d_i})} \end{aligned}$$

utilizing the imaging condition (2.1), working out the integration

$$\begin{aligned} I &= \iint \exp \left\{ -(B_i + B_j^*)P^2 - [(E_i - E_j^*)\mathbf{p} + (D_i + D_j^*)\mathbf{R}] \cdot \mathbf{P} \right\} d\mathbf{P} \\ &= \frac{\pi}{(B_i + B_j^*)} \exp \frac{[(E_i - E_j^*)\mathbf{p} + (D_i + D_j^*)\mathbf{R}]^2}{4(B_i + B_j^*)} \end{aligned} \quad (3.15)$$

and putting it all back into (3.13) and rearranging terms, the intensity on the output can be expressed as

$$\begin{aligned} \Gamma_5(R, 0) &= \sum_{i=1}^2 \sum_{j=1}^2 \frac{\pi A_i A_j^*}{\lambda^2 d_o^2 (B_i + B_j^*)} \exp -[(C_i + C_j^*) - \frac{(D_i + D_j^*)^2}{4(B_i + B_j^*)}] R^2 \\ &\times \int e^{-\frac{\mathbf{p}}{\rho_0}^{5/3} - \left| \frac{(B_i + B_j^*)}{4} - \frac{(E_i - E_j^*)^2}{4(B_i + B_j^*)} \right| p^2 - \left[\frac{1}{2}(D_i - D_j^*) - \frac{(E_i - E_j^*)(D_i + D_j^*)}{2(B_i + B_j^*)} \right] \mathbf{p} \cdot \mathbf{R}} d\mathbf{p} \end{aligned} \quad (3.16)$$

The intensity at the center of the output plane is related to the turbulence level by

$$I(0,0) = \Gamma_5(0,0) = \sum_{i=1}^2 \sum_{j=1}^2 \frac{\pi A_i A_j^*}{\lambda^2 d_o^2 (B_i + B_j^*)} \int e^{-\left(\frac{p}{\rho_o}\right)^2 - \left|\frac{(B_i + B_j^*)}{4} - \frac{(E_i - E_j^*)}{4(B_i + B_j^*)}\right|^2} p^2 dp \quad (3.17)$$

Equation (3.17) is the result for remote sensing of turbulence in the case of line of sight propagation.

Fig. 3.4 and 3.5 show the behavior of the axis intensity as a function of system parameters and strength of turbulence.

3.2.2. Speckle Propagation

Making use of (3.10) and (2.15) in (3.13), and proceeding as was done for the line of sight case, the intensity distribution on the output plane is

$$\Gamma_5(R,0) = \sum_{i=1}^2 \sum_{j=1}^2 \frac{\pi A_i A_j^*}{\lambda^2 d_o^2 (B_i + B_j^*)} \exp \left\{ - \left[(C_i + C_j^*) - \frac{(D_i + D_j^*)^2}{4(B_i + B_j^*)} \right] R^2 \right\} \times \int e^{-\left(\frac{p}{\rho_o}\right)^2 - \left|\frac{(B_i + B_j^*)}{4} - \frac{(E_i - E_j^*)}{4(B_i + B_j^*)} - \frac{1}{4\alpha_o}\right|^2 p^2 - \left|\frac{1}{2}(D_i - D_j^*) - \frac{(E_i - E_j^*)(D_i + D_j^*)}{2(B_i + B_j^*)}\right| p \cdot R} p \cdot R dp \quad (3.18)$$

The intensity at the center of output plane is obtained by putting $R = 0$ in (3.18). Thus we have

$$I(0,0) = \sum_{i=1}^2 \sum_{j=1}^2 \frac{\pi^2 U_0^2 \alpha_0^2 A_i A_j^*}{\lambda^2 d_o^2 (B_i + B_j^*)} \times$$

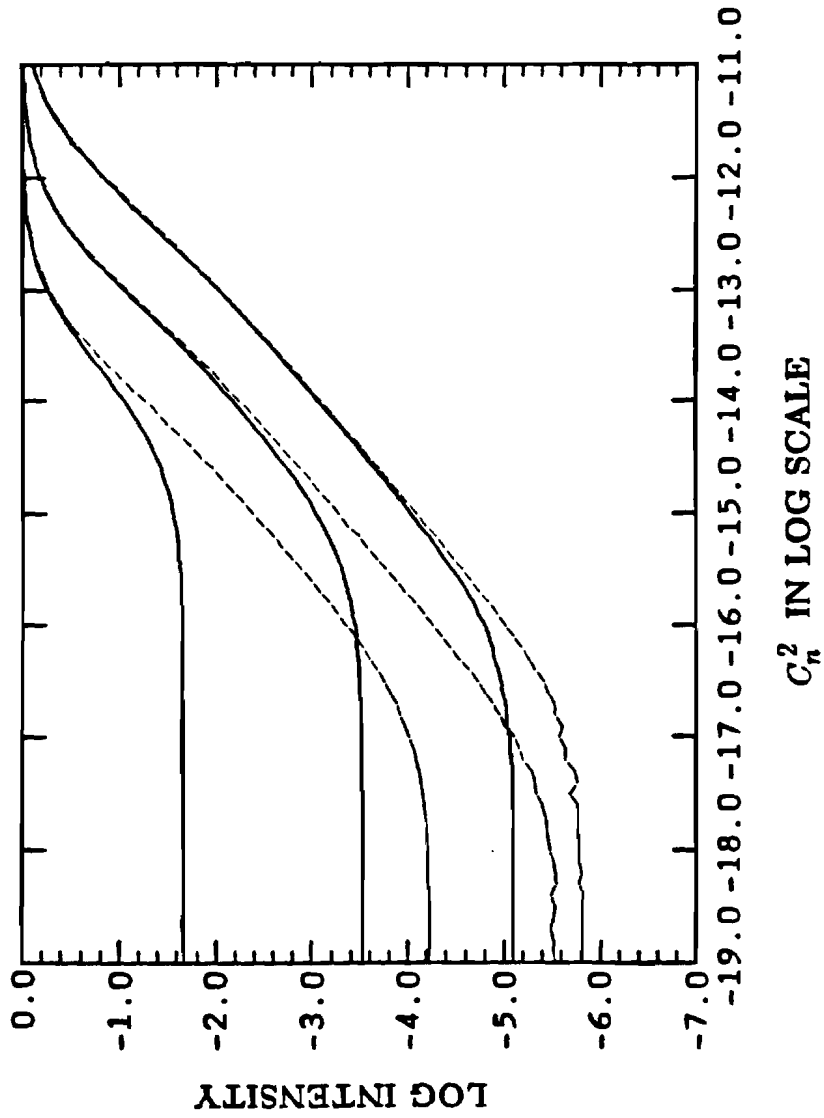


Fig. 3.4 Mean intensity of line of sight propagation. Effect of receiver aperture. The filter sizes Q_0 are 33 μm (top), 106 μm and 330 μm (bottom). Receiver aperture is 0.03 m (solid) and 0.15 m (dashed), path length = 500m.

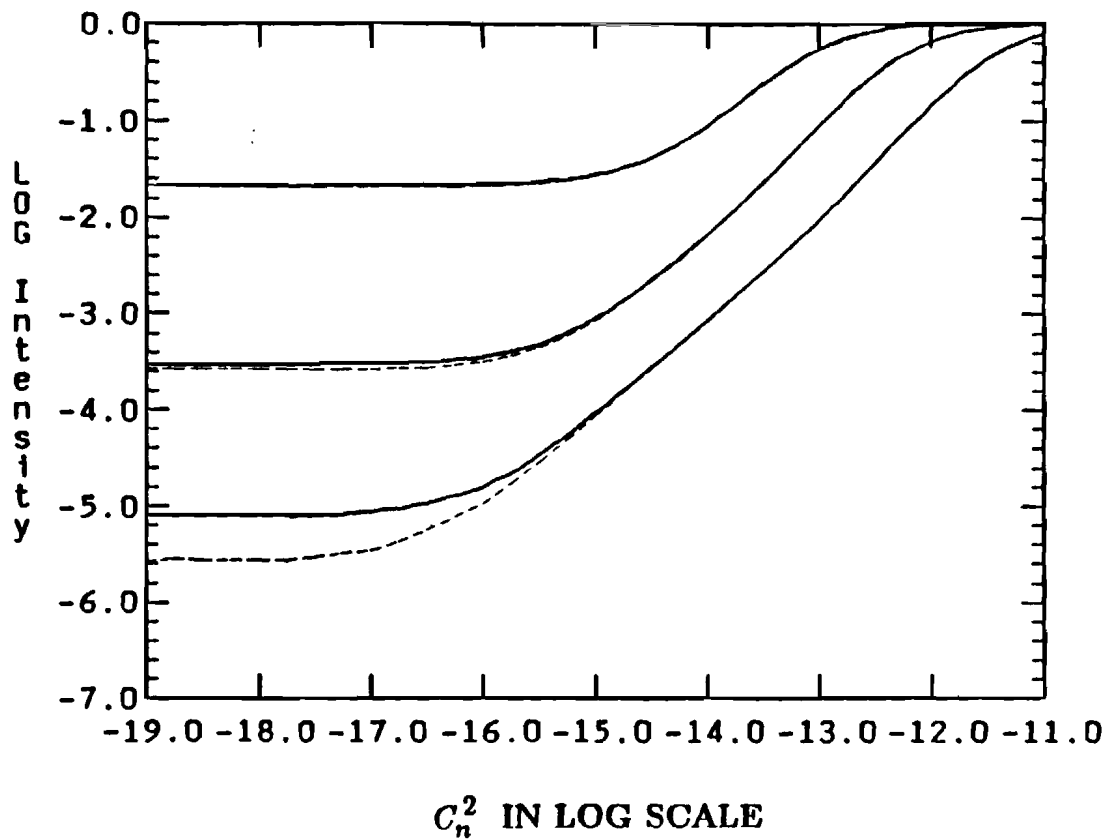


Fig. 3.5 Mean intensity of line of sight propagation. Effect of filter center transmission. Receiver aperture $a=0.03$ m. The filter sizes Q_0 are 33 μm (top), 106 μm and 330 μm (bottom). Center transmission is 1×10^{-3} (solid) and 0 (dashed), path length = 500m.

$$\int_0^{\infty} \exp \left\{ - \left[\frac{(B_i + B_j)^2 - (E_i - E_j)^2}{4(B_i + B_j)} + \frac{1}{4\alpha_0^2} \right] p^2 - 2 \left(\frac{p}{\rho_0} \right)^{5/3} \right\} p dp \quad (3.19)$$

The center intensity output of the spatial filtering system in the speckle case is shown in Fig. 3.6 and 3.7.

3.2.3. Phase Contrast Filtering

The phase contrast filtering was first suggested by Zernike⁷ for observing a phase object which is not observable using conventional microscopic techniques. Since then more complicated methods of what can collectively be called interference microscopy have been developed. The basic idea is to introduce a phase shift of $\pi/2$ to the low frequency components in the image plane of the object. It can be seen by simple calculation¹⁶ that under coherent illumination, a small phase shifts ($\theta \ll \pi$) are converted into first order intensity differences after phase contrast filtering. To consider the effect of phase shift filtering on light propagated through the atmosphere, two factors have to be taken into account. First, the light after traveling through the turbulent atmosphere loses some of its spatial coherence. This is especially true for the speckle generated by a laser beam on a diffuse target. Second, the phase shift introduced by the turbulent atmosphere is a random quantity, which under most propagation conditions exceeds several π . Hence the small phase modulation assumption is no longer valid. However, it is still

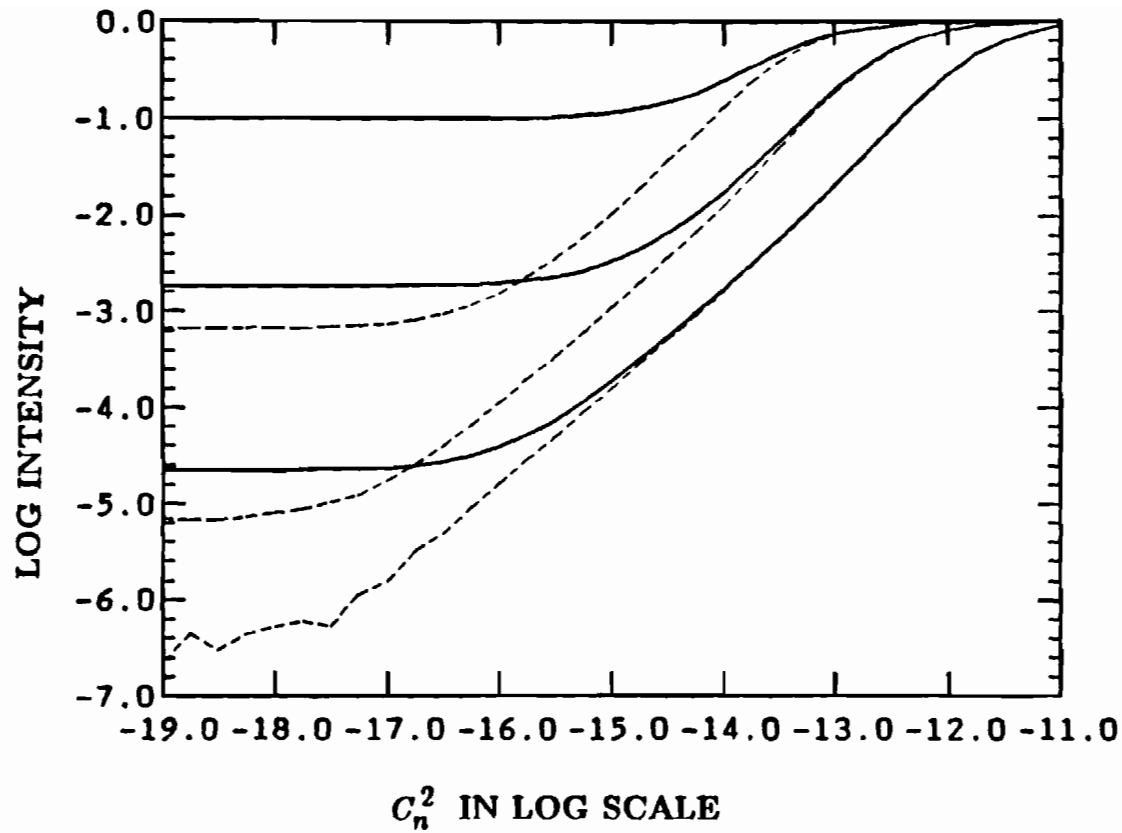


Fig. 3.6 Mean intensity of speckle propagation. Effect of transmitter aperture. The receiver aperture $a=0.15$ m. The filter sizes Q_0 are $33 \mu\text{m}$, $106 \mu\text{m}$ and $330 \mu\text{m}$. The transmission aperture is $\alpha_0 = 1 \times 10^{-2}$ m (solid) and 5×10^{-2} (dashed).

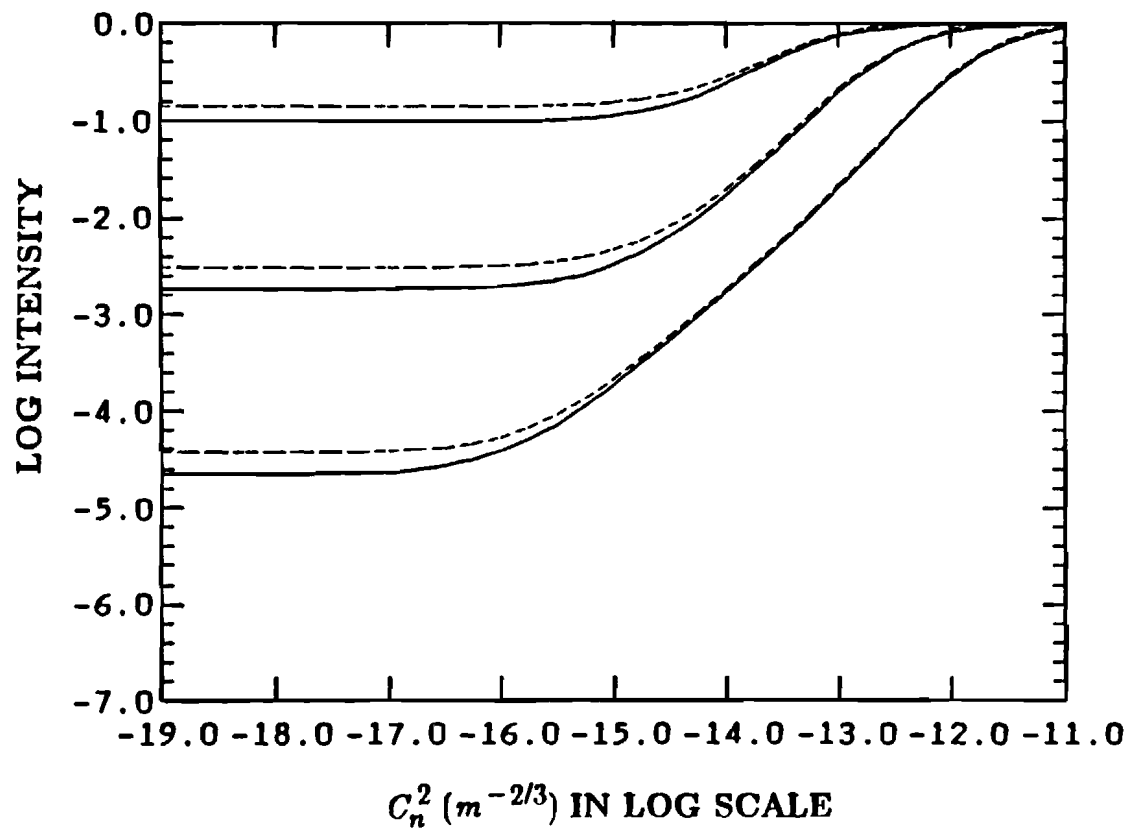


Fig. 3.7 Mean intensity of speckle propagation. Effect of receiver aperture. The transmitter aperture $a_0 = 0.01m$. The filter sizes Q_0 are $33 \mu m$, $106 \mu m$ and $330 \mu m$. The receiver aperture is $0.15 m$ (solid) and $0.03 m$ (dashed).

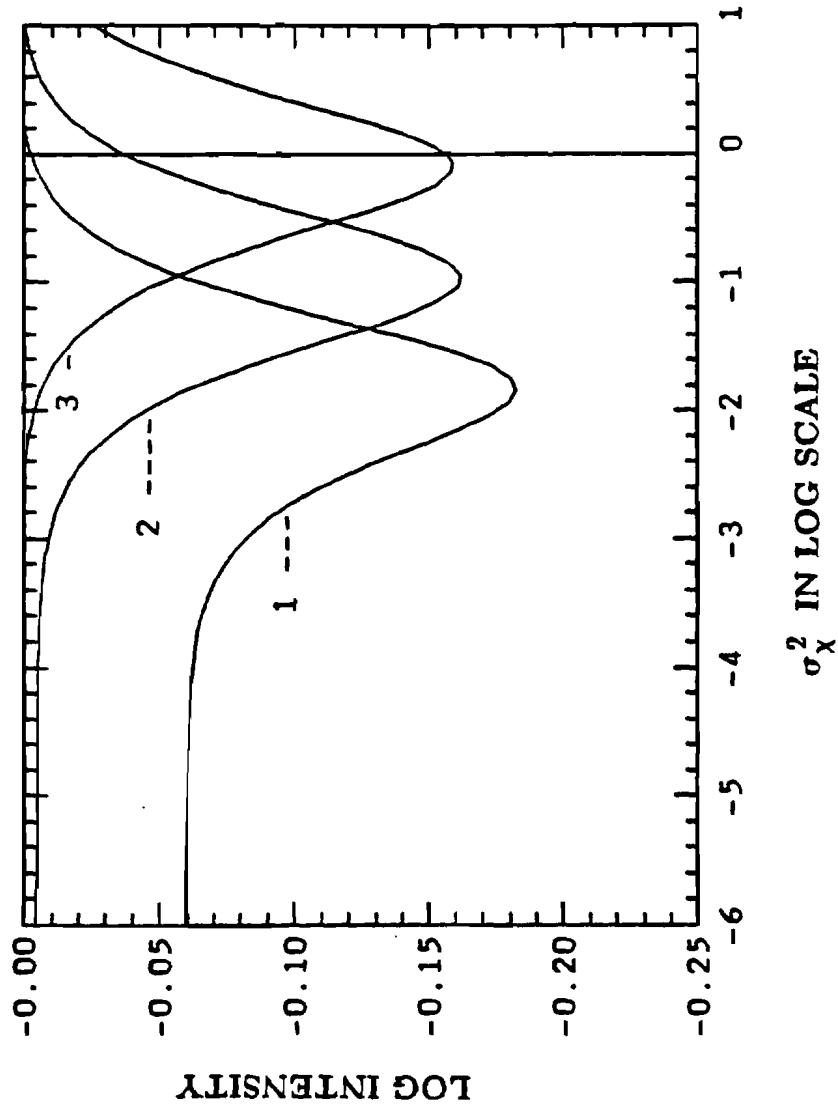


Fig. 3.8 Mean intensity of line of sight propagation. Phase contrast filter with phase shift $\pi/2$ at the center disk. Receiver aperture $a = 0.15$ m, propagation distance 1 km. Filter sizes are: 1 --- 0.01 mm, 2 - - - 0.03 mm, 3 --- 0.1 mm.

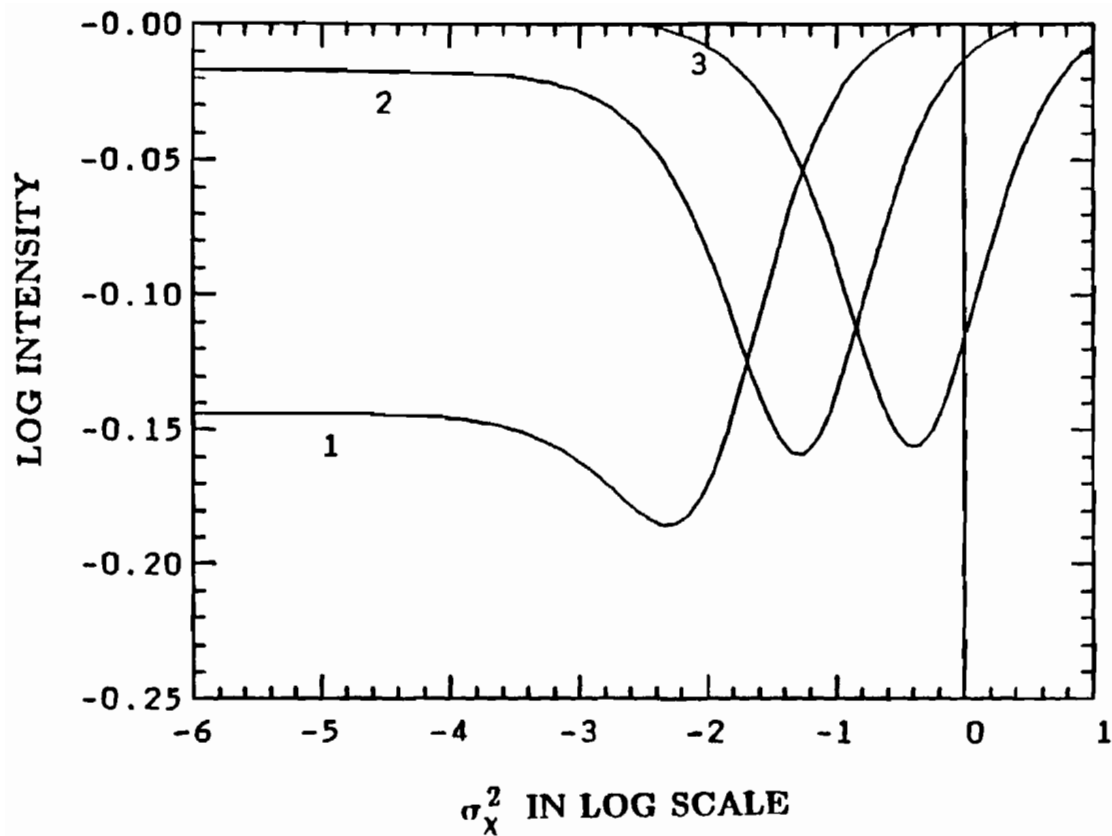


Fig. 3.9 Mean intensity of speckle propagation. Phase contrast filter with phase shift $\pi/2$ at the center disk. Receiver aperture $a = 0.15$ m, transmitter aperture $\alpha_0 = 0.05$ m, propagation distance 1 km. Filter sizes are : 1 --- 0.01 mm, 2 --- 0.03 mm, 3 -- 0.1 mm.

of interest for both theoretical and applied physicists to study the effect of phase contrast filtering on the turbulence modulated light.

Our model was designed to cover this type of spatial filter. By adjusting the parameter configurations in (3.17) and (3.19), the theoretical curves of the mean intensity under either the line of sight or speckle propagation case can be generated. In Fig. 3.8 and Fig. 3.9, the effects are shown for different system parameters.

The curves in these figures show a feature of coherent cancellation at some specific turbulence level. At low turbulence levels, most of the light energy goes through the central spot and is shifted collectively by $\pi/2$. At the high turbulence end, most of the light does not go through the center spot and the phase shift of the center part can be ignored. Thus, the output mean intensity is relatively independent of the turbulence changes. For both of these conditions in transition, some light goes through both regions and the output intensity is reduced due to destructive interference from the phase shift. However, because the light has traveled through the turbulent atmosphere and lost some of its coherence, the intensity cancellation is never complete and the response is not very sensitive to the turbulence.

3.3. Quadratic Approximation

We develop this section for two reasons. First, this section provides a direct comparison with the true numerical result for the mean intensity to

determine the error introduced by using the quadratic approximation to the wave structure function. Second, the theory of intensity variance presented in later chapters can only be solved in analytical form by using the quadratic approximation.

We define the quadratic form of wave structure function as

$$\frac{1}{2}D_{\psi}(P, Q) = \eta \frac{1}{\rho_0^2} \int_0^1 |\xi P + (1-\xi)Q|^2 d\xi = \frac{\eta}{3\rho_0^2} (P^2 + P \cdot Q + Q^2) \quad (3.20)$$

where $\rho_0 = (0.546 C_n^2 k^2 L)^{-3/6}$. The two cases of line of sight and speckle propagation will be discussed separately.

3.3.1. Line of sight propagation

By utilizing of (3.20), (3.17) is reduced to the following:

$$I(0,0) = \left[\frac{\pi}{\lambda d_0} \right]^2 \sum_1^2 \sum_1^2 \frac{A_i A_j^*}{(B_i + B_j^*) \left[\frac{E_i E_j^*}{(E_i + E_j^*)} + \frac{\eta}{3\rho_0^2} \right]} \quad (3.21)$$

In Fig. (3.10), the results of the accurate numerical integration of (3.17) are plotted along with the its quadratic form (3.20) for different values of η . The parameters used are propagation distance $L = 500m$, receiver aperture $a = 0.15m$, filter size $Q_0 = 33 \times 10^{-6}m$. The case $\eta = 3$ corresponds to the conventional approximation form. It is worthwhile to note that the slope changes substantially under the quadratic approximation. By adjusting the factor η , the slope remains the same but the average mean square error is

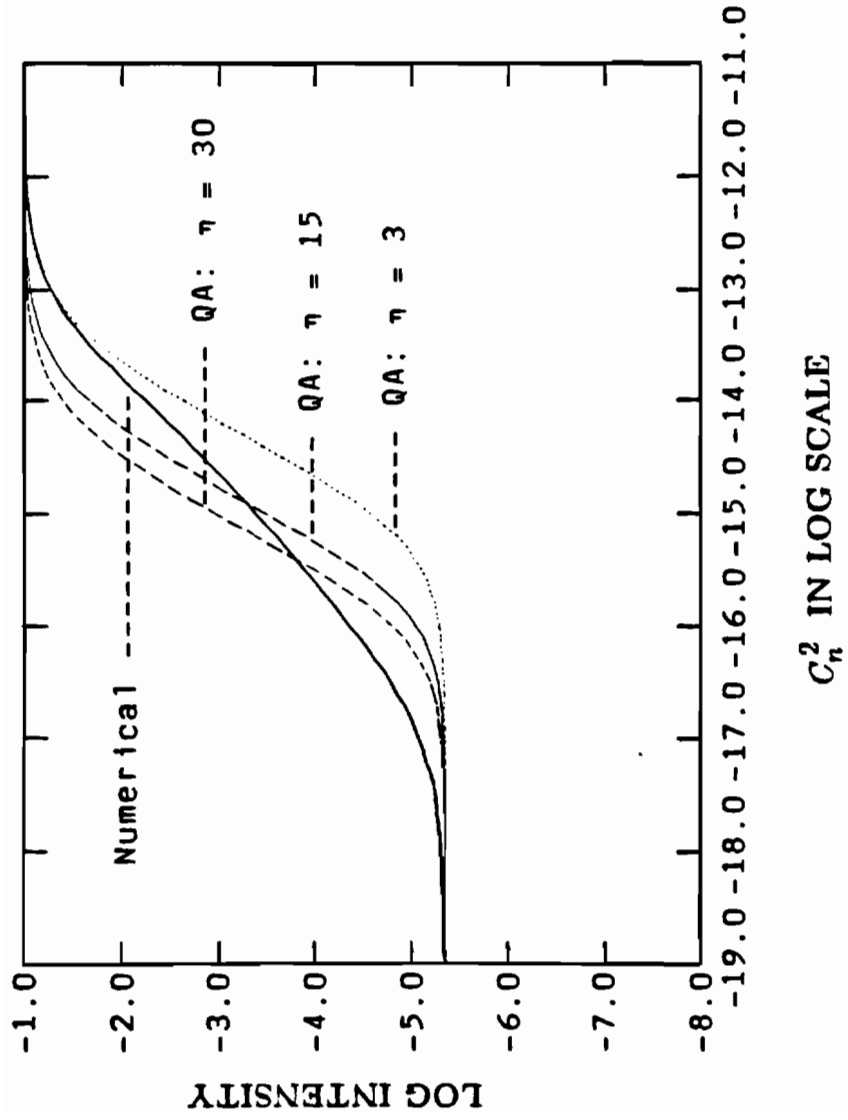


Fig. 3.10 Mean intensity of line of sight propagation. True numerical integration (solid) is compared with quadratic approximation with different factor η .

reduced. Under this criterion, the factor of $\eta = 15$ is better than the usually accepted value of $\eta = 3$.

3.3.2. Speckle propagation

The mean intensity output under quadratic approximation can be obtained by using (3.20) in (3.19). Thus we have

$$I(0,0) = \left[\frac{\pi U_0 \alpha_0}{\lambda d_0} \right]^2 \sum_1^2 \sum_1^2 \frac{A_i A_j^*}{(B_i + B_j^*) \left[\frac{E_i E_j^*}{(E_i + E_j^*)} + \frac{1}{4\alpha_0^2} + \frac{2\eta}{3\rho_0^2} \right]} \quad (3.22)$$

Both of the above results of mean intensity under quadratic approximation will be used in the analysis of the intensity variance. On Fig. 3.11, a comparison of quadratic approximation (3.22) with true numerical integration of (3.19) for speckle propagation is given. The parameters used are $L = 500 \text{ m}$, transmitter aperture $\alpha_0 = 0.01 \text{ m}$, filter size $Q_0 = 106 \times 10^{-6}$. Again, we see a better fit can be obtained by adjusting the parameter η .

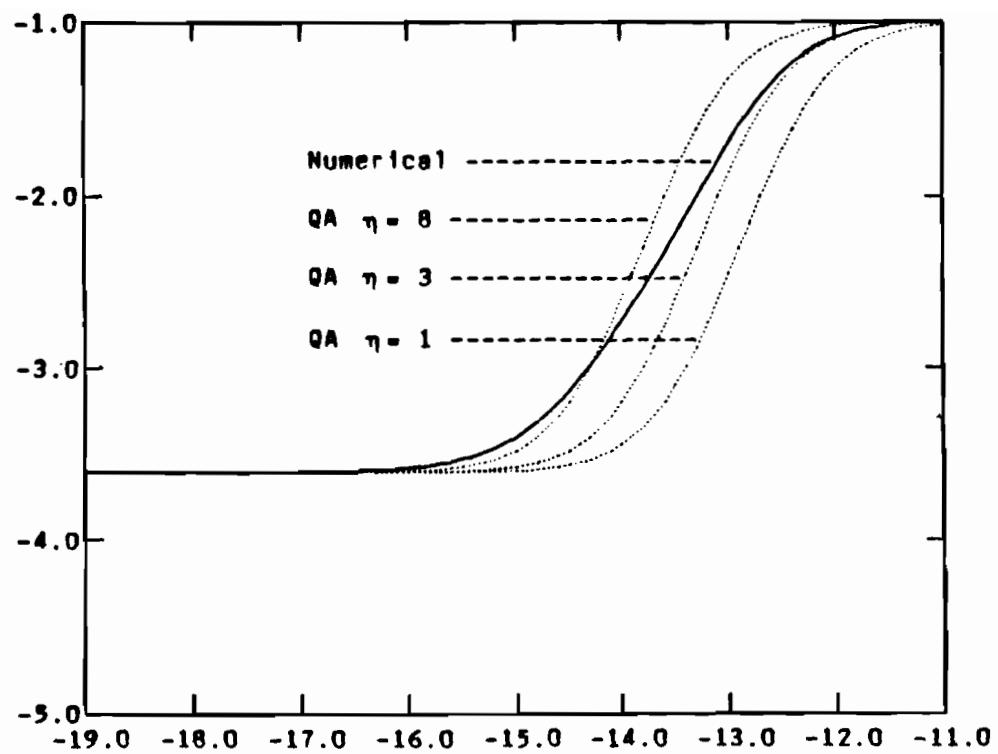


Fig. 3.11 Mean intensity of speckle propagation. True numerical integration (solid) is compared with quadratic approximation with different factor η .

4. Intensity Variance (Line of Sight Case)

4.1. Introduction

The theory of intensity variance and other second order intensity statistics of laser propagation through the turbulent atmosphere have been well developed in the two previous decades and several review papers are available^{26,27} for good reference. The significance of this study of the intensity variance of optically spatial filtered laser radiation is that by introducing a filter, the spectrum of the radiation is intentionally altered and hence it provides a different approach to access the subject. In the following, we will first develop a general formulation of the intensity correlation of the output of the spatial filtering system which applies to various propagation cases and then use this formulation to analyze two important cases of interest: line of sight propagation of coherent laser source and speckle propagation which is completely incoherent. This formulation can easily be extended to the case of partially coherent light propagation through turbulence.

4.2. General expression for intensity correlation

Using our Green-function notation, the input and output fields of the spatial filtering system are related by the following:

$$u_5(\mathbf{r}, t) = \int G_5(\mathbf{r}, \mathbf{p}) u_1(\mathbf{p}, t) d\mathbf{p} \quad (4.1)$$

where $G(\mathbf{r}, \mathbf{p})$ is the Green function of the system and is given explicitly by

$$G(\mathbf{r}, \mathbf{p}) = \sum_{i=1}^2 A_i \exp[-(B_i p^2 + C_i r^2 + D_i \mathbf{r} \cdot \mathbf{p})] \quad (4.2)$$

All the desired second order statistics of the intensity can be derived from the time-delayed intensity autocorrelation function defined as

$$B_5(\mathbf{r}_1, \mathbf{r}_2, \mathbf{r}_3, \mathbf{r}_4; \tau) = \langle u_5(\mathbf{r}_1, 0) u_5^*(\mathbf{r}_1, 0) u_5(\mathbf{r}_2, \tau) u_5^*(\mathbf{r}_2, \tau) \rangle \quad (4.3)$$

To simplify the analysis, let us calculate the correlation at points symmetrical to the origin, therefore:

$$\begin{aligned} \mathbf{r}_1 &= \frac{1}{2} \mathbf{r} \\ \mathbf{r}_2 &= -\frac{1}{2} \mathbf{r} \end{aligned}$$

The intensity correlation at the center of output plane is given by:

$$\begin{aligned} B_I(\mathbf{r}, \tau) &= \iiint \int d\mathbf{p}_1 d\mathbf{p}_2 d\mathbf{p}_3 d\mathbf{p}_4 GGGG(\mathbf{r}/2, -\mathbf{r}/2; \mathbf{p}_1, \mathbf{p}_2, \mathbf{p}_3, \mathbf{p}_4) \\ &\times \langle u_1(\mathbf{p}_1, 0) u_1^*(\mathbf{p}_1, 0) u_1(\mathbf{p}_2, \tau) u_1^*(\mathbf{p}_2, \tau) \rangle \end{aligned} \quad (4.4)$$

where $GGGG(\mathbf{r}/2, -\mathbf{r}/2; \mathbf{p}_1, \mathbf{p}_2, \mathbf{p}_3, \mathbf{p}_4)$ is given by:

$$GGGG(\mathbf{r}/2, -\mathbf{r}/2; \mathbf{p}_1, \mathbf{p}_2, \mathbf{p}_3, \mathbf{p}_4) = \sum_{i=1}^2 \sum_{j=1}^2 \sum_{k=1}^2 \sum_{l=1}^2 A_i A_j^* A_k A_l^* \exp[-(C_i + C_j^* + C_k + C_l^*)] r^2/4$$

$$\times \exp[-(B_i p_1^2 + B_j^* p_2^2 + B_k p_3^2 + B_l^* p_4^2)] - \frac{1}{2} r \cdot (D_i p_1 - D_j^* p_2 + D_k p_3 - D_l^* p_4) \quad (4.5)$$

In the case of line-of-sight propagation, the field at the receiver input is given by a distorted spherical wave:

$$u_1(\mathbf{p}, t) = \frac{e^{i d_0}}{i \lambda d_0} \exp\left(\frac{i k}{2 d_0} p^2 + \psi(\mathbf{p}, 0; t)\right)$$

The fourth moment of the input field is

$$\langle u_1(\mathbf{p}, 0) u_1^*(\mathbf{p}_2, 0) u_1(\mathbf{p}_3, \tau) u_1^*(\mathbf{p}_4, \tau) \rangle = \left[\frac{1}{\lambda d_0} \right]^4 \exp\left[\frac{i k}{2 d_0} (p_1^2 - p_2^2 + p_3^2 - p_4^2)\right] \times H \quad (4.6)$$

where H is given by

$$H = \langle \exp[\psi(\mathbf{p}_1, 0; 0) + \psi^*(\mathbf{p}_2, 0; 0) + \psi(\mathbf{p}_3, 0; \tau) + \psi^*(\mathbf{p}_4, 0; \tau)] \rangle$$

As our major concern is to study the spatial filtering effect, we will assume in the following that the function H is dominated by the phase fluctuations. In other words, the effects of log-amplitude correlation as well as the cross-correlation between phase and amplitude are ignored. Hence, the results will apply to the case of propagation in low to moderate integrated turbulence^{25, 28, 29}. Consequently,

$$H = \exp\left[-\frac{1}{2}(D_{12} - D_{13} + D_{14} + D_{23} - D_{24} + D_{34})\right]$$

where

$$\begin{aligned} D_{ij} &= \langle \psi(\mathbf{p}_i, \mathbf{p}_i; t_i) - \psi(\mathbf{p}_j, \mathbf{p}_j; t_j) \rangle \Big|_{\mathbf{p}_i = \mathbf{p}_j = 0} \\ &= \frac{2.91}{2} L k^2 \int_0^1 C_n^2(\xi) |\xi(\mathbf{p}_j - \mathbf{p}_i) - V(t_j - t_i)|^{5/3} d\xi \end{aligned}$$

where \mathbf{V} is the cross wind and $t_j - t_i$ is the time delay τ .

The final expression for the time delayed correlation of the intensity at the center of output plane is:

$$\begin{aligned}
 B_I(0, \tau) = & \iiint \int d\mathbf{p}_1 d\mathbf{p}_2 d\mathbf{p}_3 d\mathbf{p}_4 \sum_{i=1}^2 \sum_{j=1}^2 \sum_{k=1}^2 \sum_{l=1}^2 A_i A_j^* A_k A_l^* \left[\frac{1}{\lambda d_0} \right]^4 \\
 & \times \exp[-(E_i p_1^2 + E_j^* p_2^2 + E_k p_3^2 + E_l^* p_4^2)] \\
 & \times \exp \left\{ -\frac{2.91}{2} L k^2 \int_0^1 C_n^2 [|\xi(\mathbf{p}_2 - \mathbf{p}_1)|^{5/3} - |\xi(\mathbf{p}_3 - \mathbf{p}_1) - \mathbf{V}\tau|^{5/3} + |\xi(\mathbf{p}_4 - \mathbf{p}_1) - \mathbf{V}\tau|^{5/3} \right. \\
 & \left. + |\xi(\mathbf{p}_3 - \mathbf{p}_2) - \mathbf{V}\tau|^{5/3} - |\xi(\mathbf{p}_4 - \mathbf{p}_2) - \mathbf{V}\tau|^{5/3} + |\xi(\mathbf{p}_4 - \mathbf{p}_3)|^{5/3}] d\xi \right\} \quad (4.7)
 \end{aligned}$$

where $E_i = B_i - i \frac{k}{2d_0}$, etc.

Equation (4.7) is the form of time delayed intensity correlation which involves the cross-wind effect. It was observed in our experimental high-pass system that the random intensity pattern on the output plane moves with the cross wind in the same fashion as that in the case without filtering. Because the bright background has been removed, the intensity variations are much easier to observe. The cross wind can then be obtained by studying the time delayed intensity correlation. In order to retain the cross-wind effect, as we will discuss in the next section, the eight-fold integration of (4.7) has to be calculated through numerical techniques.

The 5/3 law functions within the eight-fold integration and 16-term summation make (4.7) impractical to be evaluated by conventional numerical approaches and further simplifications are needed. We have developed an expansion of the wave structure function with good accuracy which can be used to perform this type of sophisticated numerical integration [Appendix 2]. To obtain good physical insight into the subject and avoid messy ambiguous expressions, in the following we will use the quadratic form of the wave structure function in the variance analysis work, as other authors have done in the analysis of partially coherent propagation³⁰ and receiver aperture averaging effect^{20,31}. To be more flexible, we use the quadratic form with adjustable factor η to give a dimension of best fit of the theoretical result to the experiments. This simplifies the analysis and yields a result in closed form. A comparison of the 5/3 law results and the quadratic form results will be made.

4.3. Variance

The variance of the intensity at the output of the spatial filtering system will now be developed. We will use the quadratic approximation for the wave structure function. Under the quadratic approximation, the typical term in (4.7) can be written as

$$\frac{1}{2}D_{31} = \frac{\eta}{\rho_0^2} \int_0^1 [\xi(\mathbf{p}_3 - \mathbf{p}_1) - \mathbf{V}_T]^2 d\xi$$

$$= \frac{\eta}{\rho_0^2} \left[\frac{1}{3} (\mathbf{p}_3 - \mathbf{p}_1)^2 - (\mathbf{p}_3 - \mathbf{p}_1) \cdot \mathbf{V}_T + V^2 \tau^2 \right]$$

The phase structure function can thus be written as

$$H = \frac{\eta}{3\rho_0^2} [p_1^2 + p_2^2 + p_3^2 + p_4^2 + 2(p_3p_1 + p_4p_2 - p_2p_1 - p_4p_1 - p_2p_3 - p_4p_3)] \quad (4.8)$$

It can be seen from (4.8) that the cross-wind effect in the phase structure function is completely cancelled out under the quadratic approximation. Hence, this approximation can not be used to determine the cross-wind effect in the case of line of sight propagation. By utilizing (4.8), the intensity autocorrelation at zero time delay can be organized in the generalized form:

$$B_I(0,0) = \left[\frac{1}{\lambda d_0} \right]^4 \sum_{i=1}^2 \sum_{j=1}^2 \sum_{k=1}^2 \sum_{l=1}^2 A_i A_j^* A_k A_l^* \times$$

$$\iiint \int d\mathbf{p}_1 d\mathbf{p}_2 d^2 p_3 d\mathbf{p}_4 \exp[-(x_1 p_1^2 + x_2 p_2^2 + x_3 p_3^2 + x_4 p_4^2)] \times$$

$$\exp[2(x_{12} p_1 p_2 + x_{13} p_1 p_3 + x_{14} p_1 p_4 + x_{23} p_2 p_3 + x_{24} p_2 p_4 + x_{34} p_3 p_4)] \quad (4.9)$$

The eight-fold integration of (4.9) can be worked out analytically. We provide a simpler version of the integral which is essentially equivalent to the result given by Leader³⁰ in 1979. Our result is

$$J = \iiint \int d\mathbf{p}_1 d\mathbf{p}_2 d\mathbf{p}_3 d\mathbf{p}_4 \exp[-(x_1 p_1^2 + x_2 p_2^2 + x_3 p_3^2 + x_4 p_4^2)] \times$$

$$\exp[2(x_{12} p_1 p_2 + x_{13} p_1 p_3 + x_{14} p_1 p_4 + x_{23} p_2 p_3 + x_{24} p_2 p_4 + x_{34} p_3 p_4)]$$

$$= \frac{\pi^4}{x_1(x_2 - x_{12}^2/x_1)(MN - Q^2)} \quad (4.10)$$

where

$$M = x_3 - \frac{x_{13}^2}{x_1} - \frac{(x_{23} + \frac{x_{12}x_{13}}{x_1})^2}{(x_2 - \frac{x_{12}^2}{x_1})} \quad (4.11)$$

$$N = x_4 - \frac{x_{12}^2}{x_1} - \frac{(x_{24} + \frac{x_{12}x_{14}}{x_1})^2}{(x_2 - \frac{x_{12}^2}{x_1})} \quad (4.12)$$

$$Q = x_{34} + \frac{x_{13}x_{14}}{x_1} + \frac{(x_{23} + \frac{x_{12}x_{13}}{x_1})(x_{24} + \frac{x_{12}x_{14}}{x_1})}{(x_2 - \frac{x_{12}^2}{x_1})} \quad (4.13)$$

The Intensity correlation is given by the summation

$$B_I(0,0) = \left[\frac{1}{\lambda d_0} \right]^4 \sum_{i=1}^2 \sum_{j=1}^2 \sum_{k=1}^2 \sum_{l=1}^2 A_i A_j^* A_k A_l^* J(i, j, k, l) \quad (4.14)$$

In the case of line of sight propagation, the following set of parameters were used in (4.10)-(4.14):

$$x_1 = E_i + \frac{\eta}{3\rho_0^2}$$

$$x_2 = E_j^* + \frac{\eta}{3\rho_0^2}$$

$$x_3 = E_k + \frac{\eta}{3\rho_0^2}$$

$$x_4 = E_l^* + \frac{\eta}{3\rho_0^2}$$

$$x_{12} = x_{14} = x_{23} = x_{34} = \frac{\eta}{3\rho_0^2}$$

$$x_{13} = x_{24} = -\frac{\eta}{3\rho_0^2}$$

When $\eta = 3$, the result correspond to the conventional quadratic approximation. The intensity correlation can thus be calculated.

Typical behaviors of the correlation, the squared intensity, the variance and normalized variance as functions of turbulence strength are shown in Fig. (4.1) through (4.4). When plotting these figures, the wavelength of a He-Ne laser (0.6328×10^{-6}), and a receiver focal length of 2 meters were used. To reflect the realistic filter characteristics, a finite center transmission of 1 of one-millionth of power attenuation were assumed. The trivial constant $(\pi/\lambda d_o)^4$ in front of relevant expressions was omitted.

The calculation is performed using a single precision complex algorithm with an accuracy of 1×10^{-8} . The numerical noise is apparent (Fig. 4.4) when the correlation goes below 10^{-8} , this can be improved by using computers with a double precision complex algorithm in Fortran.

In fig. 4.1 and 4.5, all quantities of second order statistics are displayed. Our theory reveals the features of line of sight propagation. The intensity correlation equals the squared intensity at both low and relatively high ends of turbulence strength and so the normalized variance are zero at these ends. The system parameters were chosen so that at the low turbulence end, most light energy falls within the non-transparent center disk of the filter and thus

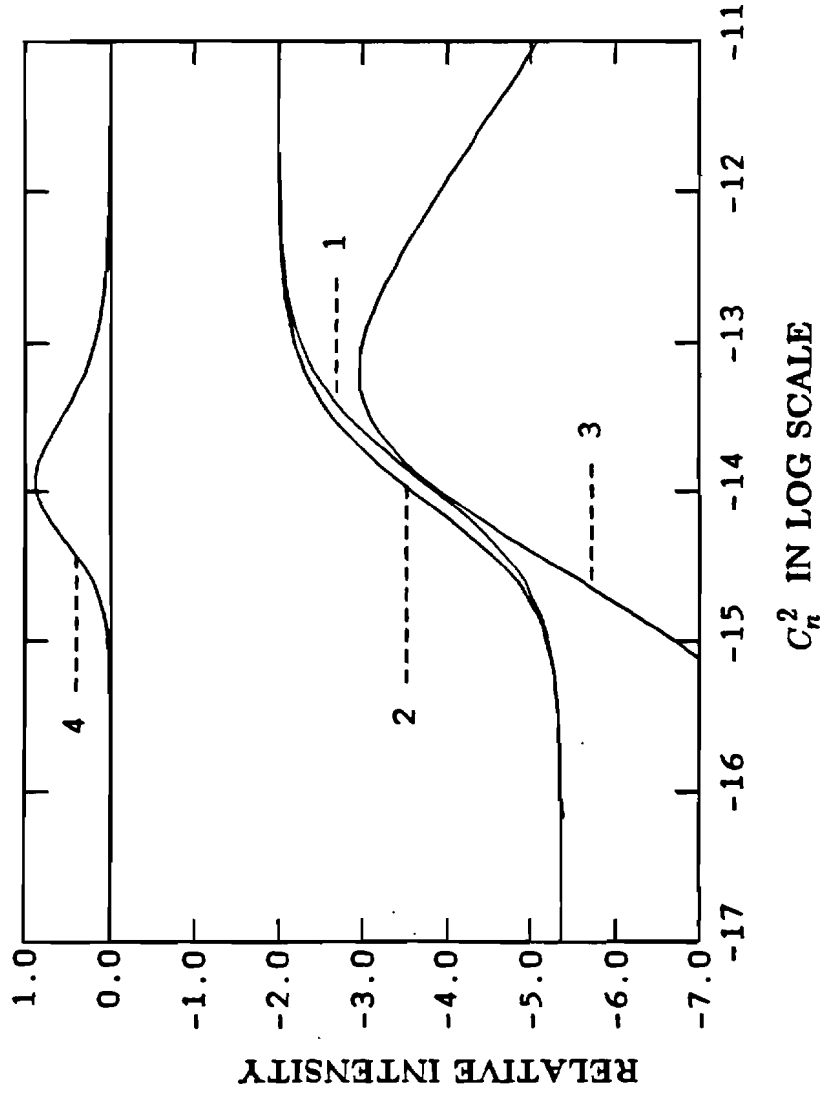
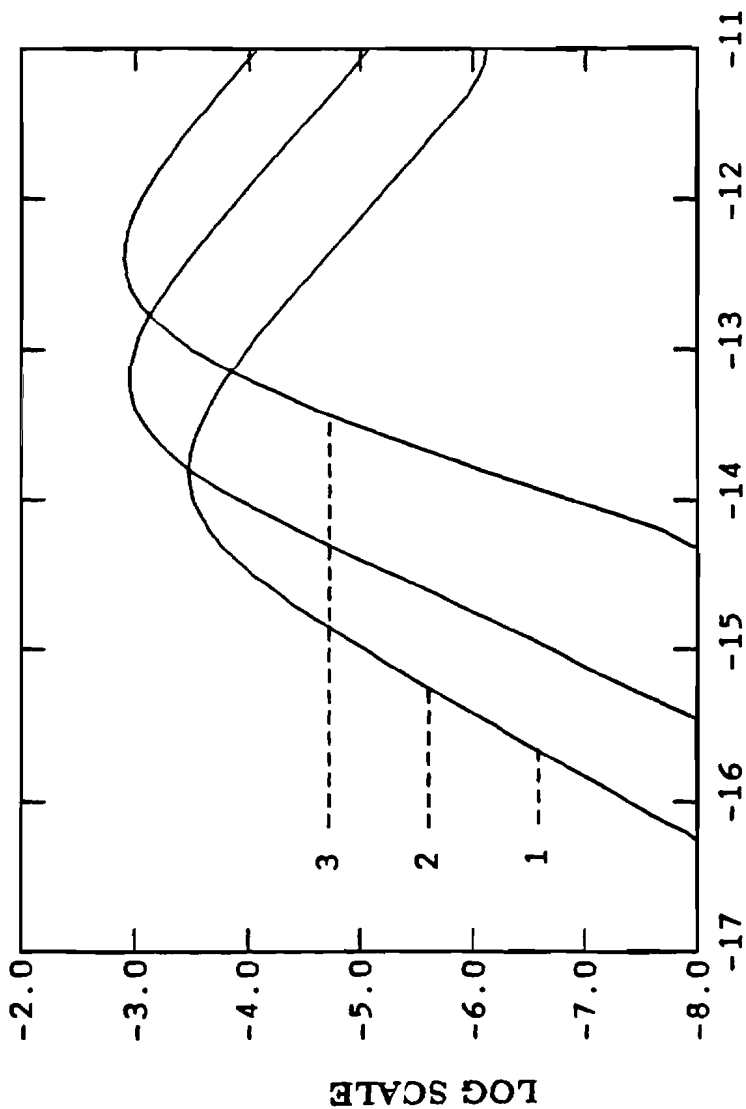


Fig. 4.1 Line of sight propagation. $L = 1\text{km}$, $\sigma = 0.03\text{m}$, high pass filter with $Q_0 = 0.033\text{mm}$. 1--- Squared intensity(log), 2--- Intensity correlation(log), 3--- Intensity variance(log), 4--- Normalized intensity variance(linear).



$C_n^2 (m^{-2/3})$ IN LOG SCALE

Fig 4.2 Intensity variance of line of sight propagation with different filter sizes. $L = 1000m$, $a = 0.03m$. High-pass filter, 1--- $Q_0 = 0.010mm$, 2--- $Q_0 = 0.033mm$, 3--- $Q_0 = 0.090mm$.

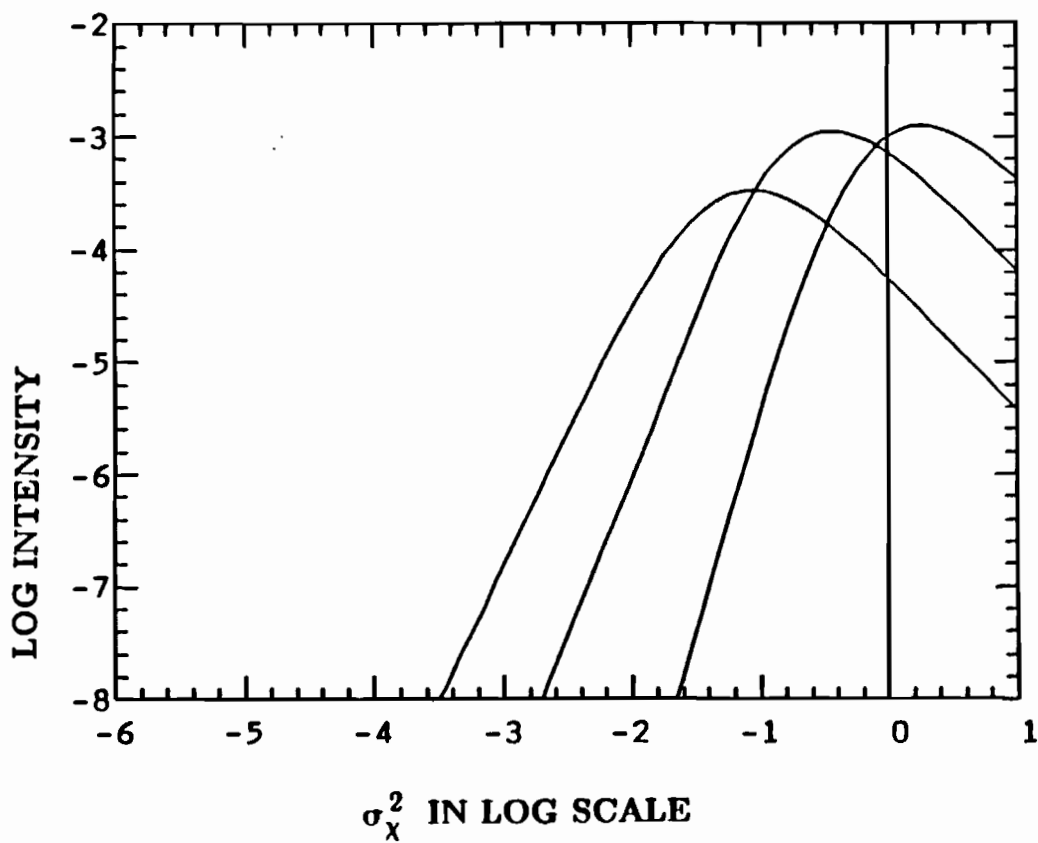
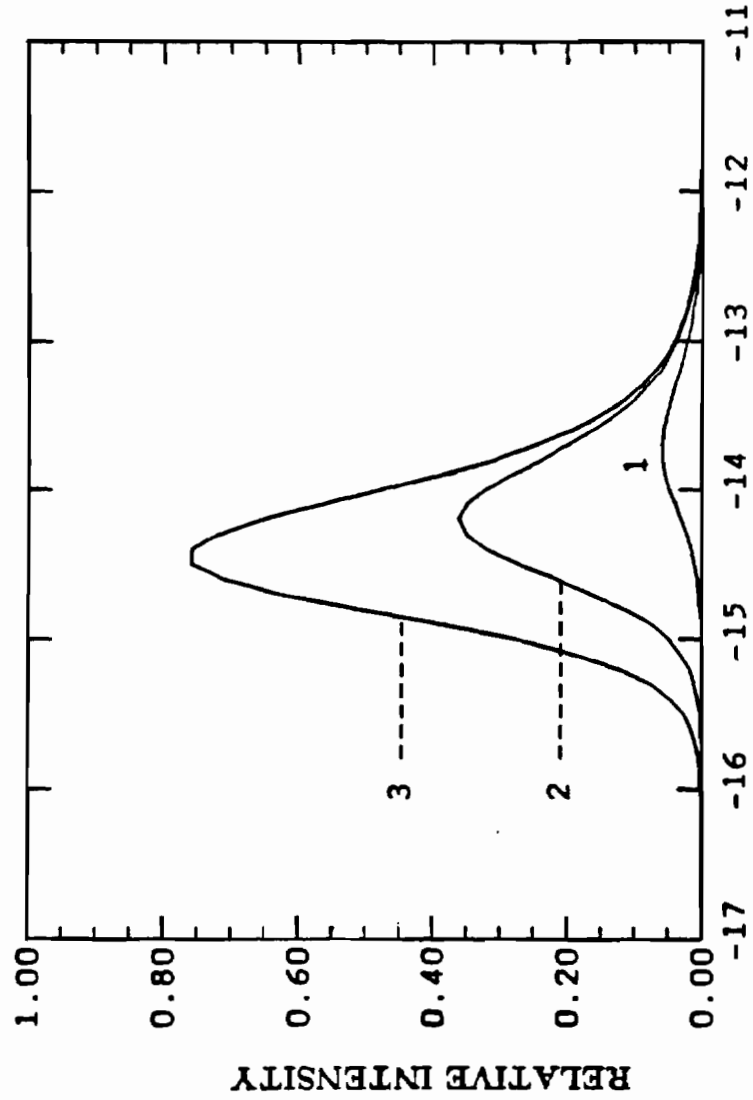


Fig 4.3 Intensity variance of line of sight propagation with different filter sizes. $L = 1000\text{m}$, $a = 0.03\text{m}$. High-pass filter, 1--- $Q_0 = 0.010\text{mm}$, 2--- $Q_0 = 0.033\text{mm}$, 3--- $Q_0 = 0.090\text{mm}$.



$C_n^2 (m^{-2/3})$ IN LOG SCALE

Fig 4.4 Normalized intensity variance of line of sight propagation with different receiver apertures. $L=1000m$, $Q_0=0.010mm$, 1--- $a = 0.03m$, 2--- $a = 0.06m$, 3--- $a = 0.09m$.

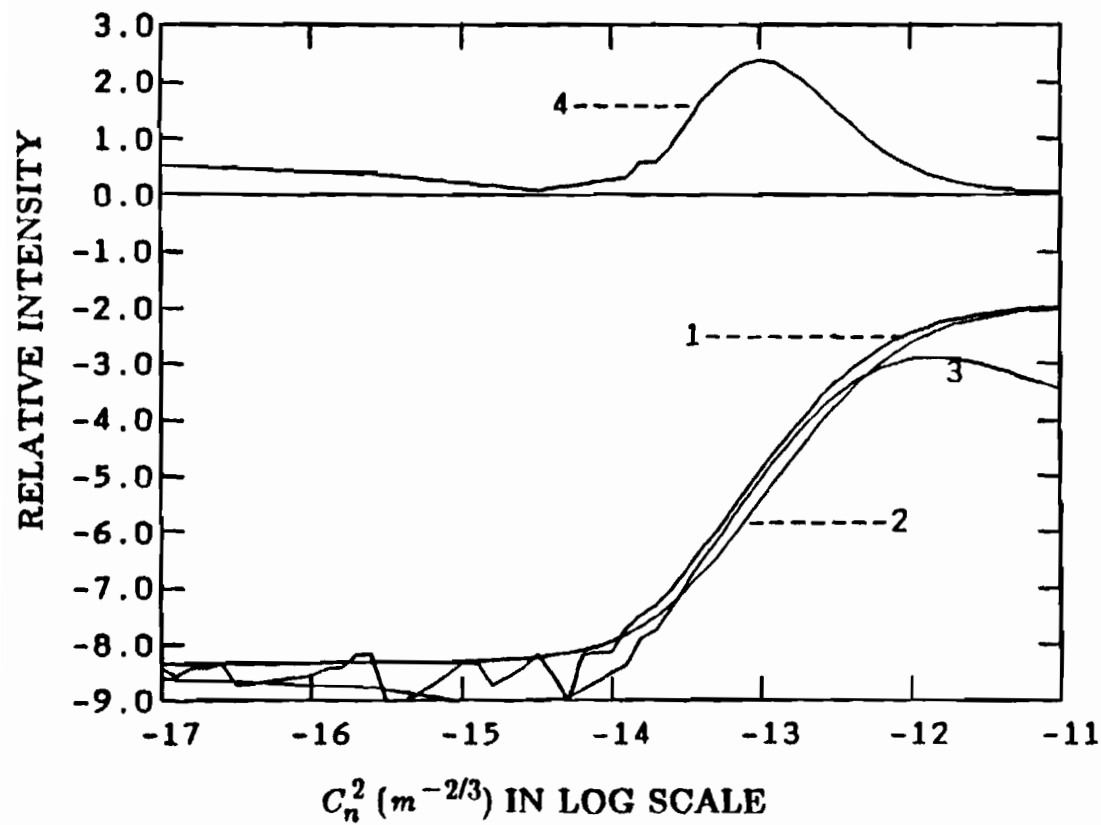


Fig. 4.5 propagation (OGC field site geometry). $L=500$, $a = 0.15m$, high pass filter with $Q_0=0.148mm$. 1--- Intensity correlation(log), 2--- Intensity variance(log), 3--- Squared intensity(log), 4--- Normalized intensity variance(linear).

is attenuated by the same amount. In this case, the system output statistics should be similar to the raw input beam in front of the receiver. On the other end, the turbulent atmosphere scatters most of the incoming beam so the image pattern is very large compared to the filter disk. The filtering effect can then be ignored, and the normalized variance should be close to that at the input of the system. In the transition region, the variance increases almost linearly in a log-log scale with the turbulence strength, then saturates at a peak and drops down. Similarly, the normalized variance increases above unity in the first half of the dynamical range and falls back to zero almost symmetrically in the second half range. It is to be noted that the normalized variance (curve 4) reaches its peak at the turbulence level where the intensity curve (2) has its largest slope.

Our theory does not predict the high turbulence end behavior correctly because of two reasons: (1) we used phase structure functions only and the correlation including log-amplitude terms are excluded; (2) we have used the quadratic approximation of (5/3) law. As has been indicated in our previous work, the introduction of the quadratic approximation changes the slope of the curves substantially. The effect of different filter parameters are shown in fig (4.2) (for normalized variance) and fig (4.3) (for variance).

5. The Intensity Variance (Speckle case)

5.1. Introduction

The speckle case is where the laser transmitter and the receiver are at the same end of the propagation path with a target located at the other end of the propagation path. Because of the mathematical complexity of the problem, we limit our discussion within the following restrictions:

1. In the forward propagation, we assume the gaussian beam is focused on the target and that the atmosphere perturbations due to the forward propagation are independent of those due to the return propagation.
2. We consider only the phase distortion by the turbulence. This is a good description for low and moderate turbulence condition but is not correct under strong turbulence
3. The quadratic approximation will be used throughout this analysis. The use of 5/3 law yields a result that includes many-fold unsolved integrations which are not practical to evaluate numerically. As we have indicated in the intensity analysis, the quadratic approximation will change the slope and range of the resultant curves. We will provide a comparison of the theory with our experimental data.

5.2. Fourth Moment of the Incoming Field

In order to find the second statistics of the intensity after spatial filtering, we need first to calculate the fourth moment of the incoming field. We assume a gaussian beam source with a diffuse target. The beam is focused on the target so that the scattered fields leaving the target have the following correlation:

$$\begin{aligned}
 & \langle u(\rho_1, 0)u^*(\rho_2, 0)u(\rho_3, \tau)u^*(\rho_4, \tau) \rangle = \\
 & = \left[\frac{4\pi}{k^2} \right] \langle I(\rho_1, 0) \rangle \langle I(\rho_3, \tau) \rangle \delta(\rho_1 - \rho_2) \delta(\rho_3 - \rho_4) + \\
 & + \left[\frac{4\pi}{k^2} \right] \langle u(\rho_4, 0)u^*(\rho_4, \tau) \rangle \langle u(\rho_2, \tau)u^*(\rho_2, 0) \rangle \delta(\rho_1 - \rho_4) \delta(\rho_2 - \rho_3) \quad (5.1)
 \end{aligned}$$

The speckles generated at the target travel back to the receiver end. By utilizing of the Extended Huygens-Fresnel principle for wave propagation in the atmosphere^{24, 32}, the time-delayed fourth moment of the field at the input of the spatial filtering system with coordinate \mathbf{p} is given in terms of integration over ρ as

$$\begin{aligned}
 B_1(\mathbf{p}_1, \mathbf{p}_2, \mathbf{p}_3, \mathbf{p}_4; \tau) = & \left[\frac{1}{\lambda L} \right]^4 \exp\left[\frac{ik}{2L} (\mathbf{p}_1^2 - \mathbf{p}_2^2 + \mathbf{p}_3^2 - \mathbf{p}_4^2) \right] \\
 & \times \iint d\rho_2 d\rho_4 \left\{ \langle I(\rho_2, 0) \rangle \langle I(\rho_4, \tau) \rangle \exp\left\{ -i\frac{k}{L} [(\mathbf{p}_1 - \mathbf{p}_2) \cdot \rho_2 + (\mathbf{p}_3 - \mathbf{p}_4) \cdot \rho_4] \right\} H_1 + \right. \\
 & \left. + \langle u(\rho_4, 0)u^*(\rho_4, \tau) \rangle \langle u(\rho_2, \tau)u^*(\rho_2, 0) \rangle \exp\left\{ -i\frac{k}{L} [(\mathbf{p}_1 - \mathbf{p}_4) \cdot \rho_4 + (\mathbf{p}_3 - \mathbf{p}_2) \cdot \rho_2] \right\} H_2 \right\} \quad (5.2)
 \end{aligned}$$

where H_1 and H_2 are the spherical wave mutual coherence functions on

the back propagation and are given by the following expressions respectively.

$$\begin{aligned}
 H_1(\mathbf{p}_1, \mathbf{p}_2, \mathbf{p}_3, \mathbf{p}_4; \rho_2, \rho_2, \rho_4, \rho_4; \tau) = \exp \left\{ -\frac{2.91}{2} L k^2 \int_0^1 C_n^2 [|\xi(\mathbf{p}_2 - \mathbf{p}_1)|^{5/3} - \right. \\
 - |\xi(\mathbf{p}_3 - \mathbf{p}_1) + (1 - \xi)(\rho_4 - \rho_2) - \mathbf{V}\tau|^{5/3} + |\xi(\mathbf{p}_4 - \mathbf{p}_1) + (1 - \xi)(\rho_4 - \rho_2) - \mathbf{V}\tau|^{5/3} + \\
 + |\xi(\mathbf{p}_3 - \mathbf{p}_2) + (1 - \xi)(\rho_4 - \rho_2) - \mathbf{V}\tau|^{5/3} - |\xi(\mathbf{p}_4 - \mathbf{p}_2) + (1 - \xi)(\rho_4 - \rho_2) - \mathbf{V}\tau|^{5/3} + \\
 \left. + |\xi(\mathbf{p}_4 - \mathbf{p}_3)|^{5/3}] d\xi \right\} \quad (5.3)
 \end{aligned}$$

$$\begin{aligned}
 H_2(\mathbf{p}_1, \mathbf{p}_2, \mathbf{p}_3, \mathbf{p}_4; \rho_2, \rho_2, \rho_4; \tau) = \exp \left\{ -\frac{2.91}{2} L k^2 \int_0^1 C_n^2 [|\xi(\mathbf{p}_2 - \mathbf{p}_1) - (1 - \xi)(\rho_4 - \rho_2)|^{5/3} - \right. \\
 - |\xi(\mathbf{p}_3 - \mathbf{p}_1) - (1 - \xi)(\rho_4 - \rho_2) - \mathbf{V}\tau|^{5/3} + |\xi(\mathbf{p}_4 - \mathbf{p}_1) - \mathbf{V}\tau|^{5/3} + \\
 + |\xi(\mathbf{p}_3 - \mathbf{p}_2) - \mathbf{V}\tau|^{5/3} - |\xi(\mathbf{p}_4 - \mathbf{p}_2) + (1 - \xi)(\rho_4 - \rho_2) - \mathbf{V}\tau|^{5/3} + \\
 \left. + |\xi(\mathbf{p}_4 - \mathbf{p}_3) + (1 - \xi)(\rho_4 - \rho_2)|^{5/3}] d\xi \right\} \quad (5.4)
 \end{aligned}$$

Equation (5.2) needs to be solved in closed form in order to calculate the effect of spatial filtering on the intensity variance. We first evaluate the time-delayed correlation of the field after leaving the diffuse target. According to Holmes *et al*²⁹, we have:

$$\langle u(\rho_4, 0) u^*(\rho_4, \tau) \rangle = \frac{2\pi}{(\lambda L)^2} u_0^2 \frac{\alpha_0^2}{2} \int d^2 r \exp \left[-\frac{r^2}{4\eta_0^2} - i \frac{k}{L} \rho_2 \cdot \mathbf{r} - \frac{1}{2} D_\psi(0, -\mathbf{r}, \tau) \right] \quad (5.5)$$

where u_0 is the amplitude of the transmitted field, α_0 is the waist radius of the transmitted gaussian beam and D_ψ is the wave structure function.

Under quadratic approximation, we assume

$$-\frac{1}{2}D_{\psi}(0, -\mathbf{r}, \tau) = -\frac{\eta}{\rho_0^2} \left(\frac{1}{3} r^2 + V^2 \tau^2 + \mathbf{r} \cdot \mathbf{V} \tau \right)$$

Here we have used the quadratic approximation with coefficient η as defined earlier. The integral of (5.5) can be worked out as given by the following:

$$\langle u(\rho_4, 0) u^*(\rho_4, \tau) \rangle = \left[\frac{u_0 \alpha_0 k}{L} \right]^2 \frac{1}{\frac{1}{\alpha_0^2} + \frac{4\eta}{3\rho_0^2}} \times$$

$$\exp \left[-\frac{\eta}{\rho_0^2} V^2 \tau^2 - \frac{\left[\frac{k^2}{L^2} \rho_4^2 - \frac{\eta^2}{\rho_0^2} V^2 \tau^2 - i \frac{2k\eta}{L\rho_0^2} \rho_4 \cdot \mathbf{V} \tau \right]}{\left[\frac{1}{\alpha_0^2} + \frac{4\eta}{3\rho_0^2} \right]} \right]$$

The mean intensity can be obtained from (5.5) by letting $\tau = 0$:

$$\langle I(\rho, 0) \rangle = \langle I(\rho, \tau) \rangle = \left[\frac{\alpha_0 u_0 k}{L} \right]^2 \frac{1}{\frac{1}{\alpha_0^2} + \frac{4\alpha}{3\rho_0^2}} \exp \left[-\frac{k^2}{L^2 \left(\frac{1}{\alpha_0^2} + \frac{4\eta}{3\rho_0^2} \right)} \rho^2 \right] \quad (5.6)$$

The functions H_1 and H_2 can also be obtained in closed form. By replacing the 5/3 law with a square in each term in H_1 and H_2 , we have the following type of approximation:

$$\frac{1}{2}D_{31} = \frac{1}{\rho_0^{5/3}} \int_0^1 |\xi(\mathbf{p}_3 - \mathbf{p}_1) + (1-\xi)(\mathbf{p}_4 - \mathbf{p}_2) - \mathbf{V} \tau|^{5/3} d\xi$$

$$= \frac{\eta}{\rho_0^2} \left\{ \frac{1}{3} \left[|(\mathbf{p}_3 - \mathbf{p}_1) - (\mathbf{p}_4 - \mathbf{p}_2)|^2 - [(\mathbf{p}_3 - \mathbf{p}_1) - (\mathbf{p}_4 - \mathbf{p}_2)] \cdot \mathbf{V} \tau \right. \right.$$

$$\left. \left. + [(\mathbf{p}_3 - \mathbf{p}_1) - (\mathbf{p}_4 - \mathbf{p}_2)] \cdot (\mathbf{p}_4 - \mathbf{p}_2) + [(\mathbf{p}_4 - \mathbf{p}_2) - \mathbf{V} \tau]^2 \right\}$$

After algebraic cancellation, the final results can be expressed in more concise form under the transformation notation described below.

$$H_1(\mathbf{p}_1, \mathbf{p}_2, \mathbf{p}_3, \mathbf{p}_4; \rho_2, \rho_2, \rho_4, \rho_4; \tau) = \exp\left[-\frac{\eta}{3\rho_0^2} u^2\right] \quad (5.7)$$

$$H_2(\mathbf{p}_1, \mathbf{p}_2, \mathbf{p}_3, \mathbf{p}_4; \rho_4, \rho_2, \rho_2, \rho_4; \tau) = \exp\left[-\frac{\eta}{3\rho_0^2} (u^2 + 2\mathbf{p}_b \cdot \mathbf{V}\tau)\right] \quad (5.8)$$

It is noticed that under the quadratic approximation, H_1 is independent of the cross wind \mathbf{V} , and both H functions are free from ρ dependence.

In order to evaluate expression (5.2), let us put these results of (5.5) through (5.8) back in (5.2). The first integral in (5.2) can be found as:

$$I_1 = \pi^2 \alpha_0^4 u_0^4 \exp\left[-\frac{k^2}{2L^2 M} p_a^2 - \left(\frac{1}{8\alpha_0^2} + \frac{\eta}{2\rho_0^2}\right) u^2\right] \quad (5.9)$$

The second integral in (5.2) is the major term for cross-wind effect under quadrature approximation. After some algebraic manipulations, we have

$$I_2 = \pi^2 \alpha_0^4 u_0^4 \exp\left[-\frac{k^2}{2L^2 M} p_b^2 - \left(\frac{1}{8\alpha_0^2} + \frac{\eta}{2\rho_0^2}\right) u^2\right] \\ \times \exp\left[-2\left(N + M \frac{\alpha^2 L^2}{k^2 \rho_0^4}\right) V^2 \tau^2 - \frac{\eta}{\rho_0^2} \left(\frac{2}{3} \mathbf{p}_b - \frac{1}{2} \mathbf{u}\right) \cdot \mathbf{V}\tau\right] \quad (5.10)$$

The time-delayed fourth order moment of the incoming field is thus given by

$$B_1(\mathbf{p}_1, \mathbf{p}_2, \mathbf{p}_3, \mathbf{p}_4; \tau) = \pi^2 \left[\frac{\alpha_0 u_0}{\lambda L} \right]^4 \exp\left[\frac{ik}{2L} (p_1^2 - p_2^2 + p_3^2 - p_4^2) - \left(\frac{1}{8\alpha_0^2} + \frac{\eta}{2\rho_0^2}\right) u^2\right] \\ \times \left\{ \exp\left(-\frac{k^2}{2L^2 M} p_a^2\right) + \exp\left[-\frac{k^2}{2L^2 M} p_b^2 - 2\left(N + M \frac{\alpha^2 L^2}{k^2 \rho_0^4}\right) V^2 \tau^2 - \frac{\eta}{\rho_0^2} \left(\frac{2}{3} \mathbf{p}_b - \frac{1}{2} \mathbf{u}\right) \cdot \mathbf{V}\tau\right] \right\} \quad (5.11)$$

For zero time delay, the correlation function is reduced to

$$B_I(0) = \pi^2 \left[\frac{\alpha_0 u_0}{\lambda L} \right]^4 \exp\left[\frac{ik}{2L} (p_1^2 - p_2^2 + p_3^2 - p_4^2) - Tu^2 \right] [\exp(-Sp_a^2) + \exp(-Sp_b^2)] \quad (5.12)$$

In the above we have used the following parameter notations:

$$M = \frac{k^2}{L^2 \left(\frac{1}{\alpha_0^2} + \frac{4\eta}{3\rho_0^2} \right)} \quad (5.13)$$

$$N = \frac{\eta \left(\frac{p_0}{\alpha_0} \right)^2 + \frac{1}{3} \eta^2}{\rho_0^4 \left(\frac{1}{\alpha_0^2} + \frac{4\eta}{3\rho_0^2} \right)} \quad (5.14)$$

$$T = \frac{1}{8\alpha_0^2} + \frac{\eta}{2\rho_0^2} \quad (5.15)$$

$$S = \frac{k^2}{2L^2 M} = \frac{1}{2} \left(\frac{1}{\alpha_0^2} + \frac{4\eta}{3\rho_0^2} \right) \quad (5.16)$$

According to Appendix 1, variables p_a, p_b, u, v are related to p_1, p_2, p_3, p_4 through a transformation matrix. We list some useful expansions below for quick reference.

$$p_a = \frac{1}{2} [(p_1 - p_2) - (p_3 - p_4)] \quad (5.17)$$

$$p_b = \frac{1}{2} [(p_1 + p_2) - (p_3 + p_4)] \quad (5.18)$$

$$u = (p_1 - p_2) + (p_3 - p_4) \quad (5.19)$$

$$v = \frac{1}{4} (p_1 + p_2 + p_3 + p_4) \quad (5.20)$$

and

$$u^2 = p_1^2 + p_2^2 + p_3^2 + p_4^2 + 2(p_1p_3 + p_2p_4 - p_1p_2 - p_3p_4 - p_1p_4 - p_2p_3)$$

$$p_a^2 = \frac{1}{4}[p_1^2 + p_2^2 + p_3^2 + p_4^2 + 2(p_1p_4 + p_2p_3 - p_1p_2 - p_1p_3 - p_2p_4 - p_3p_4)]$$

$$p_b^2 = \frac{1}{4}[p_1^2 + p_2^2 + p_3^2 + p_4^2 + 2(p_1p_2 + p_3p_4 - p_1p_3 - p_1p_4 - p_2p_3 - p_2p_4)]$$

$$v^2 = \frac{1}{16}[p_1^2 + p_2^2 + p_3^2 + p_4^2 + 2(p_1p_2 + p_3p_4 + p_1p_3 + p_1p_4 + p_2p_3 + p_2p_4)]$$

5.3. Variance of Intensity after Spatial Filtering

Similar to the case of line of sight propagation, the time-delayed intensity correlation on the output plane can be written as :

$$B_I(\mathbf{r}, \tau) = \iiint d\mathbf{p}_1 d\mathbf{p}_2 d\mathbf{p}_3 d\mathbf{p}_4 GGGG\left(\frac{\mathbf{r}}{2}, -\frac{\mathbf{r}}{2}; \mathbf{p}_1, \mathbf{p}_2, \mathbf{p}_3, \mathbf{p}_4\right) B_1(\mathbf{p}_1, \mathbf{p}_1, \mathbf{p}_1, \mathbf{p}_1; \tau) \quad (5.21)$$

where $GGGG(\mathbf{p}_1, \mathbf{p}_2, \mathbf{p}_3, \mathbf{p}_4; \mathbf{r}/2, -\mathbf{r}/2)$ is given by (2.16) and $B_1(\mathbf{p}_1, \mathbf{p}_2, \mathbf{p}_3, \mathbf{p}_4; \tau)$ is given by (5.11). The expression for $\langle I^2 \rangle$ on the optical axis is obtained by putting $\tau = 0$ and $\mathbf{r} = 0$ in (5.21). The result is

$$B_I(0,0) = \pi^2 \left[\frac{\alpha_0 u_0}{\lambda L} \right]^4 \iiint d\mathbf{p}_1 d\mathbf{p}_2 d\mathbf{p}_3 d\mathbf{p}_4 \sum_{i=1}^2 \sum_{j=1}^2 \sum_{k=1}^2 \sum_{l=1}^2 A_i A_j^* A_k A_l^* \times \exp[-(E_i p_1^2 + E_j^* p_2^2 + E_k p_3^2 + E_l^* p_4^2) - T u^2] \left\{ \exp(-S p_a^2) + \exp(-S p_b^2) \right\} \quad (5.22)$$

We first work on the eight-fold integration as we did in the case of line of sight propagation. Expanding u^2 , p_a^2 and p_b^2 in terms of p_1, p_2, p_3, p_4 and combining similar terms, these integrals reduce to the standard format contained in formula (4.10). The correlation can then be expressed in the following form

$$B_I(0,0) = \pi^2 \left[\frac{\alpha_0 u_0}{\lambda L} \right]^4 \sum_{i=1}^2 \sum_{j=1}^2 \sum_{k=1}^2 \sum_{l=1}^2 A_i A_j^* A_k A_l^* [J_1(i, j, k, l) + J_2(i, j, k, l)] \quad (5.23)$$

where $J_1(i, j, k, l)$ and $J_2(i, j, k, l)$ are of the form of (4.10), with the following entries:

For both J_1 and J_2 , use

$$x_1 = E_i + c_1$$

$$x_2 = E_j^* + c_1$$

$$x_3 = E_k + c_1$$

$$x_4 = E_l^* + c_1$$

For J_1 use

$$x_{12} = x_{34} = c_1$$

$$x_{14} = x_{23} = c_2$$

$$x_{13} = x_{24} = -c_2$$

For J_2 use

$$x_{12} = x_{34} = c_2$$

$$x_{14} = x_{23} = c_1$$

$$x_{13} = x_{24} = -c_2$$

In the above, the following notations have been used:

$$c_1 = T + \frac{S}{4} = \frac{1}{4\alpha_0^2} + 2\left(\frac{\eta}{3\rho_0^2}\right)$$

$$c_2 = T - \frac{S}{4} = \frac{\eta}{3\rho_0^2}$$

In summary, the second statistics of intensity of the speckle propagation case can be expressed in terms of system parameters.

We have intensity variance:

$$\sigma_I^2 = B_I(0,0) - [\langle I(0,0) \rangle]^2 \quad (5.24)$$

and normalized intensity variance:

$$b_I(0,0) = \frac{\sigma_I^2}{[\langle I(0,0) \rangle]^2} \quad (5.25)$$

where $B_I(0,0)$ is given by (5.23) and $\langle I(0,0) \rangle^2$ is available from our preceding result for the mean intensity.

In Fig. 5.1 through Fig. 5.5, the behavior of the intensity correlation along with other second order intensity statistics are plotted for system parameters and the strength of turbulence. The parameters common to these figures are wave length $\lambda = 0.6328 \times 10^{-6} m$, focal length of the receiver lens $f = 2m$.

Fig. 5.1 shows the general behavior of the four quantities of interest: the squared intensity, the intensity correlation (at zero time delay), the intensity variance and the normalized intensity variance. According to the theory of speckle propagation through the turbulent atmosphere²⁵, the normalized intensity variance at the receiver input stays at unity for all levels of turbulence when phase dominance is assumed. After the high-pass filtering, our theory indicates that this remains true for relatively low and high turbulence levels, but in the transition region where the mean intensity is sensitive to the turbulence, the normalized variance rises above unity.

Fig. 5.2 and 5.3 show the effect of the transmitter aperture. A larger aperture results in a smaller focused spot on the target. At the receiver image plane, this gives a smaller image spot at low turbulence levels and a wider dynamic range of the turbulence sensing. The peak of the normalized vari-

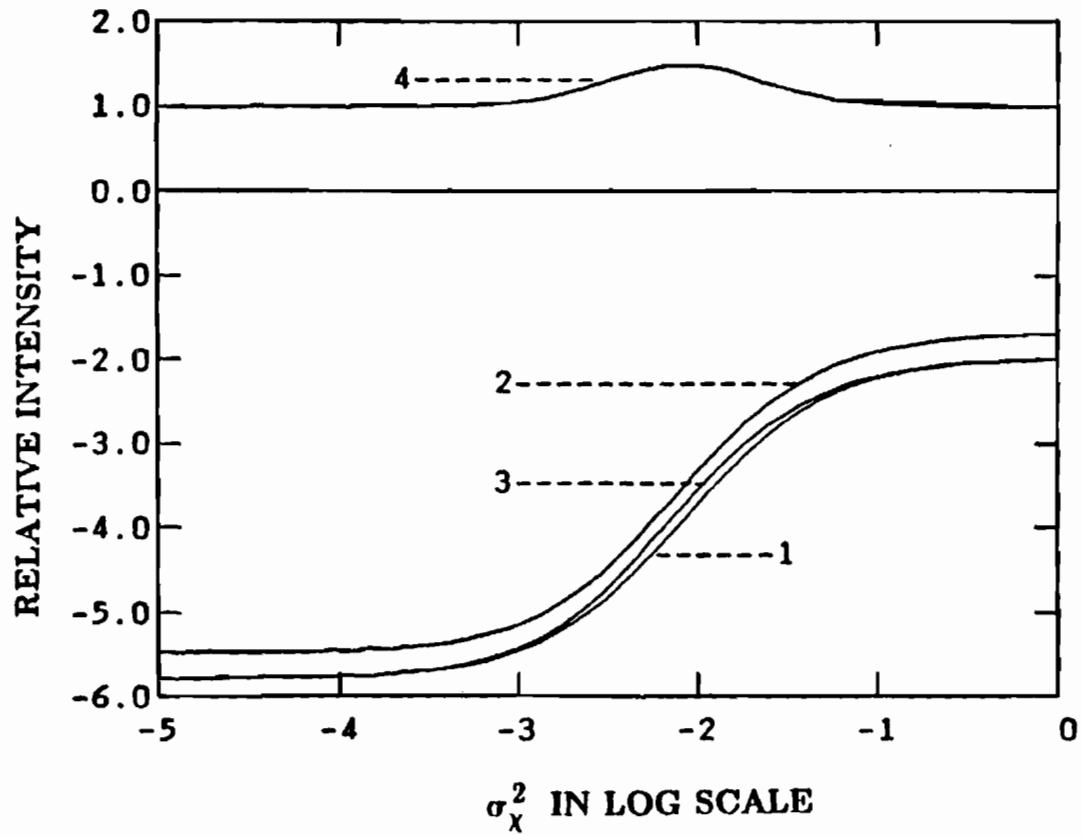
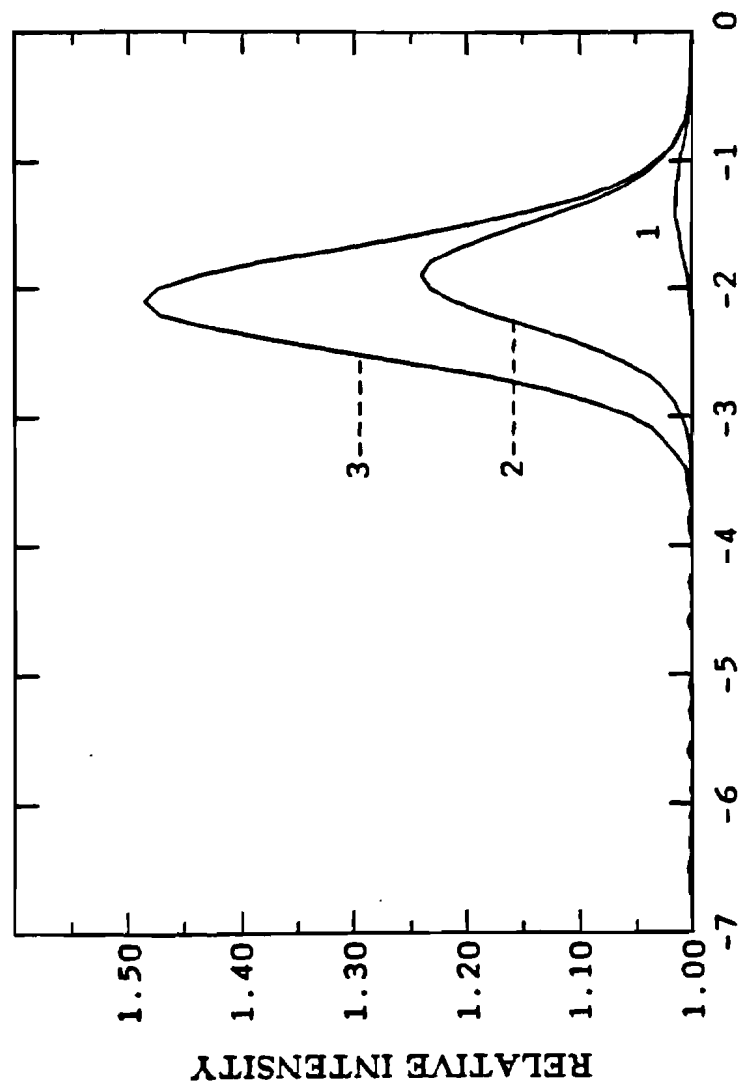


Fig. 5.1 Speckle propagation. $L=1\text{km}$, $\alpha_0 = 0.05\text{m}$, High pass filter with $Q_0=0.015\text{mm}$. 1--- Squred intensity(log), 2--- Intensity correlation(log), 3--- Intensity Variance(log), 4--- Normalized intensity variance(linear).



σ_x^2 IN LOG SCALE

Fig 5.2 Normalised intensity variance of speckle propagation with different transmitter apertures. $L = 290m$, $a = 0.15m$, high-pass filter $Q_0 = 0.015mm$.
1--- $\alpha_0 = 0.01m$, 2--- $\alpha_0 = 0.03m$, 3--- $\alpha_0 = 0.05m$.

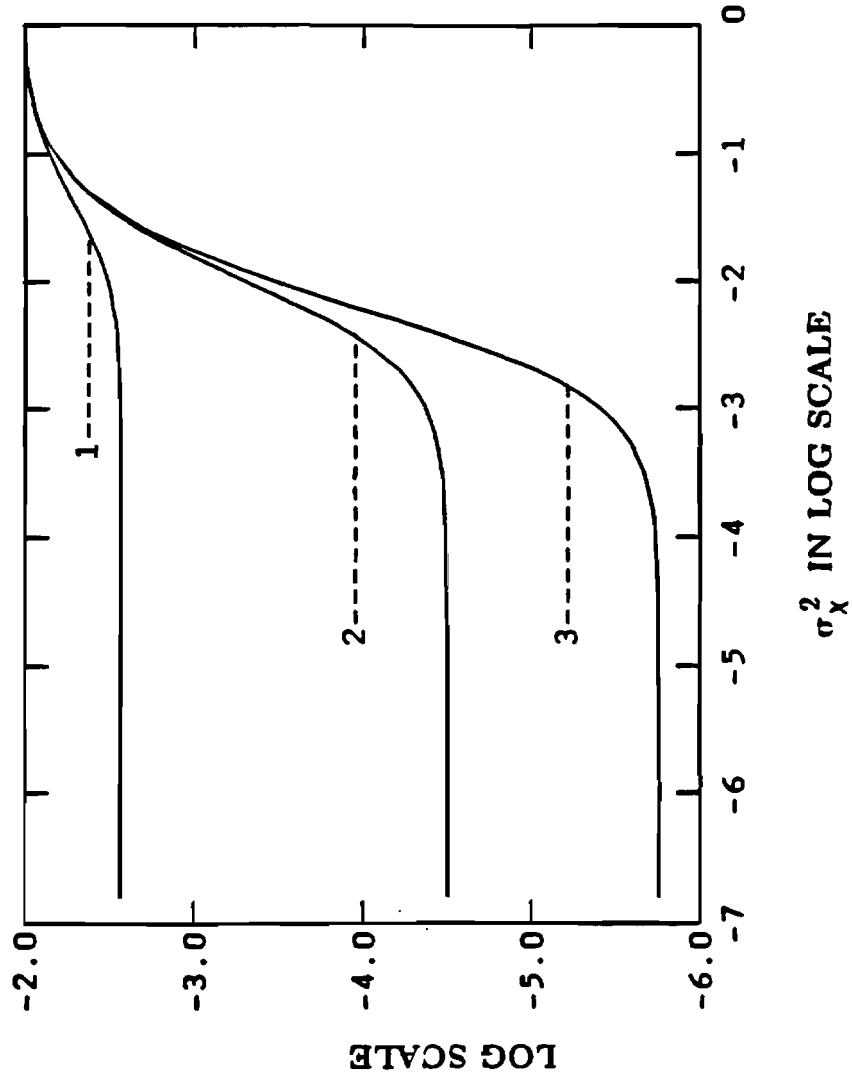


Fig 5.3 Intensity variance of speckle propagation with different transmitter apertures. $L = 200\text{m}$, $a = 0.15\text{m}$ and high-pass filter of $Q_0 = 0.015\text{mm}$. 1--- $u_0 = 0.01\text{m}$, 2--- $u_0 = 0.03\text{m}$, 3--- $u_0 = 0.05\text{m}$.

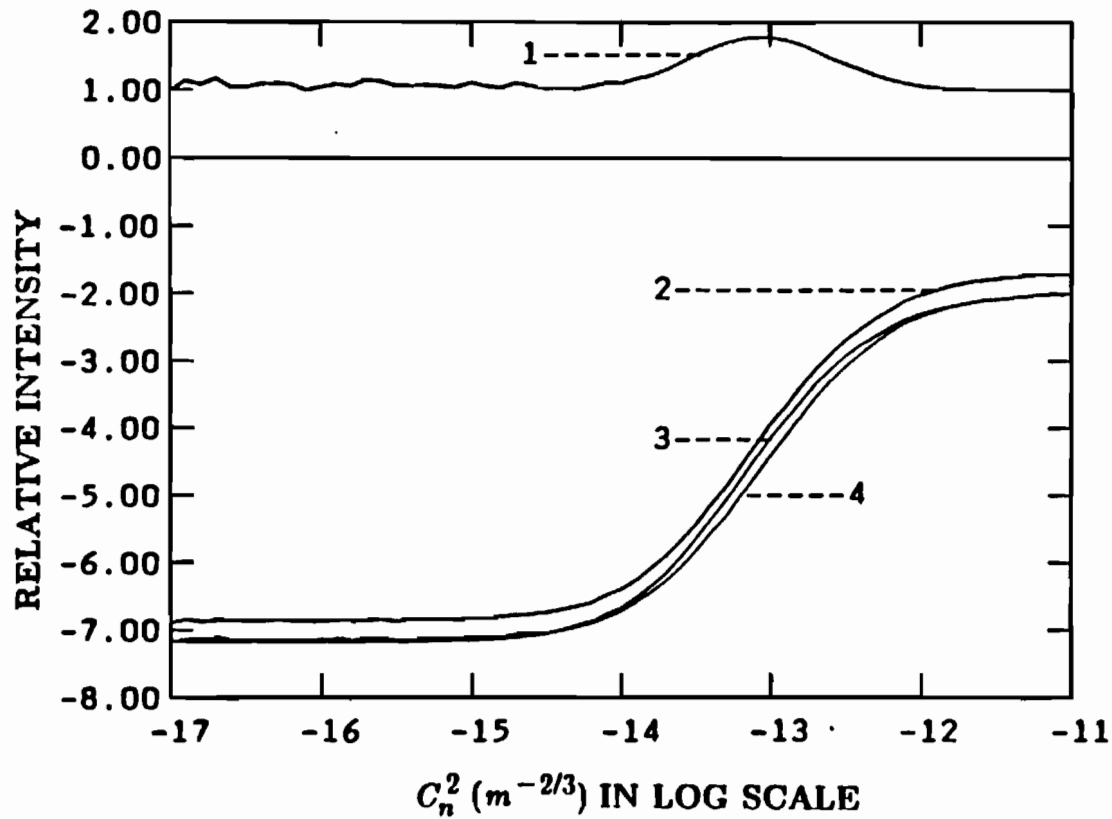
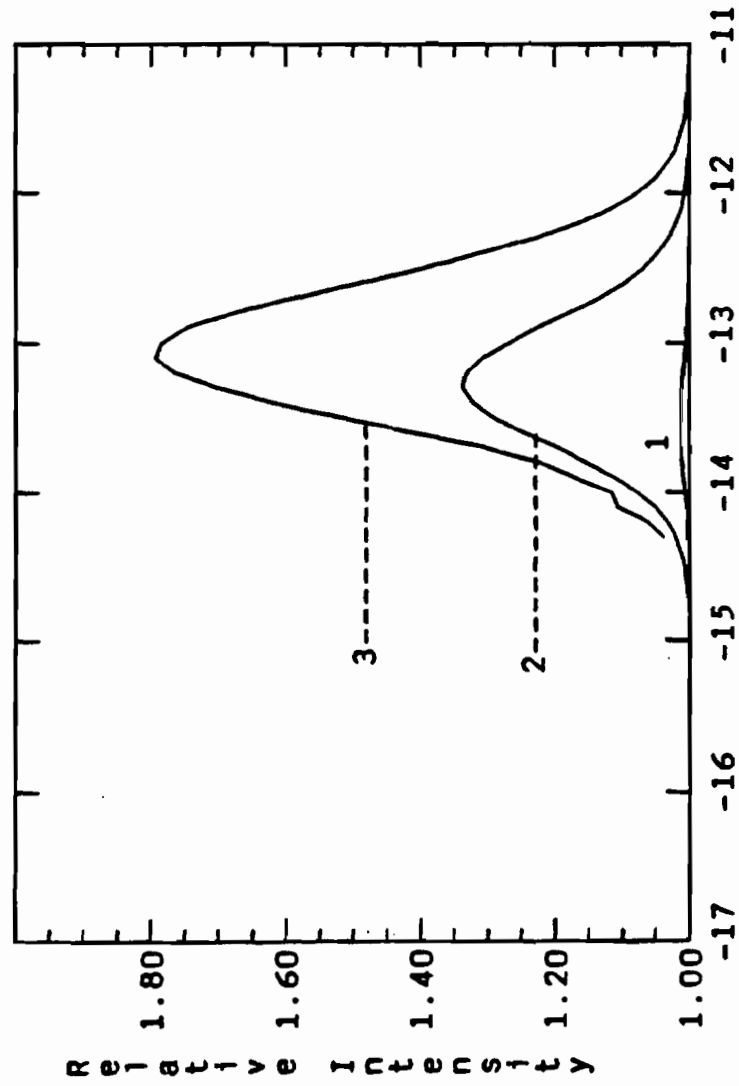


Fig. 5.4 Speckle propagation (OGC campus field geometry). $L=290m$, $\alpha_0 = 0.0108m$, high pass filter with $Q_0=0.106mm$. 1--- Normalized intensity variance(linear). 2-- Intensity correlation(log), 3--- Intensity variance(log), 4--- Squared intensity(log).



C_n^2 IN LOG SCALE

Fig 5.5 Normalized intensity variance of speckle propagation with different filter sizes. $L = 290m$, $\sigma = 0.15m$, $\alpha_0 = 0.0108m$. 1--- $Q_0 = 0.015mm$, 2--- $Q_0 = 0.053mm$, 3--- $Q_0 = 0.106mm$.

ance is thus shifted toward the low turbulence end.

Our theory also indicates that with increased turbulence strength, the variance increases faster than the squared intensity during the first half of the dynamic range, but slower during the second half. This explains the up-bump of the normalized variance. The experiment of the speckle propagation were conducted in the OGC campus field site with a propagation distance of 290 meters. Fig. 5.4 gives the curves for that specific geometry with a high-pass filter of 0.3 mm in diameter.

The effect of different filter sizes is displayed in Fig. 5.5. A very small filter has the least effect on the incoming light. Our theory indicates that the normalized variance is very close to that of raw beam at the entrance. We also noticed that with a larger filter, the peak shifts to the high turbulence direction as expected.

6. Experimental Results

6.1. Introduction

Previous work on remote sensing of turbulence strength has suggested basically two categories of instrumentation that are responsive to the changes of the turbulence strength along the light path. The first uses the linear relationship between the log intensity variance for a spherical wave and the path integrated turbulence strength at low to moderate turbulence levels. The second, which uses focal plane statistics to measure the turbulence level, was proposed by Artem'yev²² in 1969. Recent improvements were made by other Russian scientists^{19,21} in 1982 and 1984 respectively. This method uses the changes of half-width of intensity on the focal plane of the receiver lens to measure the strength of the turbulence. The arrangement includes a well designed receiver lens and a moving mechanical system at the location of the focal plane. A slow scanning mechanism consisting of a narrow slot and attached photo-sensing receiver is driven by a motor and travels back and forth across the focal plane. Mironov³³ described a typical instrument having the following system parameters:

Receiver lens: 15 cm diameter
Focal length : 1.6 m
Width of slot: $20 \times 10^{-6} m$
Scan speed: 0.113 mm/minute

The theory of above system is based on the calculation of the intensity distribution on the focal plane for a collimated laser beam. Under quadratic approximation for the wave structure function and assuming a Gaussian lens aperture, the following formulas were obtained ¹⁹ :

$$C_n^2 = \frac{0.86\mu(y_f/F^t)^{5/3}}{2.91k^{1/3}L} \quad (6.1)$$

where $\mu = 1$ for plane wave, $\mu = 1.2^{5/3}$ for space-limited Gaussian beam and $\mu = 3.0^{5/6}$ for spherical wave input.

The major disadvantage of this approach is the moving part in the receiver system and its small dynamic range.

Our theory of spatial filtering suggests a new approach of remote sensing of the path integrated turbulence which has no moving parts and can be conveniently implemented on an existing telescope by inserting a high-pass spatial filter on the image plane of the telescope and attaching a photosensitive receiver. We first discuss several aspects of experiment design for the spatial filtering receiver.

The most important parameters of the system are 1) the aperture of the receiver lens, 2) the size of the filter, 3) the system noise level, 4) the transmission ratio of the filter, and 5) the size of the pin-hole of the photoreceiver.

- 1) The aperture of receiver lens.

According to our theory, the log of the mean intensity on the output axis of the two-lens spatial filtering system is linearly related to the log of the path-integrated turbulence in a specific range. The lower limit of the linear dependence is mainly determined by the aperture of the receiver lens which is known as the diffraction limit.

2) The size of the filter.

By properly choosing the diameter of the high-pass filter, one can determine the range of turbulence level that can be measured. A smaller filter size reduces the range and shifts it toward the low turbulence end.

3) The system noise level

The thermal noise from the electronics system and the shot noise from the photomultiplier are the sources of the noise that restrict the lower limit of turbulence detection. However, another factor which behaves like a noise source is the imperfectness of all optical passages (optical noise). The measurement is based on the scattering of the light by turbulent eddies in the atmosphere. Hence, the scattering by any particle, dust or small object in the light path will also be detected. As a result, the mean intensity can not follow the variation of turbulence below a specific level determined by the optical noise.

4) The transmission of the filter.

Theoretically, a high-pass spatial filter can have zero transmission at the center. But in practice, this is technically impossible. Most filters have a finite non-zero center transmission. This needs to be taken into

consideration especially at the lower end of the turbulence level. At this end, the majority of incoming light is focused at the center. Even a tiny part of the residue transmitted center light is comparable to the light scattered by the turbulence eddies. The effect of residue center transmission is to further reduce the dynamic range at the lower end of turbulence level.

5) The aperture of the photosensitive receiver.

The theory of the mean intensity and intensity variance is developed based on a point-receiver model. The finite pin-hole size of the receiver represents spatial averaging which is more critical for intensity variance. In order to avoid aperture averaging effects, the effective diameter of the pin-hole is chosen to be much smaller than the coherence length of the incoming light. Considering the effective diameter, the ratio of focal length of the two lenses in the receiver has to be taken into account, if they are different. The mean intensity on the other hand, is not so critically related to the pin-hole size because it is already a time-averaged quantity. Therefore, spatial averaging does not deteriorate the performance under the ergodicity assumption.

The quantitative relationship of the above factors can be studied in more detail by using the figures obtained in the theoretical section. The following experiments have been designed and conducted to verify the theory.

1. Experiment in tank simulated turbulence.
2. Line of sight propagation in open field.
3. Speckle propagation in open field.

6.2. Mean Intensity Measurement

The mean intensity output of the optical high-pass filtering system is responsive to the changes of the path-integrated turbulence levels as well as other factors. In order to eliminate the effect of other meteorological parameters, the drift of laser output power and the change in background illumination condition, the intensity is normalized according to the following rule.

1) Before taking intensity data under spatial filtering, first take the saturation intensity I_s and the bias intensity I_b . I_s is the intensity output of the system without the high-pass filter, that is, the maximum intensity available at the current turbulence condition. I_b is the intensity output with the filter in place and the laser turned off. This is the total amount of background radiation that reaches the receiver output.

2) The intensity data are taken immediately after I_s and I_b . During this data taking period, special care was exercised to prevent the spatial orientation of the receiver from being affected by any foreign source of vibration and even unnecessary motion of the operator. The normalized mean intensity is thus given by the following formula:

$$\langle I_n \rangle = \frac{\langle I \rangle - \langle I_b \rangle}{\langle I_s \rangle - \langle I_b \rangle}$$

It was found from our data taking experience that the change of the meteorological conditions especially the change of beam refraction in the atmosphere due to the vertical temperature gradient can result in noticeable

displacement of the light image spot in the image plane for the line of sight case. Hence, the normalization procedure is required for each data taking period and the length of the data set is restricted to about 10 minutes when the meteorological conditions undergo swift changes such as just before and after sun set.

6.2.1. Experiment in laboratory simulated turbulence.

A tank full of alcohol equipped with heating and cooling systems³⁴ can be used to implement an artificial turbulence environment. The system provides controllable simulated turbulence with good repeatability. The measurement apparatus is shown schematically in Fig. 6.1. A point source is obtained from a He-Ne laser and a pin-hole spatial filter. The spherical wave propagates through the tank, is received by lens L_1 and enters the spatial filtering receiver. A part of the laser radiation is reflected upward by a mirror and received by photomultiplier PM2, from which the intensity variance is obtained and used to compare to the spatial filtering result. The turbulence level in the tank is monitored by a microthermal sensor array. To reduce system error, an expensive fourier transform lens with a full aperture of 7.5 cm was used for lens L_1 . The high-pass spatial filter was made by photocopying a pin-hole on a KODAK film plate and processing using a highest contrast formula. It can be seen from Fig. 6.1 that only a portion of the propagation path (the tank) is under the effect of turbulence. Hence, two

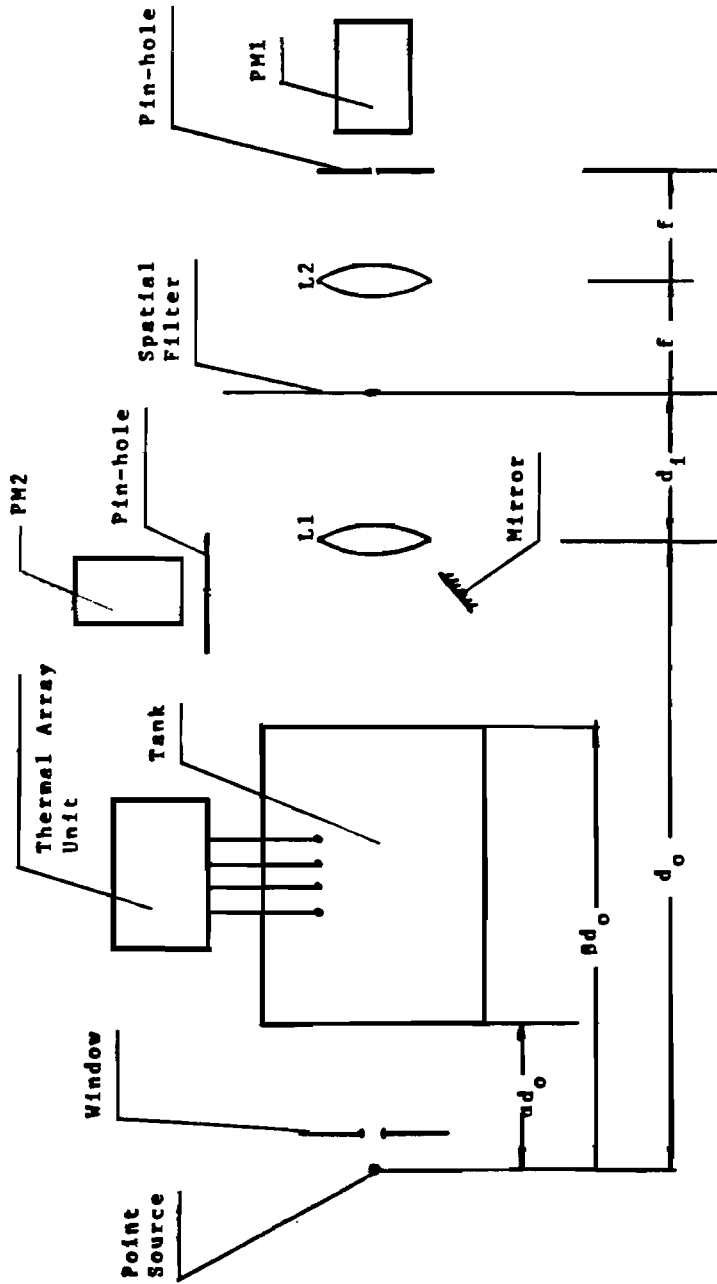


Fig. 6.1 Schematic illustration of the turbulence simulation tank and instrumentations for turbulence measurement.

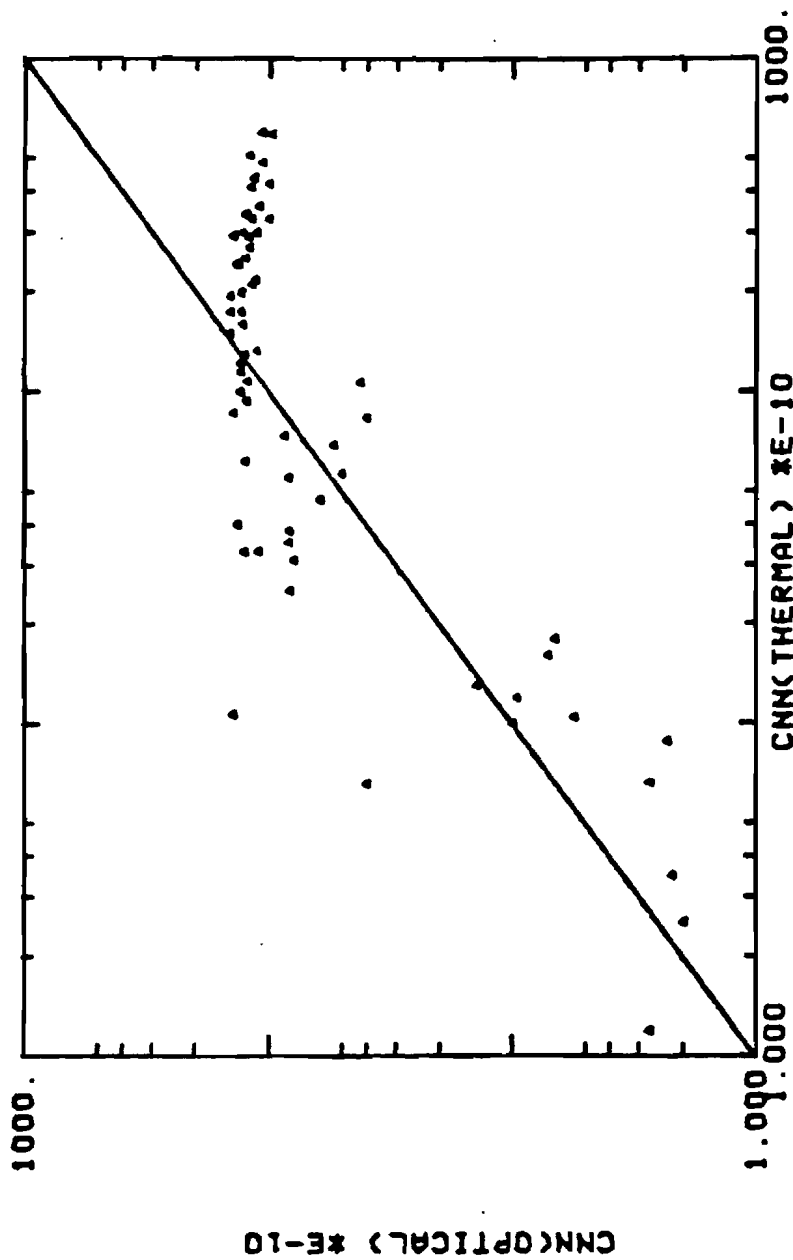


Fig. 6.2 Output of optical intensity variance vs. turbulence levels

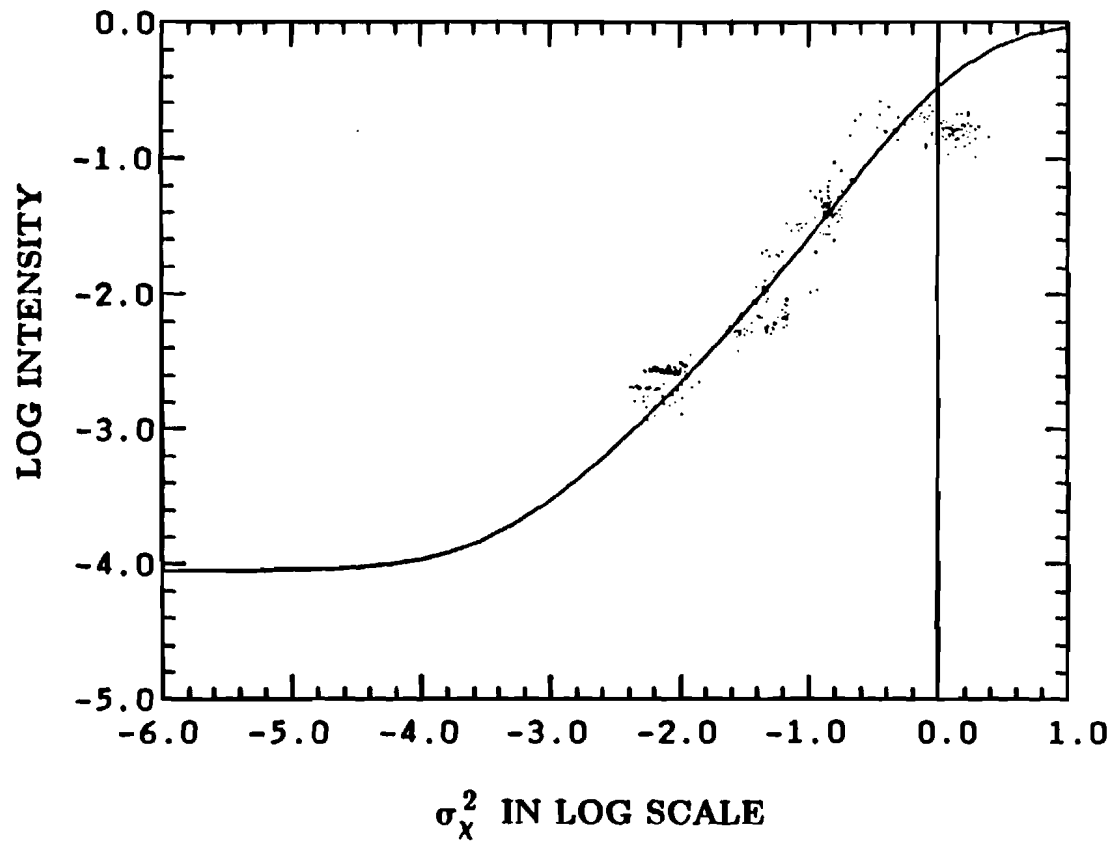


Fig. 6.4 Line of sight propagation. Experimental results of mean intensity after optical spatial filtering vs. σ_x^2 . Solid line is theoretical curve. Each dot represents the intensity averaged over 120 seconds.

under the given geometry. To further reduce the noise, a narrow band optical line filter was placed in front of the receiver pin-hole. The receiver electronics consists of a band-pass amplifier of 100 k Hz with bandwidth of 10 k Hz and a linear mean square detector.

A microthermal probe system (Model MT-2 by Oregon Graduate Center) is placed at the same height as the light path to measure the local temperature structure function data as a measure of turbulence strength. In addition, a separate optical measurement system (Laser Anemometer by Campbell Scientific Co.) is also used to provide the cross-wind and path-averaged turbulence data.

The measured data of normalized intensity output of the optical spatial filtering system is shown in Fig. 6.4 against the data of σ_x^2 obtained from the Campbell unit (at low to moderate turbulence levels) and microthermal measurement (above the level that optical measurement was saturated).

6.2.3. Speckle propagation in turbulent atmosphere

The measurement of spatially filtered mean intensity was conducted at the optical propagation site located on the campus of the Oregon Graduate Center. The structures of the transmitter and receiver are shown in Fig. 6.5 and 6.6 respectively. The diffuse reflector is located 290 meters away from the transmitter-receiver end, and the light path is around 2 meters high above the ground. The whole measurement system were redesigned and

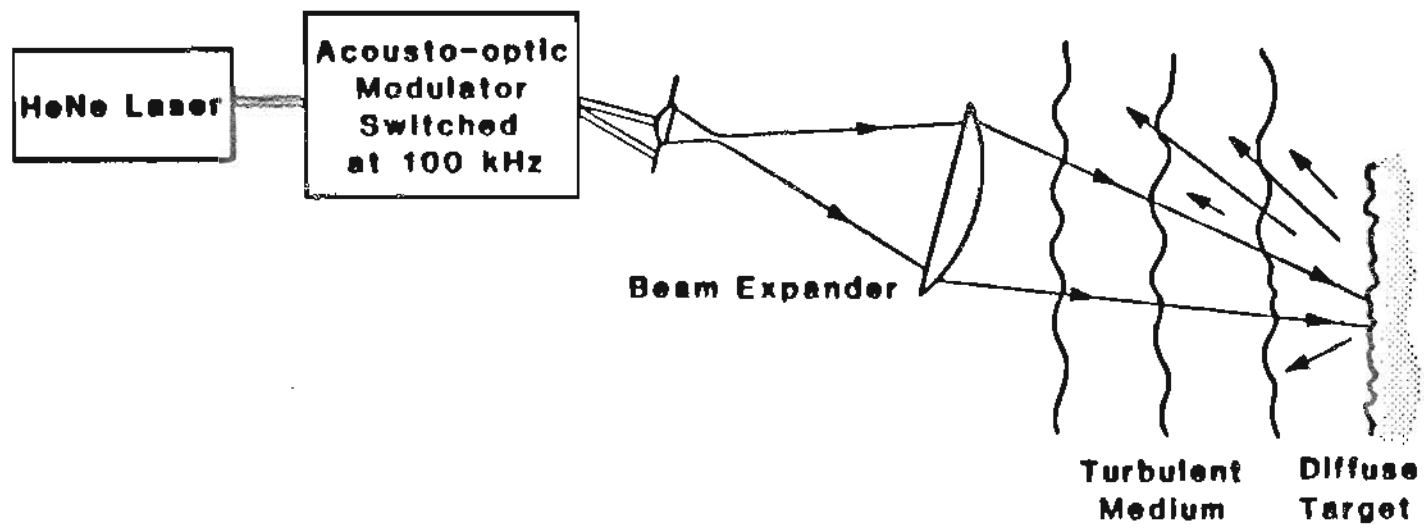


Fig. 6.5 Structure of Transmitter in a Single Ended Remote Sensing System

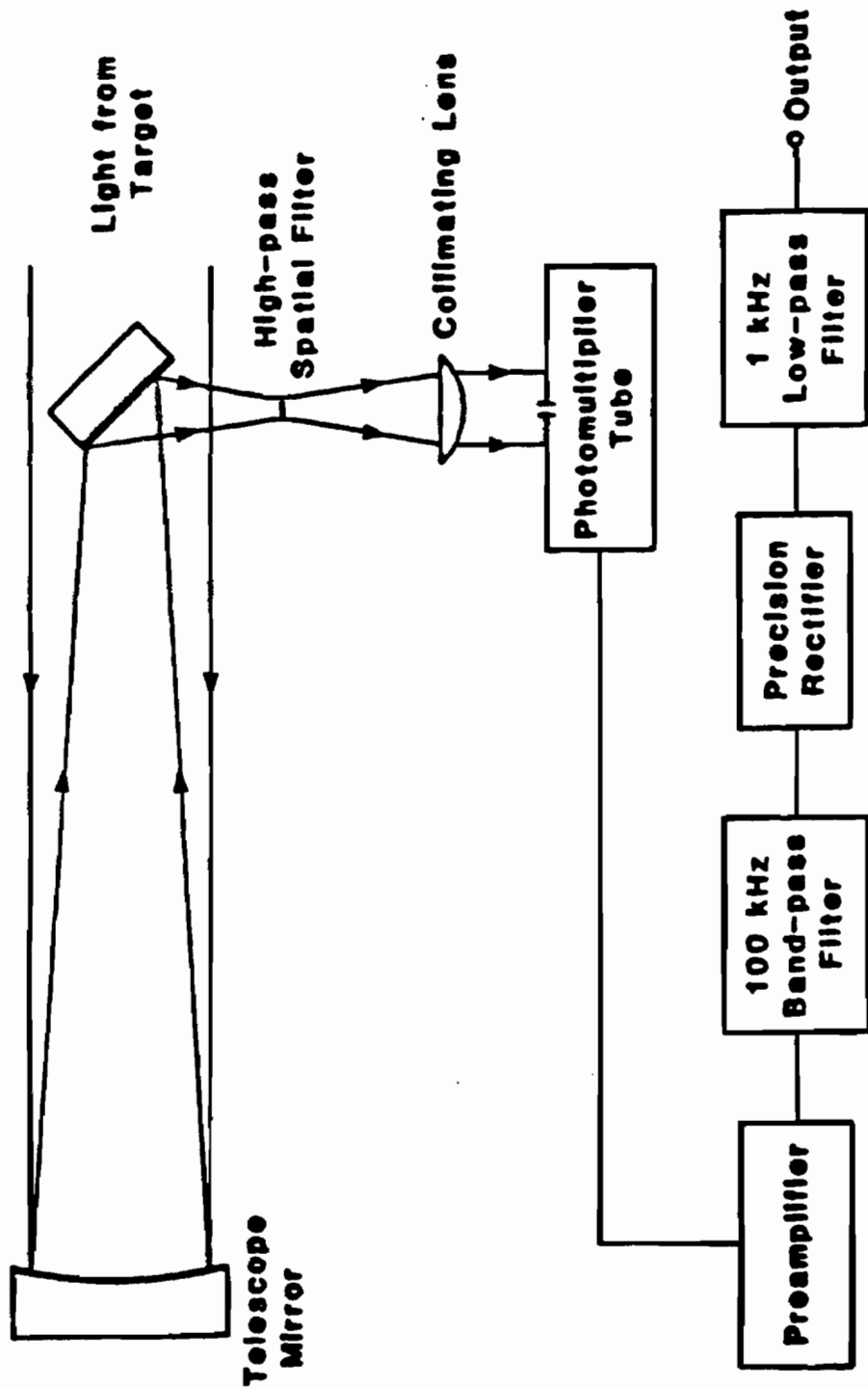


Fig. 6.6 Structure of Receiver in a Single Ended Remote Sensing System

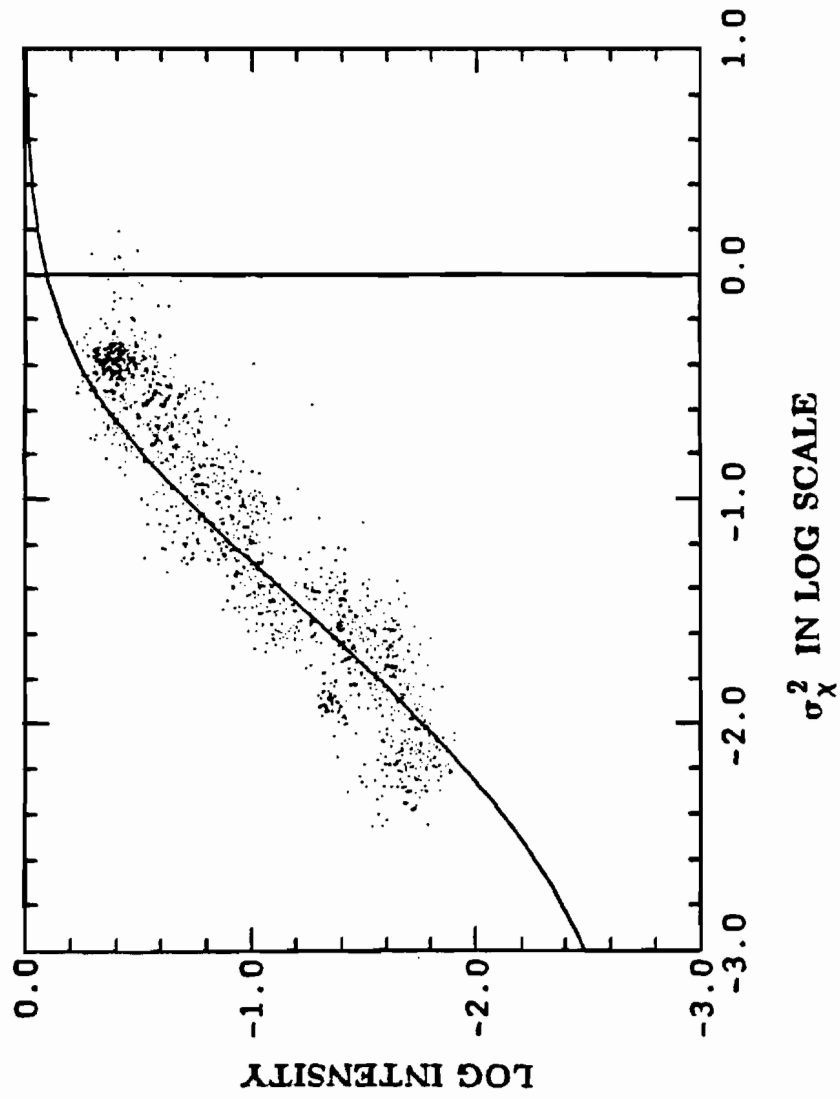


Fig. 6.7 Speckle propagation. Experimental results of mean intensity after optical spatial filtering vs. σ_x^2 . Solid line is theoretical curve. Each dot represents the intensity averaged over 6 seconds.

improved by John Hunt (senior engineer) and Todd Cloninger (graduate student) of Oregon Graduate Center. The transmitter is based on a 5-mw He-Ne laser, with an acoustic-optical modulator and a high quality beam expander. The average power of the exit beam is two milliwatt (chopped at 50-50 duty cycle) with a beam width of 3 cm, focusing on the target. The target is made of Scotchlite reflector (3M Sprint Marking Paper) with a directional return which realizes a gain in signal strength of 1000 to 1 over the perfect Lambertian surface. To improve the signal to noise ratio, the high-pass spatial filter is made by metal evaporation technology, providing a center transmission below one of one-millionth in power ratio. A high-sensitivity photomultiplier is sealed in a receiver box with a pin-hole of 100 micrometer diameter. The pin-hole size is determined so that its equivalent diameter is less than the coherence length of the incoming speckle and hence aperture averaging can be ignored. In Fig. 6.7, the experimental mean intensity output were plotted against the turbulence level obtained from the data of σ_x from the Campbell anemometer.

6.3. Intensity Variance

The intensity variance measurement were conducted for the speckle propagation case. The variance data are normalized by the squared intensity and are displayed in Fig. 6.8. As a comparison, two theoretical curves with different value of the parameter η are plotted. The theory of the normalized variance for the speckle propagation predicts a bump above unity at

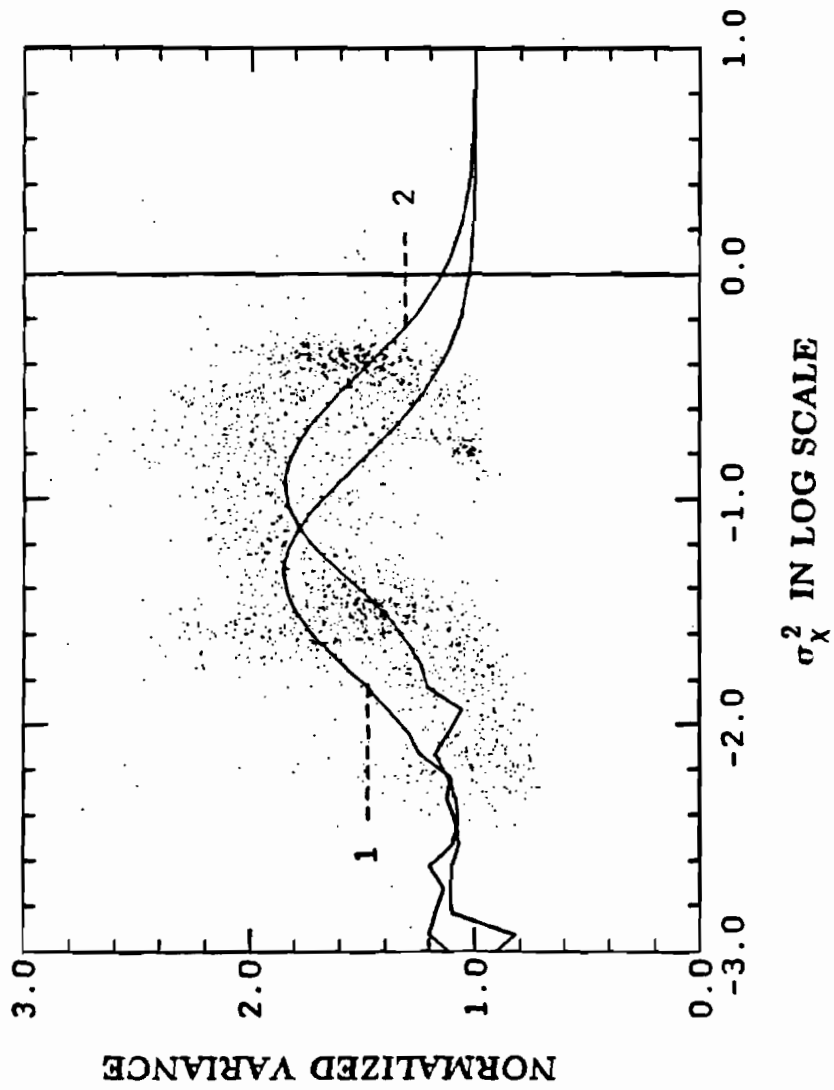


Fig. 6.8 Speckle propagation. Experimental results of normalized variance vs. σ_X^2 . Solid line is theoretical curve, 1--- $\alpha=3$, 2--- $\alpha=1$. Each dot represents 6 seconds averaged value.

intermediate turbulence levels. Even with some apparent ghost signals that come from vehicles passing across the path as well as from the scattering by water mist, the experimental data correctly reflect these features. It is worthwhile to note further that in the theory for the variance, the quadratic approximation was used in both the mean and correlation statistics of the intensity. Along with Fig. 3.10, our work shows that for precision measurement, the quadratic approximation needs factoring adjustment. This is because the optical spatial filtering process includes cancellation of several terms: four in the mean calculation and 16 in the correlation calculation. Consequently, the error due to using the quadratic approximation is highly enhanced.

7. Conclusions

We have studied the general theory of an optical spatial filtering system with application to remote sensing of atmosphere turbulence. The OSF technique has been analyzed fully in quantitative description and the application of optical high-pass filtering to remote sensing of turbulence has also been studied in detail.

(1) A system model was proposed which leads to a closed form for the Green function of a conventional spatial filtering system. In order to get a closed form, a Gaussian lens and filter profile was assumed. In the development, Fresnel diffraction formulation was used throughout the analysis. This model contains all of the system parameters and thus can be used elsewhere to analyze the quantitative effects of such a system in image processing, feature recognition, and other applications.

(2) It was found theoretically and verified by our experiments that the log of the mean output intensity is linearly related to the log of the path-integrated turbulence within a specific range. According to the theory, system parameters such as transmitter and receiver lens aperture, focal length, filter size, etc. can be so chosen in a combination that the linear range will meet the requirements of most remote sensing circumstances.

(3) The averaged intensity variance of the output of the optical spatial filtering receiver is given in closed form. It is shown that the normalized out-

put intensity variance rises above zero for line of sight propagation and above unity for the speckle propagation case at an intermediate level of the path-integrated turbulence level. The location of the peak corresponds to the turbulence value at which the mean intensity changes most sharply.

The 5/3 law model of refractivity fluctuations which can be justified by analysis and supported by experiments, remains a major obstacle in obtaining expressions in closed form. This becomes more serious for problems involving higher order statistics or complex processing steps. It is then a common practice to use quadratic in stead of 5/3 law as an approximation in the analysis of more complex problems. However, this can lead to serious error in the results^{35,36}.

In the process of this research, we approached this question in two ways. First, we have developed a closed form expansion for the integrals involving fractional power (Appendix 2). This expansion has good accuracy and can be used in the numerical analysis to solve complex problems in the wave propagation through turbulence. Second, we have developed the formulas for the intensity after optical spatial filtering process under both 5/3 and quadratic structure functions. By comparing with the experimental data, the model errors of quadratic approximation for different turbulence levels are fully displayed. Our result show that the major effect under this approximation is that the slope of the intensity curve changes substantially, which can not be explained satisfactorily by the traditional estimate of 4% change in coherence length.

References

1. E. Abbe, *Archiv. Mikroskopische Anat.*, vol. 9, p. 413, 1893.
2. A. B. Porter, "On the diffraction theory of microscope vision," *Phil. Mag.*, vol. 6, p. 11:154, 1906.
3. M. Born and E. Wolf, *Principles of Optics*, Pergamon Press, New York, 1959.
4. A. Toepler, *Pogg. Ann. Phys. Chem.*, vol. 127, p. 556, 1866.
5. H. Taylor and J. Waldrum, *J. Sci. Inst.*, vol. 10, p. 378, 1933.
6. R. Edmonson, E. Gayhart, and J. Olsen, *J. Opt. Soc. Am.*, vol. 42, p. 989, 1952.
7. F. Zernike, "Phase contrast, a new method for the microscopic observation of transparent objects," *Physica*, vol. 9, pp. 686-698, 974-986, 1942.
8. E. L. O'Neill, "Spatial filtering in optics," *IRE Trans. Inf. Theo.*, pp. 56-65, June 1956.
9. L. J. Cutrona, E. N. Leith, C. J. Palermo, and L. J. Porcello, "Optical data processing and filtering systems," *IRE Trans. Inf. Theo.*, pp. 386-400, June 1960.
10. M. W. Taylor, "An application of the method of phase contrast to gas flow visualization," *Proc. AIAA Inter. Meeting & Tech. Display*, Baltimore, May 1980.
11. R. C. Anderson and M. W. Taylor, "Phase contrast flow visualization," *Appl. Opt.*, vol. 21, pp. 528-536, Feb. 1982.

12. P. Mohana Shanker and H. M. Gupta, "Spatial filtering in speckle," *Opt. Letters*, vol. 4, pp. 99-101, March 1979.
13. J. A. Blodgett and R. L. Easton, Jr, "Two-stage spatial filtering for diffraction pattern analysis," *Appl. Opt.*, vol. 20, pp. 1050-1055, March 1981.
14. M. Francon, "Laser speckle and related phenomena, edited by J. C. Dainty," *Topics in Applied Physics, Vol. 9*, Springer, Berlin, 1975.
15. J. B. Chen and F. P. Chiang, "Statistical analysis of whole-field filtering of specklegram and its upper limit of measurement," *J. Opt. Soc. Am.*, vol. 1, pp. 845-849, Aug. 1984.
16. J. W. Goodman, *Introduction to Fourier Optics*, McGraw-Hill, 1978.
17. E. Hecht, *Optics, second Ed.*, Addison-Wesley, 1987.
18. N. G. Denisov and V. I. Tatarskii, *Izv. Vyssh. Uchebn. Zaved. Radiofiz.*, vol. 6, pp. 488-494, 1963.
19. M. S. Belen'kii, V. V. Boronoev, N. Ts. Gomboev, and V. L. Mironov, "Measurement of atmospheric-turbulence-structure parameter using a space-limited laser beam," *Opt. Letters*, vol. 5, pp. 67-69, Feb. 1982.
20. M. S. Belen'kii, A. I. Kon, and V. L. Mironov, "Turbulent distortions of the spatial coherence of a laser beam," *Sov. J. Quantum Electron*, vol. 7, pp. 287-290, March 1977.
21. V. P. Aksenov, V. A. Banakh, V. M. Buldakov, V. L. Mironov, and O. V. Tikhomirova, "Intensity fluctuations of light in the focal plane of a receiving telescope caused by round-trip propagation through a

- turbulent atmosphere," *Opt. letters*, vol. 10, pp. 107-109, April 1984.
22. A. V. Artem'yev, "Distortion of coherence by atmospheric turbulence," *Radio Eng. Elec. Phys.*, vol. 14, pp. 469-471, 1969.
 23. A. R. Lewis and V. H. Rumsey, *J. Opt. Soc. Am.*, vol. 67, pp. 178-181, 1977.
 24. R. F. Lutomirski and H. T. yura, "Propagation of a finite optical beam in an inhomogeneous medium," *Appl. Opt.*, vol. 10, pp. 1652-1658, July 1971.
 25. M. H. Lee, J. F. Holmes, and J. R. Kerr, "Statistics of speckle propagation through the turbulent atmosphere," *J. Opt. Soc. Am.*, vol. 66, pp. 1164-1172, Nov. 1976.
 26. A. Ishimaru, "Theory and application of wave propagation and scattering in random media," *Proc. IEEE*, vol. 65, pp. 1030-1061, July 1977.
 27. R. L. Fante, *Proc. IEEE*, vol. 68, pp. 1424-1444, Nov. 1980.
 28. S. F. Clifford, G. R. Ochs, and R. S. Lawrence, "Saturation of optical scintillation by strong turbulence," *J. Opt. Soc. Am.*, vol. 64, pp. 148-154, Feb. 1974.
 29. J. F. Holmes, M. H. Lee, and J. R. Kerr, "Effect of the log-amplitude covariance function on the statistics of speckle propagation through the turbulent atmosphere," *J. Opt. Soc. Am.*, vol. 70, pp. 355-360, Apr. 1980.
 30. J. C. Leader, "Intensity fluctuations resulting from partially coherent light propagating through atmospheric turbulence," *J. Opt. Soc. Am.*,

- vol. 69, pp. 73-84, Jan. 1979.
31. S. J. Wang, Y. Baykal, and M. A. Plonus, "Receiver-aperture averaging effects for the intensity fluctuation of a beam wave in the turbulent atmosphere," *J. Opt. Soc. Am.*, vol. 73, pp. 831-837, June 1983.
 32. H. T. Yura, "Mutual coherence function of a finite cross section optical beam propagating in a turbulent medium," *Appl. Opt.*, vol. 11, pp. 1399-1406, June 1972.
 33. V. L. Mironov, *Rasprastranenie Lasernovo Puchka v Turbulentnoi Atmosfere*, <nauka>, novosibirsk, 1981.
 34. R. A. Elliott, J. R. Kerr, and P. Pincus, "Optical propagation in laboratory-generated turbulence," *Appl. Opt.*, vol. 18, pp. 3315-3323, Oct. 1979.
 35. J. C. Leader, "Atmospheric propagation of partially coherent radiation," *J. Opt. Soc. Am.*, vol. 68, pp. 175-185, Feb. 1978.
 36. S. C. H. Wang and M. A. Plonus, "Optical beam propagation for a spatially coherent source in the turbulent atmosphere," *J. Opt. Soc. Am.*, vol. 69, pp. 1297-1304, Sept. 1979.

Appendix 1

On Multidimensional Integration

Summary

Through two successive linear transformations, we proved that the 8-fold integral associated with the intensity fluctuation of a laser beam propagating through the turbulent atmosphere is equivalent to a 5-fold integral and thus direct numerical evaluation of the optically processed intensity fluctuation is feasible. The resultant integration formulas are directly applicable to the calculation of the intensity fluctuations of a laser beam after the receiver lens and/or the optical spatial filtering system.

1. Introduction

Consider the optical processing of the laser beam that has propagated through the turbulent atmosphere. The major difficulty associated with the second order statistics is the evaluation of the 8-fold integral which has no closed form solution and direct numerical evaluation takes too much computer time and is hard to implement. This similar problem has been approached in three ways. Wang *et al*,¹ utilized the quadrature approximation to the wave structure function to obtain a closed form for the intensity fluctuation. But the quadrature approximation is not well justified for the fourth moments of the field. Asymptotic method have been adopted to

evaluate the behavior of the intensity fluctuations under extreme conditions, but the behavior in the transition region remains unsolved. The Monte-Carlo method has also been used to solve the integration. But this method becomes very inefficient for high dimensions. In the following, we introduce a two-step linear transformation method and show that the 8-fold integral is equivalent to a 5-fold integral.

Consider the following general form of the integration:

$$I = \iiint\int d^2p_1 d^2p_2 d^2p_3 d^2p_4 \exp[-(B_i p_1^2 + B_j^* p_2^2 + B_k p_3^2 + B_l^* p_4^2)] \times H((p_2 - p_1), (p_3 - p_1), (p_4 - p_1), (p_3 - p_2), (p_4 - p_2), (p_4 - p_3)) \quad (1.1)$$

Where H is the fourth order MCF of the input field and is given by:

$$H = \exp - \left\{ \frac{2.91}{2} C_n^2 L k^2 \int_0^1 [|t(p_2 - p_1)|^{5/3} - |t(p_3 - p_1) - V\tau|^{5/3} + |t(p_4 - p_1) - V\tau|^{5/3} + |t(p_3 - p_2) - V\tau|^{5/3} - |t(p_4 - p_2) - V\tau|^{5/3} + |t(p_4 - p_3)|^{5/3}] dt \right\}$$

2. Linear Transformation (1)

Introduce

$$\begin{bmatrix} p_a \\ p_b \\ u \\ v \end{bmatrix} = \begin{bmatrix} 1/2 & -1/2 & -1/2 & 1/2 \\ 1/2 & 1/2 & -1/2 & -1/2 \\ 1 & -1 & 1 & -1 \\ 1/4 & 1/4 & 1/4 & 1/4 \end{bmatrix} \begin{bmatrix} p_1 \\ p_2 \\ p_3 \\ p_4 \end{bmatrix} \quad (1.1)$$

The inverse transformation is given by

$$\begin{bmatrix} p_1 \\ p_2 \\ p_3 \\ p_4 \end{bmatrix} = \begin{bmatrix} 1/2 & 1/2 & 1/4 & 1 \\ -1/2 & 1/2 & -1/4 & 1 \\ -1/2 & -1/2 & 1/4 & 1 \\ 1/2 & -1/2 & -1/4 & 1 \end{bmatrix} \begin{bmatrix} p_a \\ p_b \\ u \\ v \end{bmatrix}$$

It is easy to verify that the Jacobian of the transformation is $J = 1$.

Under this transformation, the arguments of the function H are given by

$$|p_2 - p_1| = |p_a + \frac{1}{2}u| = (p_a^2 + \frac{1}{4}u^2 + p_a u \cos(\theta_a - \theta_u))^{\frac{1}{2}}$$

$$|p_4 - p_3| = |p_a - \frac{1}{2}u| = (p_a^2 + \frac{1}{4}u^2 - p_a u \cos(\theta_a - \theta_u))^{\frac{1}{2}}$$

$$|p_1 - p_4| = |p_b + \frac{1}{2}u| = (p_b^2 + \frac{1}{4}u^2 + p_b u \cos(\theta_b - \theta_u))^{\frac{1}{2}}$$

$$|p_2 - p_3| = |p_b - \frac{1}{2}u| = (p_b^2 + \frac{1}{4}u^2 - p_b u \cos(\theta_b - \theta_u))^{\frac{1}{2}}$$

$$|p_1 - p_3| = |p_a + p_b| = (p_a^2 + p_b^2 + 2p_a p_b \cos(\theta_a - \theta_b))^{\frac{1}{2}}$$

$$|p_4 - p_2| = |p_a - p_b| = (p_a^2 + p_b^2 - 2p_a p_b \cos(\theta_a - \theta_b))^{\frac{1}{2}}$$

thus the function H can be expressed as:

$$H = H_1(p_a, p_b, u, \theta_a - \theta_u, \theta_b - \theta_u, \theta_a - \theta_b) \quad (1.2)$$

It can be seen from (1.2) that the variables v and θ_u are not included in the function H explicitly and thus the integration regarding to these two

variables can be worked out analytically.

Under this transformation, the exponential terms take the form:

$$\begin{aligned}
 F &= (B_i p_1^2 + B_j^* p_2^2 + B_k p_3^2 + B_l^* p_4^2) \tag{1.3} \\
 &= \frac{1}{4}(B_i + B_j^* + B_k + B_l^*) \times (p_a^2 + p_b^2 + \frac{1}{4}u^2 + 4v^2) + \\
 &\quad + \frac{1}{2}(B_i - B_j^* + B_k - B_l^*) p_a \cdot p_b + \frac{1}{4}(B_i + B_j^* - B_k - B_l^*) p_a \cdot u \\
 &\quad + (B_i - B_j^* - B_k + B_l^*) p_a \cdot v + \frac{1}{4}(B_i - B_j^* - B_k + B_l^*) p_b \cdot u \\
 &\quad + (B_i + B_j^* - B_k - B_l^*) p_b \cdot v + \frac{1}{2}(B_i - B_j^* + B_k - B_l^*) u \cdot v
 \end{aligned}$$

To further simplify the integral, introduce the following notation:

$$\begin{aligned}
 B_{tt}(kk) &= \frac{1}{4}(B_i + B_j^* + B_k + B_l^*) \\
 B_{ab}(kk) &= \frac{1}{2}(B_i - B_j^* + B_k - B_l^*) \\
 B_{au}(kk) &= \frac{1}{4}(B_i + B_j^* - B_k - B_l^*) \\
 B_{av}(kk) &= (B_i - B_j^* - B_k + B_l^*) \\
 B_{bu}(kk) &= \frac{1}{4}(B_i - B_j^* - B_k + B_l^*) \\
 B_{bv}(kk) &= (B_i + B_j^* - B_k - B_l^*) \\
 B_{uv}(kk) &= \frac{1}{2}(B_i - B_j^* + B_k - B_l^*)
 \end{aligned}$$

where we have the sequential index $kk = 8(i-1) + 4(j-1) + 2(k-1) + l$.

The function F can be written in a simple form as

$$F = B_{tt}(kk)(p_a^2 + p_b^2 + \frac{1}{4}u^2 + 4v^2) + B_{ab}(kk)\mathbf{p}_a \cdot \mathbf{p}_b + B_{au}(kk)\mathbf{p}_a \cdot \mathbf{u} + B_{av}(kk)\mathbf{p}_a \cdot \mathbf{v} + \\ + B_{bu}(kk)\mathbf{p}_b \cdot \mathbf{u} + B_{bv}(kk)\mathbf{p}_b \cdot \mathbf{v} + B_{uv}(kk)\mathbf{u} \cdot \mathbf{v} \quad (1.4)$$

The integral on v can be worked out and the integral (1) takes the following form:

$$I = \frac{\pi}{4B_{tt}(kk)} \int \int \int dp_a^2 dp_b^2 du^2 \exp \left\{ - [P_{aa}(kk) p_a^2 + P_{bb}(kk) p_b^2 + P_{uu}(kk) u^2 + \\ + P_{ab}(kk) \mathbf{p}_a \cdot \mathbf{p}_b + P_{au}(kk) \mathbf{p}_a \cdot \mathbf{u} + P_{bu}(kk) \mathbf{p}_b \cdot \mathbf{u}] \right\} \quad (1.5)$$

Where :

$$P_{aa}(kk) = (16B_{tt}(kk)^2 - B_{av}(kk)^2) / 16B_{tt}(kk) \\ P_{bb}(kk) = (16B_{tt}(kk)^2 - B_{bv}(kk)^2) / 16B_{tt}(kk) \\ P_{uu}(kk) = (16B_{tt}(kk)^2 - B_{uv}(kk)^2) / 16B_{tt}(kk) \\ P_{ab}(kk) = (16B_{tt}(kk) \times B_{ab}(kk) - 2B_{av}(kk) \times B_{bv}(kk)) / 16B_{tt}(kk) \\ P_{au}(kk) = (16B_{tt}(kk) \times B_{au}(kk) - 2B_{av}(kk) \times B_{uv}(kk)) / 16B_{tt}(kk) \\ P_{bu}(kk) = (16B_{tt}(kk) \times B_{bu}(kk) - 2B_{bv}(kk) \times B_{uv}(kk)) / 16B_{tt}(kk)$$

Particularly, we consider the case when $B_i = B_j = B_k = B_l = B$, we have

$$F = \frac{1}{2}(B + B^*)(p_a^2 + p_b^2 + \frac{1}{4}u^2 + 4v^2) + (B - B^*)(\mathbf{p}_a \cdot \mathbf{p}_b + \mathbf{u} \cdot \mathbf{v}) \quad (1.6)$$

Thus the integral with respect to \mathbf{v} can be worked out:

$$I_v = \int \int \exp[-2(B + B^*)v^2 - (B - B^*)\mathbf{u} \cdot \mathbf{v}] d^2v \\ = \left[\frac{\pi}{2(B + B^*)} \right] \exp\{[(B - B^*)^2 u^2 / 8(B + B^*)]\}$$

After the first transformation, the explicit form of the integral I is given by

$$I = \iiint d^2 p_a d^2 p_b d^2 u \exp \left\{ - \left[\frac{1}{2} (B+B^*) (p_a^2 + p_b^2) + \frac{|B|^2}{2(B+B^*)} u^2 + (B-B^*) p_a \cdot p_b \right] \right\} \\ \times H \left(- \left(p_a + \frac{1}{2} u \right), - \left(p_a + p_b \right), - \left(p_b + \frac{1}{2} u \right), - \left(p_b - \frac{1}{2} u \right), p_a - p_b, p_a - \frac{1}{2} u \right) \quad (1.7)$$

We rewrite H in the following form:

$$H = H_1 (p_a, p_b, u ; \theta_a - \theta_u, \theta_b - \theta_u, \theta_a - \theta_b)$$

The angular integral will be discussed further in the next section.

3. Linear Transformation (2)

Consider the general form of the angular part of the above integration:

$$I_\theta = \int_0^{2\pi} \int_0^{2\pi} \int_0^{2\pi} S (\theta_a - \theta_u, \theta_b - \theta_u, \theta_a - \theta_b) d\theta_a d\theta_b d\theta_u$$

Introduce the transformation:

$$\begin{bmatrix} \theta_1 \\ \theta_2 \\ \theta_3 \end{bmatrix} = \begin{bmatrix} 1 & 0 & -1 \\ 0 & 1 & -1 \\ 1/2 & 1/2 & 0 \end{bmatrix} \begin{bmatrix} \theta_a \\ \theta_b \\ \theta_u \end{bmatrix} \quad (1.8)$$

The inverse transformation is

$$\begin{bmatrix} \theta_a \\ \theta_b \\ \theta_u \end{bmatrix} = \begin{bmatrix} 1/2 & -1/2 & 1 \\ -1/2 & 1/2 & 1 \\ -1/2 & -1/2 & 1 \end{bmatrix} \begin{bmatrix} \theta_1 \\ \theta_2 \\ \theta_3 \end{bmatrix}$$

The Jacobian is also unity. This transformation maps the cube with sides 2π in the $\theta_a\theta_b\theta_u$ space into a rhomb in the new space of $\theta_1\theta_2\theta_3$. The vertexes (a-h) are related by the following correspondence:

$$\begin{array}{l}
 \theta_a\theta_b\theta_u \text{-----} \theta_1\theta_2\theta_3 \\
 a = (0, 0, 0) \text{-----} a = (0, 0, 0) \\
 b = (2\pi, 2\pi, 2\pi) \text{-----} b = (0, 0, 2\pi) \\
 c = (0, 2\pi, 0) \text{-----} c = (0, 2\pi, \pi) \\
 d = (0, 2\pi, 2\pi) \text{-----} d = (-2\pi, 0, \pi) \\
 e = (0, 0, 2\pi) \text{-----} e = (-2\pi, -2\pi, 0) \\
 f = (2\pi, 0, 2\pi) \text{-----} f = (0, -2\pi, \pi) \\
 g = (2\pi, 0, 0) \text{-----} g = (2\pi, 0, \pi) \\
 h = (2\pi, 2\pi, 0) \text{-----} h = (2\pi, 2\pi, 2\pi)
 \end{array}$$

The correspondences are displayed in Fig. A1.1. We noticed that under this transformation, the variable θ_3 is not included in the function S. Indeed, we have

$$I = \iiint S (\theta_1, \theta_2, \theta_1 - \theta_2) d\theta_1 d\theta_2 d\theta_3 \quad (1.9)$$

Denoting the projection of the rhomb on $\theta_1\theta_2$ plane by D (Fig. A1.2), the integral over θ_3 can be worked out. To do this, the region D is cut into 6 sub-regions (I, II, III, I', II', III') and integrals are performed separately.

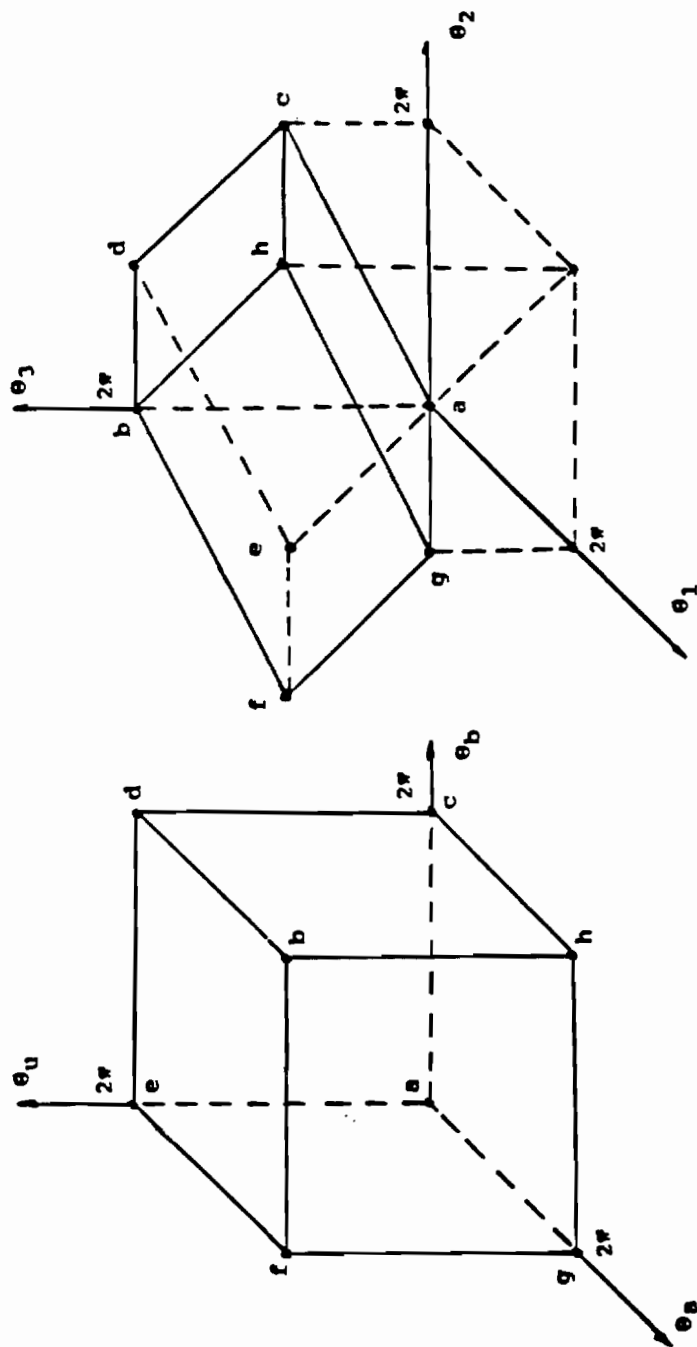


Fig. A1.1 Original space and new space

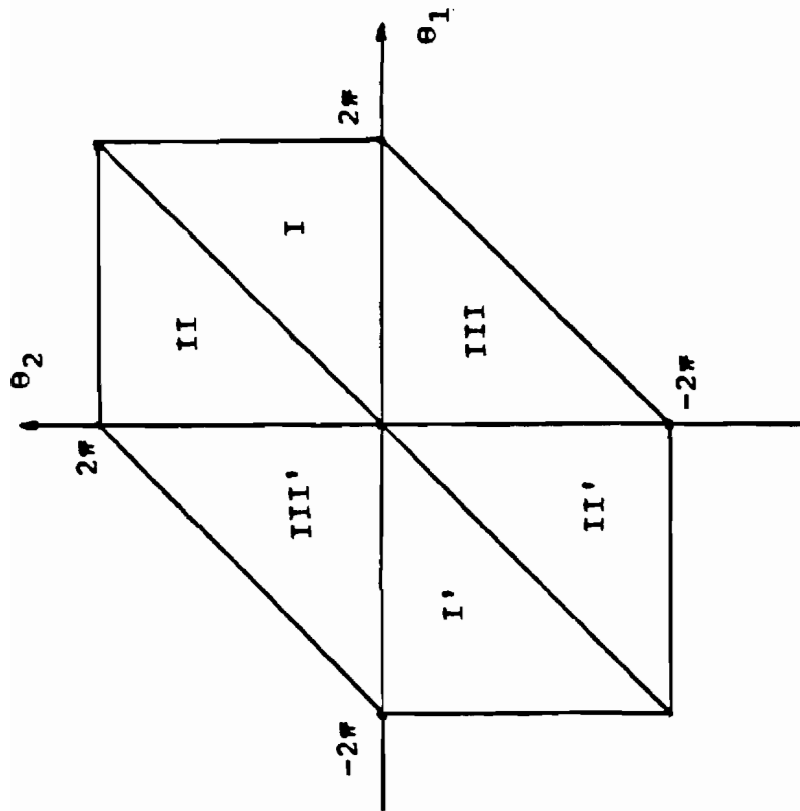


Fig. A1.2 Integration Region on θ_1, θ_2 Plane.

The final result is given by:

$$\begin{aligned}
 I_0 = & 2 \int_0^{2\pi} d\theta_1 (2\pi - \theta_1) \int_0^{\theta_1} S(\theta_1, \theta_2, \theta_1 - \theta_2) d\theta_2 \\
 & + 2 \int_0^{2\pi} d\theta_1 \int_{\theta_1}^{2\pi} (2\pi - \theta_2) S(\theta_1, \theta_2, \theta_1 - \theta_2) d\theta_2 \\
 & + 2 \int_0^{2\pi} d\theta_1 \int_0^{2\pi - \theta_1} (2\pi - \theta_1 - \theta_2) S(\theta_1, \theta_2, \theta_1 + \theta_2) d\theta_2
 \end{aligned} \tag{1.10}$$

Combine these two transformations together, the final expression of the integral (1) is

$$\begin{aligned}
 I = & \frac{\pi}{2(B+B^*)} \int_0^\infty \int_0^\infty p_a dp_a p_b dp_b u du \exp \left\{ - \left[\frac{1}{2}(B+B^*)(p_a^2 + p_b^2) + \frac{|B|^2}{2(B+B^*)} u^2 \right] \right\} \\
 & \times \left\{ \begin{aligned}
 & 2 \int_0^{2\pi} d\theta_1 (2\pi - \theta_1) \int_0^{\theta_1} d\theta_2 H_1(p_a, p_b, u; \theta_1, \theta_2, \theta_1 - \theta_2) \exp[-(B-B^*)p_a p_b \cos(\theta_1 - \theta_2)] \\
 & + 2 \int_0^{2\pi} d\theta_1 \int_{\theta_1}^{2\pi} d\theta_2 (2\pi - \theta_2) H_1(p_a, p_b, u; \theta_1, \theta_2, \theta_1 - \theta_2) \exp[-(B-B^*)p_a p_b \cos(\theta_1 - \theta_2)] \\
 & + 2 \int_0^{2\pi} d\theta_1 \int_0^{2\pi - \theta_1} d\theta_2 (2\pi - \theta_1 - \theta_2) H_1(p_a, p_b, u; \theta_1, \theta_2, \theta_1 + \theta_2) \exp[-(B-B^*)p_a p_b \cos(\theta_1 - \theta_2)]
 \end{aligned} \right\}
 \end{aligned} \tag{1.11}$$

Consequently, the original 8-fold integral has been converted to a 5-fold integral. To check the validity of the result above, let us calculate a simple

integration.

$$I = \int \int \int \int d^2 p_1 d^2 p_2 d^2 p_3 d^2 p_4 \exp[-(p_1^2 + p_2^2 + p_3^2 + p_4^2)]$$

This can be worked out as

$$I = \left(\int d^2 p e^{-p^2} \right)^4 = \pi^4$$

According to formula (11), we have

$$\begin{aligned} I &= \frac{\pi}{4} \int_0^\infty \int_0^\infty \int_0^\infty p_a dp_a p_b dp_b u du \exp \left[- \left(p_a^2 + p_b^2 + \frac{1}{4} u^2 \right) \right] \\ &\times 2 \left\{ \int_0^{2\pi} (2\pi - \theta_1) d\theta_1 \int_0^{\theta_1} d\theta + \int_0^{2\pi} d\theta \int_{\theta_1}^{2\pi} (2\pi - \theta_2) d\theta_2 + \int_0^{2\pi} d\theta_1 \int_0^{2\pi - \theta_1} (2\pi - \theta_1 - \theta_2) \right\} \\ &= 2\pi^4 \int_0^\infty e^{-p_a^2} p_a dp_a \int_0^\infty e^{-p_b^2} p_b dp_b \int_0^\infty e^{-\frac{u^2}{4}} u du \\ &= \pi^4 \end{aligned}$$

References

1. S. J. Wang, Y. Baykal, and M. A. Plonus, "Receiver-aperture averaging effects for the intensity fluctuation of a beam wave in the turbulent atmosphere," *J. Opt. Soc. Am.*, vol. 73, pp. 831-837, June 1983.

Appendix 2

Closed Form Expansions of the Four-point, Wave Structure Function for a Turbulent Atmosphere

1. Introduction

In the study of laser beam propagation through turbulent atmosphere, the end-processing of received light by optical instrument is often required. In imaging and communication system, telescope of all types are utilized to increase the sensitivity by collect more light using a larger entrance aperture^{1,2}. The receiver-aperture averaging effect were analyzed by several authors³⁻⁵. We have performed analysis on the effect of optical spatial filtering system on the statistics of laser radiation propagating through turbulence⁶⁻⁸. In optical communication system, to analyse the signal-to-noise ration (analog) or error rate (digital), the variance of received signal has to be evaluated⁹ and an calculation of the four-point wave structure function of the input wave is a necessary step. The four-point structure function is laso needed in the study of specklele propagation through turbulence¹⁰.

In the case of spherical wave propagation, the fourth moment of the input field is

$$\langle u_1(\mathbf{p}_1, 0) u_1^*(\mathbf{p}_2, 0) u_1(\mathbf{p}_3, \tau) u_1^*(\mathbf{p}_4, \tau) \rangle = \left(\frac{1}{\lambda d_o} \right)^4 \exp\left[\frac{ik}{2d_o} (p_1^2 - p_2^2 + p_3^2 - p_4^2) \right] \times H$$

(1)

and the wave structure function H is

$$H = \langle \exp[\psi(\mathbf{p}_1, 0; 0) + \psi^*(\mathbf{p}_2, 0; 0) + \psi(\mathbf{p}_3, 0; \tau) + \psi^*(\mathbf{p}_4, 0; \tau)] \rangle$$

Under weak turbulence assumption, the the wave structure function is dominant by phase. The mutual coherence function can be written as

$$H = \exp\left[-\frac{1}{2}(D_{12} - D_{13} + D_{14} + D_{23} - D_{24} + D_{34})\right]$$

where

$$\begin{aligned} D_{ij} &= \langle \psi(\mathbf{p}_i, \mathbf{p}_i; t_i) - \psi(\mathbf{p}_j, \mathbf{p}_j; t_j) \rangle \Big|_{\mathbf{p}_i = \mathbf{p}_j = 0} \\ &= \frac{2.91}{2} L k^2 \int_0^1 C_n^2(t) |t(\mathbf{p}_j - \mathbf{p}_i) - V(t_j - t_i)|^{5/3} dt \end{aligned}$$

where V is the cross wind and $t_j - t_i$ is the time delay.

The integration of concern is:

$$H(\mathbf{p}_1, \mathbf{p}_2, \mathbf{p}_3, \mathbf{p}_4; V\tau) =$$

$$\begin{aligned} &= \left\{ -\frac{2.91}{2} L k^2 \int_0^1 C_n^2 [|t(\mathbf{p}_2 - \mathbf{p}_1)|^{5/3} - |t(\mathbf{p}_3 - \mathbf{p}_1) - V\tau|^{5/3} + |t(\mathbf{p}_4 - \mathbf{p}_1) - V\tau|^{5/3} \right. \\ &\quad \left. + |t(\mathbf{p}_3 - \mathbf{p}_2) - V\tau|^{5/3} - |t(\mathbf{p}_4 - \mathbf{p}_2) - V\tau|^{5/3} + |t(\mathbf{p}_4 - \mathbf{p}_3)|^{5/3}] dt \right\} \quad (2) \end{aligned}$$

(2) is the form contained in time delayed intensity correlation which involves the cross-wind effect. Due to the high complexity, direct numerical evaluation of these integrals are very costly. In addition, D_{ij} is usually the argument of an exponential and to complicate matters further, the whole

expression usually needs to be integrated with respect to \mathbf{P} or \mathbf{Q} . If we introduce the quadratic assumption as defined below³⁻⁵:

$$\begin{aligned} \frac{1}{2}D_{31} &= \frac{1}{\rho_0^2} \int_0^1 [t(\mathbf{p}_3 - \mathbf{p}_1) - \mathbf{V}\tau]^2 dt \\ &= \frac{1}{\rho_0^2} \left[\frac{1}{3}(\mathbf{p}_3 - \mathbf{p}_1)^2 - (\mathbf{p}_3 - \mathbf{p}_1) \cdot \mathbf{V}\tau + V^2\tau^2 \right] \end{aligned}$$

It can be seen by direct substitution, that the cross wind effect is completely canceled out under the quadratic assumption:

$$H = \frac{1}{3\rho_0^2} [p_1^2 + p_2^2 + p_3^2 + p_4^2 + 2(p_3p_1 + p_4p_2 - p_2p_1 - p_4p_3 - p_2p_3 - p_4p_3)]$$

Another words, the quadratic assumption is not applicable to describe the cross-wind effect in the structure function of line of sight propagation and an efficient numerical algorithm is needed to perform the above integration.

2. Analysis

Consider the four-point time delayed wave structure function as defined below:

$$D_{\psi}(\mathbf{P}, \mathbf{Q}, \mathbf{V}, \tau) = \int_0^1 C_n^2(t) |t\mathbf{P} + (1-t)\mathbf{Q} - \mathbf{V}\tau|^{5/3} dt \quad (3)$$

where $C_n^2(t)$ is the index of refraction structure constant, \mathbf{V} is the cross wind, \mathbf{P} and \mathbf{Q} are two-dimensional spatial coordinate vectors, τ is the time delay and t is the normalized propagation distance from the source to the receiver.

To simplify the discussion, uniform turbulence is first considered, i.e. C_n^2 is a constant and not a function of position along the propagation path. The non-uniform turbulence case can then be handled by exactly the same technique as will be used for the uniform case. Thus for the uniform turbulence case and suppressing C_n^2 , the integral to be considered is

$$I = \int_0^1 |tP + (1-t)Q - V_T|^{5/3} dt \quad (3)$$

Making the following changes of variable:

$$R = P - Q \quad (4)$$

$$M = V_T - Q \quad (5)$$

The integral becomes

$$\begin{aligned} I &= \int_0^1 |tR - M|^{5/3} dt \\ &= \int_0^1 (M^2 + t^2 R^2 - 2tR \cdot M)^{5/6} dt \end{aligned}$$

where

$$\begin{aligned} M &= [M \cdot M]^{1/2} = [(V_T - Q) \cdot (V_T - Q)]^{1/2} \\ &= [V_T^2 + Q^2 - 2V_T \cdot Q]^{1/2} \end{aligned} \quad (7)$$

$$\begin{aligned} R &= [R \cdot R]^{1/2} = [(P - Q) \cdot (P - Q)]^{1/2} \\ &= [P^2 + Q^2 - 2P \cdot Q]^{1/2} \end{aligned} \quad (8)$$

$$R \cdot M = (V_T - Q) \cdot (P - Q)$$

$$= Q^2 - Q \cdot P - \tau V \cdot Q + \tau V \cdot P \quad (9)$$

If P, Q and V are now expressed in vector form as

$$P = \hat{x} P \cos\theta_p + \hat{y} P \sin\theta_p \quad (10)$$

$$Q = \hat{x} Q \cos\theta_q + \hat{y} Q \sin\theta_q \quad (11)$$

$$V = \hat{x} V \quad (12)$$

Then equations (7) - (9) can be expressed as

$$M = [V^2\tau^2 + Q^2 - 2\tau VQ \cos\theta_q]^{1/2} \quad (13)$$

$$R = [P^2 + Q^2 - 2PQ \cos(\theta_p - \theta_q)]^{1/2} \quad (14)$$

$$R \cdot M = RM \cos\theta = Q^2 - PQ \cos(\theta_q - \theta_p) - V\tau Q \cos\theta_q + V\tau P \cos\theta_p \quad (15)$$

It should be noted that no loss of generality will result from aligning the x axis with the wind so long as the wind direction does not change along the path length. The factor M^2 is now removed from the integrand which yields

$$I = M^{5/3} \int_0^1 (t^2 \rho^2 + 1 - 2t \rho \cos\theta)^{5/6} dt \quad (16)$$

where θ is the angle between M and R and can be determined from equations (7), (8) and (9) and $\rho = R/M$. For the case of $M = 0$, the integral can be evaluated directly and yields

$$I = \int_0^1 |tR - M|^{5/3} dt = \frac{8}{3} R^{5/3} \quad (17)$$

Also when $R = 0$,

$$I = \int_0^1 |tR - M|^{5/3} dt = M^{5/3} \quad (18)$$

The next step is to find an expansion for the function I that is accurate enough for all values of ρ and θ and also simple enough to be useful.

3. Approximate Expansion

What is desired is an efficient approximation for the integration of the type shown in Eq.(16) which is a function of two variables ρ and θ . The general behaviors of the integral (16) with respect to argument ρ and θ are shown in Fig. A2.1 and A2.2 respectively. The general approach of two-dimensional polynomial fitting was tried and the result was not satisfactory. It requires at least 6th order power polynomials in ρ dependence for a relative error of 5% in the range $0 < \rho < 10$, and each term requires another polynomial in θ to fit the angle variation. The resultant two-variable polynomial expression has 35 coefficients which must be determined from non-linear fitting. Also, the resultant formulation applies only for a finite range of $0 \leq \rho \leq 10$, due to the non-integer power of the integrand.

Another possible approach is to use the Gegenbauer function expansion¹¹ based on the following generating function

$$(1-2xz + z^2)^{-\alpha} = \sum_0^{\infty} C_n^{\alpha} z^n \quad (19)$$

This expansion has one restriction that z (in our case, ρ) is limited ($0 \leq z \leq 1$). It is in reality also a two-dimensional polynomial expansion.

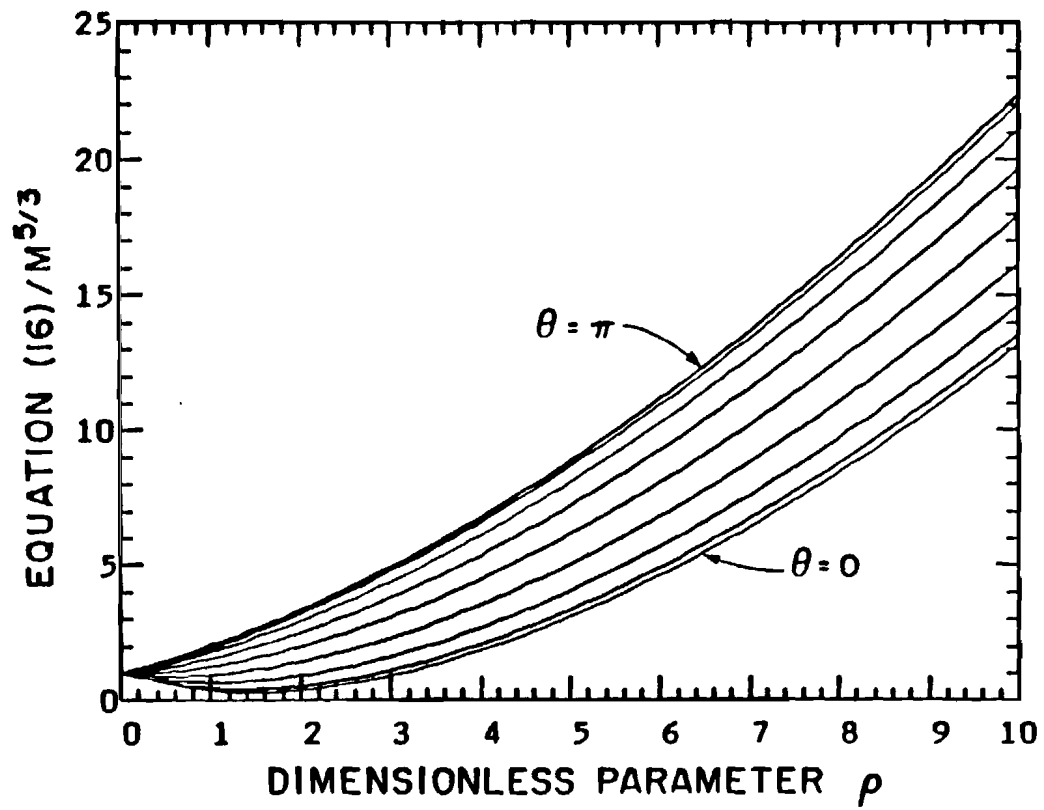


Fig. A2.1 Numerical integration of 1 as a function of ρ .

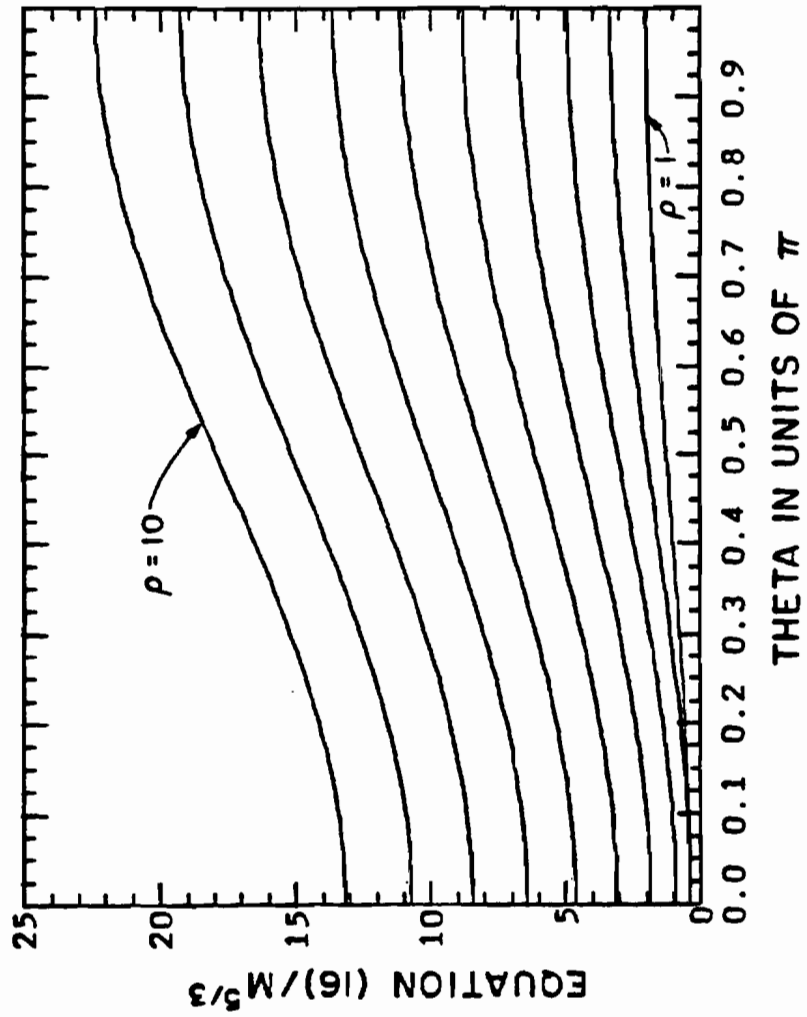


Fig. A2.2 Numerical integration of I as a function of θ .

Consequently it has the same problems with the non-integer power as the regular polynomial expansion.

In an attempt to find a useful expansion for Eq.(16), numerical work was done to gain some insight on how the expression behaves as a function of ρ and θ . It was found that: for a given ρ , the integral reaches its minimum at $\theta = 0$ and maximum at $\theta = \pi$; the angle dependence of the integral is symmetrical about π , and is periodic for each 2π increment; the ρ dependence is of fractional power; and for sufficiently large ρ , the integral has an asymptotic approximation of $I \approx \frac{3}{8} \rho^{5/3}$, which cannot be fitted with just a few integer power polynomials.

Based on this information, our approach was to expand the integral in a harmonic series in θ with coefficients dependent on ρ , solve the dependence on ρ explicitly for the first two terms as the foundation of the expression, and then to empirically fit the other coefficients in the series. This is advantageous because the $\rho^{5/3}$ dependence is preserved. Consequently, the expansion was accomplished using the following steps:

Obtain accurate analytical expressions $F_1(\rho)$ and $F_2(\rho)$ for I at $\theta = 0$ and $\theta = 2\pi$ respectively;

Solve the 1-D fitting problem for the a_i , at various values of ρ by using the formula

$$I(\rho, \theta) = [c(\rho) - d(\rho)\cos\theta] + a_1(\rho)|\sin\theta| + a_2(\rho)\cos(2\theta) + a_3(\rho)|\sin(2\theta)| + \dots \quad (20)$$

where

$$c(\rho) = (F_2(\rho) + F_1(\rho))/2 \quad (21)$$

is the average of Eq.(16) for $\theta = 0$ and π

and

$$d(\rho) = (F_2(\rho) - F_1(\rho))/2 \quad (22)$$

is the amplitude of the $\cos\theta$ dependence; then determine appropriate functions to approximate the $a_n(\rho)$. It should be noted that the absolute value signs on the sin functions are needed to accommodate the symmetrical nature of the integral with respect to $\theta = \pi$.

3.1. Step 1:

For $\theta = 0$ and π , Eq.(16) can be simplified to

$$I = \int_0^1 |1 \pm t\rho|^{5/3} dt$$

Performing the integrations, the results are

$$F_1(\rho) = \int_0^1 |1 - t\rho|^{5/3} dt = \frac{3}{8\rho} [1 - |1 - \rho|^{8/3}] \quad (\theta = 0) \quad (23)$$

$$F_2(\rho) = \int_0^1 |1 + t\rho|^{5/3} dt = \frac{3}{8\rho} [|\rho + 1|^{8/3} - 1] \quad (\theta = \pi) \quad (24)$$

$$F_1(\rho) = F_2(\rho) = 1.0 \quad (\rho = 0) \quad (25)$$

3.2. Step 2:

Depending on the required accuracy, the proper number of harmonic terms can be chosen from the expansion

$$H(\rho, \theta) = F_0(\rho, \theta) + a_1(\rho) |\sin \theta| + a_2(\rho) \cos(2\theta) + a_3(\rho) |\sin(2\theta)| + \dots \quad (26)$$

where

$$F_0(\rho) = c(\rho) - d(\rho) \cos \theta \quad (27)$$

and the $a_i(\rho)$'s are unknown functions of ρ . Then minimum mean square error fitting of the function $H(\rho, \theta)$ to the integral $I(\rho, \theta)$ can be used to generate a set of coefficients (a_1, a_2, \dots, a_k) for discrete values of ρ and θ . This is accomplished by solving the minimization problem

$$\frac{\partial E_i}{\partial a_j} = 0 \quad j = 1, 2, 3$$

where $E_i = [I(\rho_i, \theta_m) - H(\rho_i, \theta_m)]^2$ and $i = 1, 2, \dots, k$; $m = 1, 2, \dots, k$.

This process generates a matrix equation of order k which can be solved for the unknown a_i 's. A numerical study of the error distribution with respect to θ revealed that the error is dominated by small θ values. Consequently, to better optimize the fit more weight was put on small values of θ . This reduces the maximum error and results in a more uniform error distribution. The resultant coefficients and associated maximum relative errors are listed in tables 1-3 for the following three expansions:

$$H_1(\rho, \theta) = F_0(\rho, \theta) + a_1(\rho) |\sin \theta| \quad (28)$$

$$H_{12}(\rho, \theta) = F_0(\rho, \theta) + a_1(\rho) |\sin \theta| + a_2(\rho) \cos(2\theta) + a_3(\rho) |\sin(2\theta)| \quad (29)$$

and

$$H_{13}(\rho, \theta) = F_0(\rho, \theta) + a_1(\rho) |\sin \theta| + a_4(\rho) \cos(3\theta) + a_5(\rho) |\sin(3\theta)| \quad (30)$$

respectively.

Comparing the errors in tables 2 and 3, it can be seen that the next dominant term after the first harmonic is the 3rd rather than the second order harmonics. Consequently the three expansions that are proposed are expansion (28) with $a_1(\rho) = 0$; expansion (28) and expansion (30). In principle, additional harmonic terms could be included to further improve the accuracy, but this does not appear to be necessary. The coefficients in the tables could be used with a table look up scheme and interpolation to generate the function I. However, it is more convenient to use analytic forms for the coefficients and these will be generated in the next section.

3.3. Step 3:

The coefficients obtained from step 2 can now be fitted into appropriate functions of ρ . A study of the error distribution obtained from the second step shows that as ρ increases, the relative error decreases monotonically and the maximum error occurs at $\rho = 2$. Since the formulations that use the wave structure function are of the form $\exp(-I)$, for small ρ I is small and contributes the most to any integral formulation such as Eq.(2). Consequently, functions $a_i(\rho)$ were chosen that are close to the numerical data a_i 's for $\rho \leq 3$, exactly equal at $\rho=2$ and have a tolerable deviation from the data

at

larger ρ values. After studying the dependency of a_i with ρ , the following functional form was chosen:

$$a_i(\rho) = C_i(1 - \exp(-b_i\rho^2))$$

which automatically satisfies the requirement that $a_i(0) = 0$. The coefficients b_i and C_i were chosen by minimizing the mean square error (as a function of θ) at $\rho = 1$.

4. Final Results

Completing Step 3, the final results for the three expansions are as follows:

$$I = \frac{3}{8}R^{5/3} \quad (M = 0, \text{ all expansions}) \quad (31)$$

$$I = M^{5/3} \quad (R = 0, \text{ all expansions}) \quad (32)$$

Expansion 1 yields: (error $\leq 14\%$)

$$I = M^{5/3}F_0(\rho, \theta) \quad (33)$$

Expansion 2 yields: (error $\leq 2.88\%$)

$$I = M^{5/3}\{F_0(\rho, \theta) + 0.146(1 - \exp(-0.6684\rho^2))|\sin(\theta)|\} \quad (34)$$

Expansion 3 yields: (error $\leq 1.66\%$)

$$I = M^{5/3}\left\{F_0(\rho, \theta) + 0.1519(1 - \exp(-0.69\rho^2))|\sin\theta| - 0.33 \times 10^{-2}[1 - \exp(-0.59\rho^2)]\cos(3\theta) - 0.01[1 - \exp(-0.518\rho^2)]|\sin(3\theta)|\right\} \quad (35)$$

Where M , R , θ , and F_o are related back to the original problem variables by equations (13), (14), (15), and (27), $\rho = R/M$, and F_o is obtained from equations (21)-(25) and (27).

The relative errors of the three models are displayed in Figs. A2.3-A2.5 respectively. The ρ dependence in these figures is restricted to $\rho \leq 10$ because the error decreases continuously as ρ increases beyond $\rho = 10$. Although the expansion was made for the case of uniform turbulence, this same approach can be used for non-uniform turbulence. However, different coefficients will be obtained for each different $C_n^2(t)$ profile.

5. Example: Line-of-sight spherical wave propagation

By using the above approximation of (33), the four-point, time delay mutual coherence function of (1) can be given in a closed form as below:

$$H(\mathbf{P}_1, \mathbf{P}_2, \mathbf{P}_3, \mathbf{P}_4; \mathbf{V}_\tau) = -\frac{2.91}{2} L k^2 C_n^2 \left\{ \frac{3}{8} [|\mathbf{P}_2 - \mathbf{P}_1|^{5/3} + |\mathbf{P}_4 - \mathbf{P}_3|^{5/3}] + \right. \\ \left. |\mathbf{V}_\tau|^{5/3} \sum_{i=3}^4 \sum_{j=1}^2 \left[\frac{3}{16 \rho_{ij}} [(|\rho_{ij} + 1|^{8/3} - |1 - \rho_{ij}|^{8/3}) - 2(|\rho_{ij} + 1|^{8/3} + |1 - \rho_{ij}|^{8/3} - 2) \cos \theta_{ij}] \right] \right\}$$

where

$$\rho_{ij} = \frac{|\mathbf{P}_i - \mathbf{P}_j|}{|\mathbf{V}_\tau|}$$

$$\theta_{ij} = \text{angle}(\mathbf{P}_i - \mathbf{P}_j, \mathbf{V}_\tau)$$

This can be evaluated efficiently by using a Fortran subroutine. Higher accuracy can be reached by using a better approximations of (34)-(35).

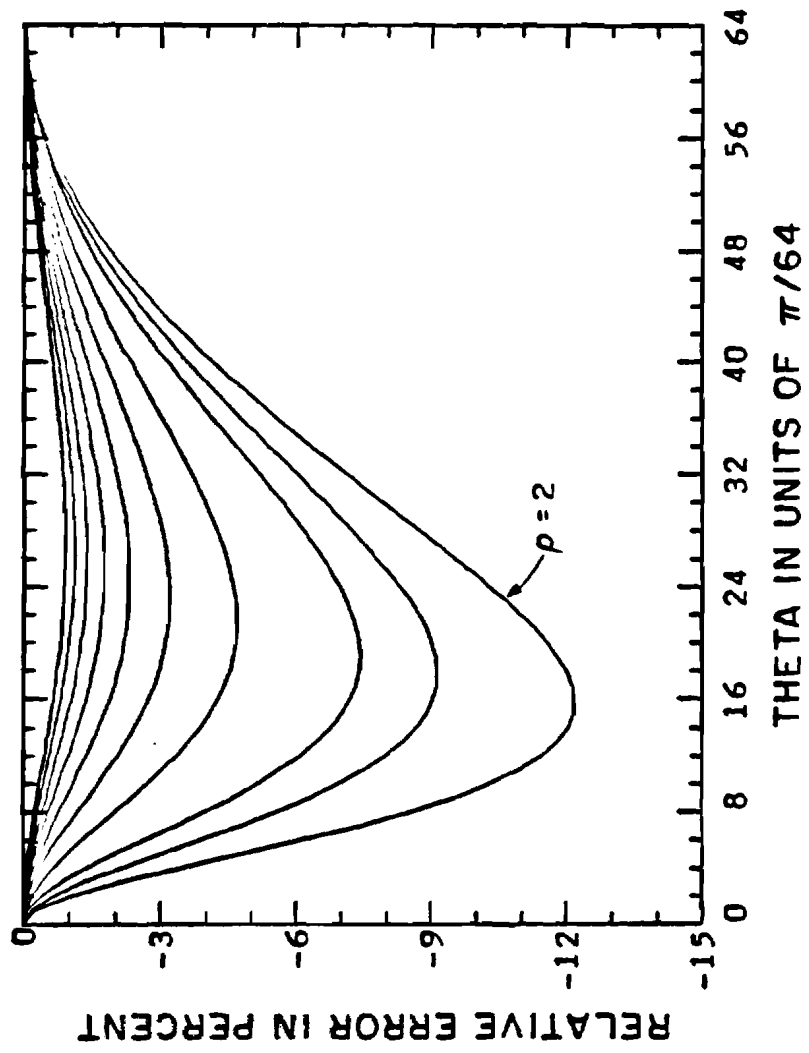


Fig. A2.3 Relative error of expansion 1.

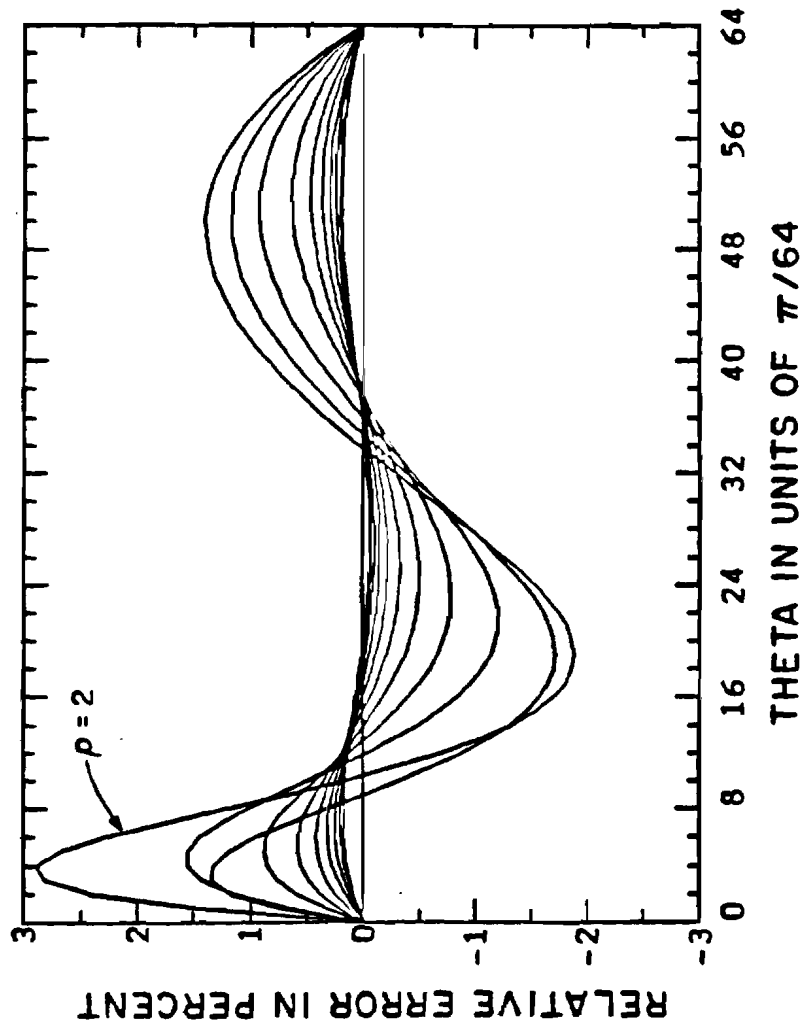


Fig. A2.4 Relative error of expansion 2.

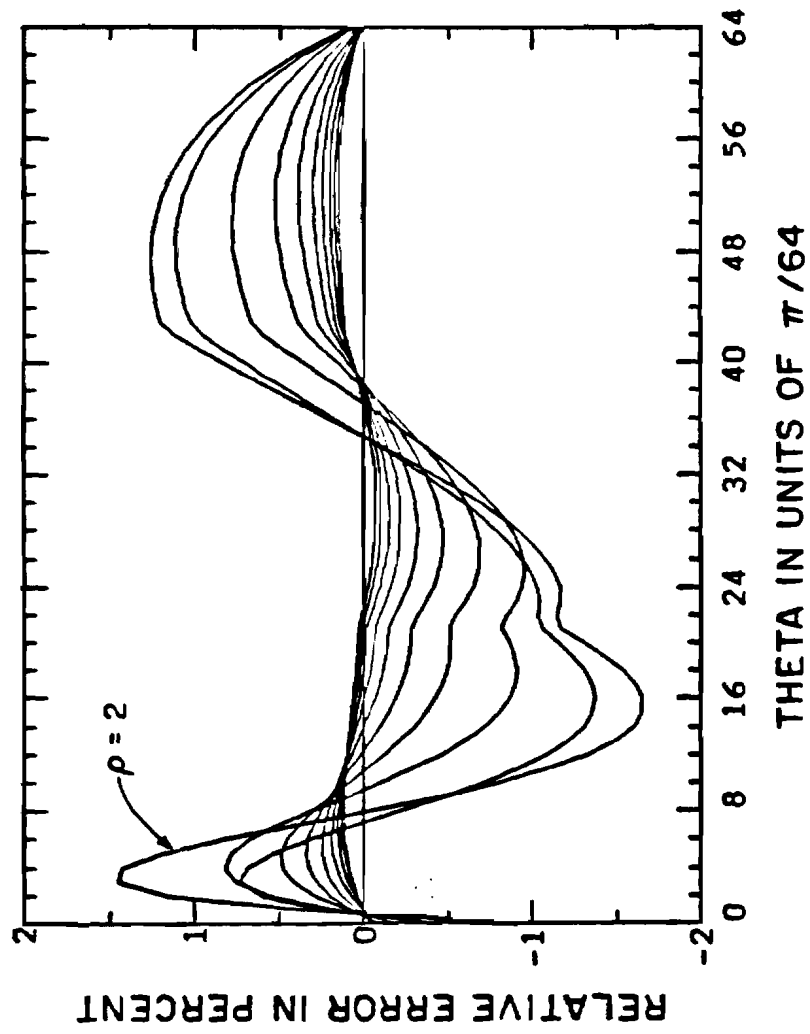


Fig. A2.5 Relative error of expansion 3.

$$\rho = 0 \quad a_1 = .0000E+00$$

$$\rho = 1 \quad a_1 = .7483E-01$$

$$\rho = 2 \quad a_1 = .1372E+00$$

$$\rho = 3 \quad a_1 = .1461E+00$$

$$\rho = 4 \quad a_1 = .1454E+00$$

$$\rho = 5 \quad a_1 = .1424E+00$$

$$\rho = 6 \quad a_1 = .1388E+00$$

$$\rho = 7 \quad a_1 = .1354E+00$$

$$\rho = 8 \quad a_1 = .1322E+00$$

$$\rho = 9 \quad a_1 = .1298E+00$$

$$\rho = 10 \quad a_1 = .1252E+00$$

max. relative error = 2.94%

Table 1 Coefficients for first harmonics

$$\rho = 0 \quad a_1 = .0000E+00 \quad a_2 = .0000E+00 \quad a_3 = .0000E+00$$

$$\rho = 1 \quad a_1 = .6970E-01 \quad a_2 = -.2060E-02 \quad a_3 = .6717E-02$$

$$\rho = 2 \quad a_1 = .1292E+00 \quad a_2 = -.4023E-02 \quad a_3 = .1064E-01$$

$$\rho = 3 \quad a_1 = .1428E+00 \quad a_2 = -.4671E-02 \quad a_3 = .5024E-02$$

$$\rho = 4 \quad a_1 = .1459E+00 \quad a_2 = -.4720E-02 \quad a_3 = .4270E-03$$

$$\rho = 5 \quad a_1 = .1449E+00 \quad a_2 = -.5544E-02 \quad a_3 = -.1906E-02$$

$$\rho = 6 \quad a_1 = .1435E+00 \quad a_2 = -.4994E-02 \quad a_3 = -.4820E-02$$

$$\rho = 7 \quad a_1 = .1403E+00 \quad a_2 = -.3404E-02 \quad a_3 = -.5381E-02$$

$$\rho = 8 \quad a_1 = .1389E+00 \quad a_2 = -.3342E-02 \quad a_3 = -.7489E-02$$

$$\rho = 9 \quad a_1 = .1369E+00 \quad a_2 = -.2984E-02 \quad a_3 = -.8156E-02$$

$$\rho = 10 \quad a_1 = .1331E+00 \quad a_2 = -.4039E-02 \quad a_3 = -.8850E-02$$

max. relative error = 2.66%

Table 2 Coefficients for 2nd harmonics

$\rho = 0$	$a_1 = .0000E+00$	$a_4 = .0000E+00$	$a_5 = .0000E+00$
$\rho = 1$	$a_1 = .7705E-01$	$a_4 = -.1582E-02$	$a_5 = -.3796E-02$
$\rho = 2$	$a_1 = .1423E+00$	$a_4 = -.2988E-02$	$a_5 = -.8739E-02$
$\rho = 3$	$a_1 = .1547E+00$	$a_4 = -.2996E-02$	$a_5 = -.1472E-01$
$\rho = 4$	$a_1 = .1560E+00$	$a_4 = -.2675E-02$	$a_5 = -.1823E-01$
$\rho = 5$	$a_1 = .1540E+00$	$a_4 = -.3294E-02$	$a_5 = -.1982E-01$
$\rho = 6$	$a_1 = .1510E+00$	$a_4 = -.2684E-02$	$a_5 = -.2096E-01$
$\rho = 7$	$a_1 = .1476E+00$	$a_4 = -.1083E-02$	$a_5 = -.2107E-01$
$\rho = 8$	$a_1 = .1446E+00$	$a_4 = -.9243E-03$	$a_5 = -.2130E-01$
$\rho = 9$	$a_1 = .1421E+00$	$a_4 = -.6741E-03$	$a_5 = -.2121E-01$
$\rho = 10$	$a_1 = .1382E+00$	$a_4 = -.1438E-02$	$a_5 = -.2233E-01$

max. relative error \approx 1.66%

Table 3 Coefficients for 3rd harmonics

References

1. R. M. Gagliardi and S. Karp, *Optical Communications*, p. Chpt. 5, Wiley-Interscience, New York, 1976.
2. J. H. Shapiro, "Optimal spatial modulation for reciprocal channels," *Res. Lab. Electron. Tech. Rept.*, p. 476, M.I.T., 1970.
3. J. C. Leader, "Intensity fluctuations resulting from partially coherent light propagating through atmospheric turbulence," *J. Opt. Soc. Am.*, vol. 69, pp. 73-84, Jan. 1979.
4. M. S. Belen'kii, A. I. Kon, and V. L. Mironov, "Turbulent distortions of the spatial coherence of a laser beam," *Sov. J. Quantum Electron*, vol. 7, pp. 287-290, March 1977.
5. S. J. Wang, Y. Baykal, and M. A. Plonus, "Receiver-aperture averaging effects for the intensity fluctuation of a beam wave in the turbulent atmosphere," *J. Opt. Soc. Am.*, vol. 73, pp. 831-837, June 1983.
6. J. F. Holmes, Myung H. Lee, and L. Sun, "Remote sensing of atmosphere turbulence by utilizing spackle-turbulence interaction and optical spatial filtering," *Proc. Topical Meeting on Optical Techniques for Remote Probing of the Atmosphere*, Incline Village, Nevada, Jan 11-12, 1983.
7. L. Sun and J. F. Holmes, "Optical high-pass spatial filtering in laser remote sensing of turbulence," *Proc. Annual Meeting of OSA*, San Diego, Oct. 29-Nov. 2, 1984.

8. L. Sun and J. F. Holmes, "Measurement of spatially filtered laser radiation in atmospheric turbulence," *Proc. Annual Meeting of OSA*, Washington DC, Oct. 14-18, 1985.
9. J. W. Strohbehn, ed., *Laser Beam Propagation in the Atmosphere*, Springer-Verlag, New York, 1978.
10. J. F. Holmes, M. H. Lee, and J. R. Kerr, "Effect of the log-amplitude covariance function on the statistics of speckle propagation through the turbulent atmosphere," *J. Opt. Soc. Am.*, vol. 70, pp. 355-360, Apr. 1980.
11. M. Abramowitz and I. A. Stegun, *Handbook of Mathematical Functions*, Dover Publications Inc., New York, 1972.

VITA

The author was born in Yunnan, China on March 1, 1944. He moved to Beijing in 1948 and stayed there until 1968. After finishing his high school in 1962, he entered the Chinese University of Science and Technology. He received his B.S. diploma in 1968.

After 10 years working experience, he entered the Graduate School of CUST and obtained his M.S. degree from Chinese Academy of Sciences in 1981. In 1982, he joined Oregon Graduate Center and began his Ph.D. studies. He completed all requirement for Ph.D. degree in Applied Physics in 1988.

While at OGC, the author received an academic scholarship from SPIE in 1984 and coauthored the following journal and conference papers:

1. J. Fred Holmes, Myung H. Lee, and Libo Sun, "Remote sensing of atmosphere turbulence by utilizing speckle-turbulence interaction and optical spatial filtering," *Proc. Topical Meeting on Optical Techniques for Remote Probing of the Atmosphere,* , Incline Nevada, Jan 11-12, 1983.

2. Libo Sun and J. Fred Holmes, "Optical high-pass spatial filtering in laser remote sensing of turbulence," *Proc. Annual Meeting of OSA,* San Diego, Oct. 29-Nov.2, 1984.

3. Libo Sun and J. Fred Holmes, "Measurement of spatially filtered laser radiation in atmospheric turbulence," *Proc. Annual Meeting of OSA*, Washington DC, Oct. 14-18, 1985.

4. Libo Sun and J. Fred Holmes, "Closed form expansion of the four-point, wave structure function for a turbulent atmosphere," accepted for publication in *J. Opt. Soc. Am.-A*.

5. Libo Sun and J. Fred Holmes, "Remote sensing of atmospheric turbulence by using speckle-turbulence interaction and coherent optical spatial filtering--- Line of sight case," will be submitted to *J. Opt. Soc. Am.*

6. Libo Sun, J. Fred Holmes Todd L. Cloninger, and John M. Hunt, "Remote sensing of atmospheric turbulence by using speckle-turbulence interaction and coherent optical spatial filtering--- Single ended case," will be submitted to *J. Opt. Soc. Am.*